

國立成功大學
機械工程學系
博士論文

整合電動馬達與齒輪減速機之設計
On the Design of Integrated Electric Motors
with Gear Mechanisms

研究生：陳冠辰 Guan-Chen Chen
指導教授：顏鴻森 Hong-Sen Yan

Dissertation for Doctor of Philosophy
Department of Mechanical Engineering
National Cheng Kung University
October 2017

中華民國一百零六年十月

國立成功大學

博士論文

整合電動馬達與齒輪減速機之設計

On the Design of Integrated Electric Motors with
Gear Mechanisms

研究生：陳冠辰

本論文業經審查及口試合格特此證明

論文考試委員：

蔡明禮 藍北杰 黃文敏
吳益勳 王心德 顏鴻森

指導教授：顏鴻森

系(所)主管：楊元祥

中華民國 106 年 10 月 7 日

摘要

現有馬達與齒輪減速機是分別設計與製造後再選配，存在動力傳輸路徑較長、機器組成元件較多、整體安裝空間較大等缺點。本研究提出一套整合設計流程，用以有系統地將電動馬達之電磁場設計與齒輪減速機的運動設計結合。依據電動馬達及齒輪減速機的構造特性與運動原理，歸納設計需求與限制，藉由圖論表示法與創意性機構設計方法，提出整合設計構想。建立一維及二維等效磁路法分析模型，解析整合裝置的電磁特性與輸出性能，並配合有限元素分析進行驗證，其誤差值分別為 3.21 % 與 3.06 %。引入卡特係數建立槽開口與齒型之磁導模型，探討齒輪輪廓對馬達電磁場之影響，結果顯示齒型不影響馬達之磁交鏈、磁通密度、及電磁轉矩。提出齒輪系的設計方法，包含齒形、齒數、齒輪系構形、及齒輪強度分析。最後，分別以現有直流有刷馬達整合行星齒輪減速機，及交流感應馬達整合一般齒輪系為設計實例，有系統並完成整合裝置的設計。齒輪強度分析結果顯示，透過矽鋼片堆疊之齒型，可承受之最大應力為 312 MPa，齒輪之動態負載，直流有刷馬達為 7.94 MPa，交流感應馬達為 98.32 MPa，足夠承受傳輸需求。由性能分析結果得知，該整合裝置滿足現有設計的傳動能力，大幅降低直流有刷馬達的頓轉扭矩 92.02% 及轉矩漣波 50.14%，降低交流感應馬達轉矩漣波 14.23%，且分別提高直流馬達與交流馬達之轉矩密度 16.66% 與 1.75%，改善整合裝置的電磁與輸出特性，其頓轉扭矩、轉矩漣波，及軸向空間的使用，皆較現有設計有更佳的性能表現。

關鍵詞：電動馬達、齒輪減速機、整合設計、創意性機構設計

Abstract

This work presents a novel design procedure for integrating electric motors with gear mechanisms. Based on the configurations of electric motors and the kinematic structure of gear trains, the design requirements and constraints are concluded. By applying the graph representations and creative mechanism design methodology, feasible design concepts are successfully generated systematically. The open-circuit magnetostatic field analysis of a DC commutator motor conducted by applying 1-D and 2-D equivalent magnetic circuit methods are obtained and verified using FEA. The differences in the air-gap flux density are 3.21% and 3.06% for 1-D and 2-D methods, respectively. The Carter's coefficient is applied to model the permeance of the slot and gear-teeth space. The affection of the integrated gear-teeth on the flux linkage and the first derivative of the flux linkage can be ignored. The design methods for gear trains, gear profiles, number of gear teeth, and gear strength are also introduced. The maximum stress of the gear profile is 312 MPa, and the results show that the gear train can be used for transmission purposes. A DC commutator motor with a planetary gear mechanism and an AC induction motor with an ordinary gear train are applied as examples. A feasible integrated DC commutator motor device is presented that reduces the cogging torque and the torque ripple by 92.02% and 50.14%, respectively, while increasing the torque density by 16.66%. The torque of the AC induction motor is reduced by 8.96%, and the torque ripple is reduced by 14.23%. In addition, the torque density is increased by 1.75%. This indicates that the integrated devices provide more stable and efficiency output torque than the existing design.

Keywords: Electric motor, Gear train, Integrated design,

Creative mechanism design

Acknowledgement

Accomplishing this dissertation is a difficult work, I would never have been able to finish this work without support and help from several people. I would like to express my greatest appreciation here.

First of all, I would like to express my sincere gratitude to my advisor, Prof. Hong-Sen Yan, for his incessant encouragement, invaluable guidance, and financial support in past years.

I also appreciate the dissertation committee members, including Prof. Mi-Ching Tsai from National Cheng Kung University (NCKU), Prof. Wen-Miin Hwang from NCKU, Prof. Chao-Chieh Lan from NCKU, Prof. Yi-Chang Wu from National Yunlin University of Science and Technology, and Prof. Hsin-Te Wang from National Kaohsiung University of Applied Sciences, for their worthwhile and insightful suggestions and comments to this work.

I would like to thank the members from NCKU Electric Motor Technology Research Center for their help and assistance on motor performance measurements.

Furthermore, I appreciate the assistance from the former and present fellows of the Creative Machine Design E&R Laboratory at NCKU. I appreciate the assistance that I have received from them, and I enjoyed the time of working and studying with them for these years.

Finally, I deeply appreciate my parents and my parents in law for their profoundest love and endless support. In addition, I would like to thank my dear wife for her patience and encouragement to accompany me to overcome the difficulties. This dissertation is cordially devoted to all of them.

Contents

摘要.....	I
Abstract.....	II
Acknowledgement.....	III
List of Tables.....	VII
List of Figures.....	IX
Nomenclature.....	XII
Chapter 1 Introduction.....	1
1-1 Motivation.....	1
1-2 Literature review.....	6
1-2-1 Motor design and electromagnetic field analysis.....	6
1-2-2 Gear train design.....	8
1-2-3 Integrated device design.....	9
1-3 Objectives.....	10
1-4 Dissertation organization.....	11
Chapter 2 Conceptual Design.....	13
2-1 Electric motors.....	13
2-2 Gear trains.....	18
2-3 Integrated design concepts.....	22
2-4 Summary.....	25
Chapter 3 Design Procedure.....	27
3-1 Design procedure.....	27
3-2 Creative design methodology.....	31
3-2-1 Graph representations.....	31

3-2-2 Creative design methodology.....	33
3-3 Summary.....	37
Chapter 4 Magnetostatics Analysis.....	39
4-1 1-D method.....	39
4-2 2-D method.....	46
4-3 FEA method.....	52
4-4 Optimal design.....	60
4-5 Summary.....	62
Chapter 5. Gear Train Design.....	64
5-1 Gear teeth design.....	64
5-2 Speed ratio design.....	66
5-3 Strength analysis of gear profiles.....	68
5-4 Summary.....	73
Chapter 6 Effects of Integrated Gear Teeth.....	74
6-1 Flux linkage analysis.....	74
6-2 Cogging torque analysis.....	75
6-3 Electromagnetic torque and torque ripple analyses.....	81
6-4 Summary.....	83
Chapter 7 Design Examples.....	84
7-1 Design example 1.....	84
7-2 Design example 2.....	94
7-3 Summary.....	101
Chapter 8 Conclusions and Suggestions.....	103
8-1 Conclusions.....	103
8-2 Suggestions.....	106

References108
Copyright122



List of Tables

Table 3-1	Fixed parameters	29
Table 3-2	Graphic representations of members of gear trains	32
Table 3-3	Graph representations of members in motors	32
Table 3-4	Graph representations of members with two inputs	32
Table 3-5	Graphic representations of armature and air-gap direction.....	33
Table 4-1	Specifications of a DC commutator motor	45
Table 4-2	Results of the 1-D equivalent magnetic circuit method.....	46
Table 4-3	Results of optimal design.....	61
Table 5-1	Standard ratios of metric involute gear teeth	65
Table 5-2	Standard modulus of involute gears.....	65
Table 5-3	Diameter of the addendum circles	66
Table 5-4	Combinations of a simple PGT.....	67
Table 5-5	Parameters of the sun gear	72
Table 5-6	Results of gear loading.....	72
Table 6-1	Parameters of the integrated device	74
Table 6-2	The n-th harmonic components generate the cogging torque.....	80
Table 6-3	Cogging torque comparison.....	81
Table 6-4	Electromagnetic and torque ripple analyses	82
Table 7-1	Design specifications of the integrated device.....	85
Table 7-2	Fixed parameters of the integrated device	85
Table 7-3	FEA parameters of the integrated device	87
Table 7-4	Results of the magnetostatic analysis	90
Table 7-5	Comparison of the performance of the integrated device.....	94

Table 7-6	Parameters of the AC induction motor.....	96
Table 7-7	Parameters of the gear train	99
Table 7-8	Loading results of the gear train	99
Table 7-9	Comparison of the output performance	101



List of Figures

Fig. 1-1	Machine systems	1
Fig. 1-2	A BLDC motor with a gear head.....	3
Fig. 1-3	A commercial DC commutator motor with a gear head [20].....	3
Fig. 1-4	An integrated starter/alternator [24].....	5
Fig. 1-5	An integrated motor/pump/controller [25].....	5
Fig. 1-6	An integrated motor/steering assembly [26].....	5
Fig. 1-7	An integrated motor/pump [27]	5
Fig. 1-8	Research structure of Yan’s research group	10
Fig. 1-9	Dissertation structure.....	12
Fig. 2-1	Mechanism of a DC commutator motor.....	14
Fig. 2-2	Planetary gear trains	19
Fig. 2-3	Integrated design concept.....	24
Fig. 2-4	Cross-section of the integrated gear teeth	25
Fig. 3-1	Integrated design procedure	28
Fig. 3-2	Creative design methodology.....	34
Fig. 3-3	Graphs of (a) three-link and (b) four-link gear trains	36
Fig. 3-4	Atlas of feasible three-link gear trains	36
Fig. 3-5	Atlas of feasible three-link integrated device.....	37
Fig. 3-6	Atlases of feasible integrated AC induction motor with three-link and four-link gear trains	38
Fig. 4-1	Topology of the linear translational motor.....	40
Fig. 4-2	Equivalent magnetic circuit.....	41
Fig. 4-3	Simplified circuit.....	42

Fig. 4-4	Simplest circuit.....	42
Fig. 4-5	Geometric parameters of a DC commutator motor.....	44
Fig. 4-6	Linear translation of coil windings	45
Fig. 4-7	Division of a DC commutator motor	47
Fig. 4-8	The permeance in the circumferential and radial directions.....	48
Fig. 4-9	The concept of fluxes flowing into a node.....	50
Fig. 4-10	A 3x3 equivalent magnetic circuit net.....	50
Fig. 4-11	Flux density comparison of the FEA result and the 2-D method.....	52
Fig. 4-12	Mesh model	55
Fig. 4-13	B-H curve of silicon steel type 50CS1300 [133]	55
Fig. 4-14	Flux linkage result.....	56
Fig. 4-15	The first derivative of the flux linkage result.....	56
Fig. 4-16	Magnetic flux density distribution	58
Fig. 4-17	Average air-gap flux density	58
Fig. 4-18	Output torque waveform	59
Fig. 4-19	Flux densities of the optimal design.....	62
Fig. 5-1	A two-stage planetary gear train	68
Fig. 5-2	Equivalent elastic system of two meshed gears	70
Fig. 5-3	Stress analysis of the gear mechanism.....	72
Fig. 6-1	Flux linkage comparison	75
Fig. 6-2	The first derivative of the flux linkage comparison.....	75
Fig. 6-3	Representation of the presence of the tooth spaces and the corresponding permeance function	77
Fig. 6-4	Cogging torque comparison	81
Fig. 6-5	Electromagnetic torque comparison.....	83

Fig. 7-1	Mesh model of the integrated design	87
Fig. 7-2	Flux linkages of the coil windings	88
Fig. 7-3	Flux distribution of the integrated device	88
Fig. 7-4	Air gap flux distribution of the integrated device	89
Fig. 7-5	Cogging torque of the integrated device	89
Fig. 7-6	Electromagnetic torque of the integrated device.....	90
Fig. 7-7	Configuration of the proposed integrated design.....	93
Fig. 7-8	Explosion drawing of the proposed integrated design.....	93
Fig. 7-9	Prototype structure	93
Fig. 7-10	The cross-section of the gear profile integrated on the rotor	95
Fig. 7-11	FEA model of the integrated device.....	96
Fig. 7-12	Comparison of the current.....	97
Fig. 7-13	Comparison of the induced voltage.....	97
Fig. 7-14	Comparison of the flux linkages	97
Fig. 7-15	A feasible gear train design	98
Fig. 7-16	3D model of the concept in Fig. 3-6 (b).....	99
Fig. 7-17	FEA gear strength results	100
Fig. 7-18	Comparison of the electromagnetic torque	101

Nomenclature

Label	Definitions
A_p	Magnetic potential energy
B	Magnetic flux density
$B(\phi)$	Flux density of the air gap without considering the rotor slots
B_a	Allowed steel flux density
$B_g(\theta, \phi)$	Magnetic flux density of the air gap
B_r	Remanence of the magnet
D_c	Diameter of the coil
D_{ps}	Depth of the pole shoe
E_b	Back-EMF
$E_g(\theta)$	Magnetic energy stored in the air gap
F	Electromagnetic force
F_p	Degrees of freedom
H	Magnetic field intensity
I	Rated conduct current
J	Current density
K_E	Back-EMF constant
K_t	Torque constant
L_g	Air gap length
L_s	Stack length
l	Length of the wire
l_m	Magnet thickness
N_c	Number of coils per armature tooth

N_J	Number of joints
N_{JG}	Number of gear pairs
N_{JR}	Number of revolute pairs
N_L	Number of links
N_p	Number of magnet poles
N_{ph}	Number of phases
N_{sl}	Number of armature slots
N_{st}	Number of stacks
n	Number of gears in a PGT
P	Number of magnet poles
R_c	Radius of commutator
R_{ro}	Outer radius of rotor
R_{sh}	Radius of shaft
R_{si}	Inner radius of stator
R_{so}	Outer radius of stator
r	Radius of coil
r_v	Velocity ratio of member i to member j
S	Number of armature slots
T	Number of teeth integrated on the rotor
$T_c(\theta)$	Cogging torque
T_i	Number of teeth in gear i
T_P	Number of teeth in the planet gear
T_R	Number of teeth in the ring gear
T_S	Number of teeth in the sun gear
$u_t(\theta, \phi)$	Step function representing the presence of tooth

	spaces
V	Rated voltage
v	Conductor moving velocity
W_{so}	Width of slot opening
W_t	Tooth width of rotor
w	Width of the tooth space along the pitch circle
α_m	Position of the tooth space
ε	Induced voltage
θ	Rotor position with respect to the stator
θ_m	Magnet arc
μ_0	Permeability of free space
μ_r	Relative permeability
τ	Electromagnetic torque
ϕ	Arbitrary angle in the air gap
ω	Rotating speed
ω_i	Angular velocity of member i
ω_{ik}	Relative angular velocity of member i to member k
ω_R	Rated rotating speed

Chapter 1 Introduction

With the development of industrial applications, electric motors and gear mechanisms are being widely used. However, electric motor and gear heads are designed and manufactured independently. Although these devices can still achieve the desired functions, there are drawbacks, such as a longer transmission path and more constituent elements. Therefore, there has been a general trend toward integrating electric motors with peripheral devices for the purposes of improving system performance, reliability, and reducing product costs. This study proposes a design process and a novel configuration of integrated electric motors and gear trains.

1-1 Motivation

Machine systems can be divided into three subsystems: the power sources, the transmissions, and the working machines [1], Fig. 1-1. The power sources provide desired energy, such as electric energy, heat energy, magnetic energy, and luminous energy. The transmissions can transfer the rotational energy into kinematic energy in a linear or rotational direction. The working machines transfer the kinematic energy into desired work.

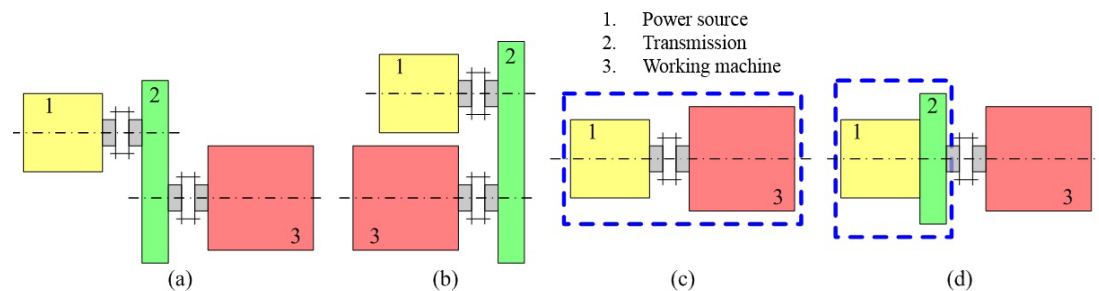


Fig. 1-1 Machine systems

Combinations of electric motors and gear reducers are considered to be typical examples of mechatronics, which are frequently adopted in present day machinery. Based on patents in Taiwan [2-7], USPTO patents [8-17], EPO patent [18], and commercial products [19-21], the traditional design strategy is to design electric motors and gear reducers independently. In order to meet needed drive requirements, users integrate these two devices within expected functions for the purpose of transforming speed and torque. The combined devices are widely used in high driving torque and/or low angular velocity applications, e.g., power tools, electric vehicles, factory conveying equipment, etc. Intermediary mechanical components, such as couplings or power-transmitting elements, are further employed for transmitting motion and/or power from the electric motors to the gear heads. This traditional configuration simplifies the complexity of design tasks due to independent designs of the electric motors and the gear heads. Since the efficiency of an electric motor is related to its rotational speed, the main advantage of the traditional configuration is the capability of operating in a motor's most efficient state because the output speed is mechanically reduced by the reducer. Fig. 1-2 shows a brushless DC motor (BLDC) with a gear head, and Fig. 1-3 shows a commercial DC commutator motor with a gear head.

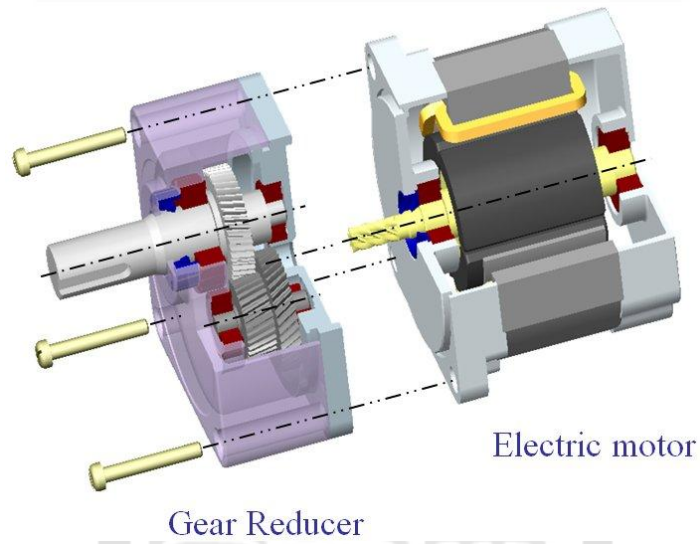


Fig. 1-2 A BLDC motor with a gear head

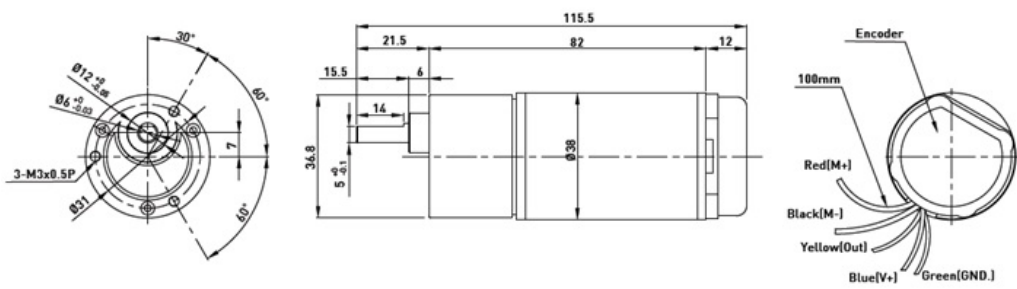


Fig. 1-3 A commercial DC commutator motor with a gear head [20]

However, this type of design suffers from three disadvantages.

1. The first one is the use of couplings or power-transmitting elements, which comprise the primary failure source and increase the maintenance complexity and manufacturing costs.
2. Secondly, the additional mechanical loss caused by the friction of intermediary components results in undesirably low efficiency.
3. The third is the incompact workspace arrangements due to the individual design of the electric motor and the gear reducer, which makes it difficult to reduce the overall size.

Therefore, a combination of an electric motor and a gear reducer should be developed from the perspective of system integration to overcome the above shortcomings.

In recent years, integrated design concepts have been applied to the research and design of novel vehicles and ships, such as integrated starters/alternators, specifically for the idle free and regenerative braking function, Fig. 1-4 [22, 24]. Another example is the use of an integrated motor/pump/controller in a vehicle cooling system intended to make the available space more efficient, as shown in Fig. 1-5 [25]. Moreover, integrated motor/steering assemblies that combine the position sensors and steering mechanisms shown in Fig. 1-6 can reduce the engine output loss and improve the arrangement of needed space [26]. In addition, the use of an integrated motor/pump system for underwater craft that combines the permanent magnets of the motors and pump blades, as shown in Fig. 1-7, can reduce the use of coupling and the axial spaces [27].



Fig. 1-4 An integrated starter/alternator [24]

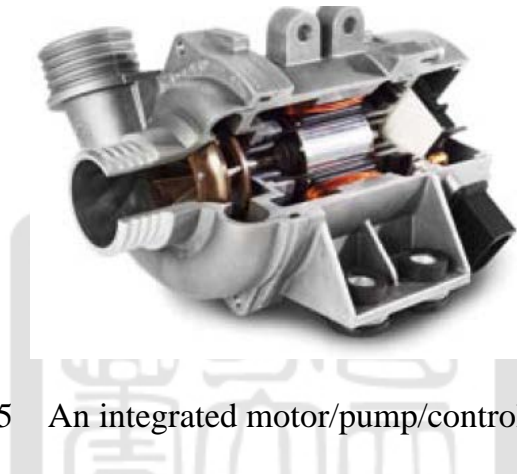


Fig. 1-5 An integrated motor/pump/controller [25]

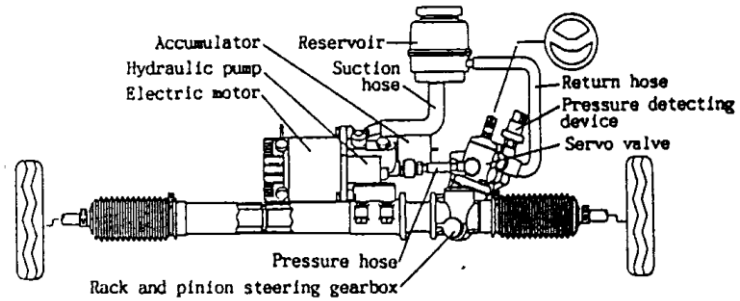


Fig. 1-6 An integrated motor/steering assembly [26]

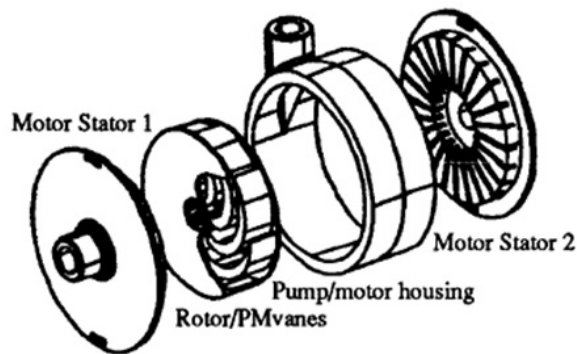


Fig. 1-7 An integrated motor/pump [27]

An innovative geared motor should be designed to overcome the above defects while simultaneously maintaining existing advantages. Therefore, the design and analysis of an electric motor and gear head are worthy research objectives.

1-2 Literature review

This study is mainly aimed at the integration of a motor and gear head. Therefore, the design approaches related to the motor, the gear trains, and the integrated device are discussed separately. The literature search and review section, then, is divided into three sub-sections: (1) motor design and electromagnetic field analysis, (2) gear train design, and (3) integrated device design.

1-2-1 Motor design and electromagnetic field analysis

In motor design, Miller [28], Hanselman [29], Akiyama [30], and Tang [31] introduced typical design procedures. These design procedures took into consideration magnetic materials, magnetic circuit structures, control systems, optimal design, machine design, and computer aided design (CAD). Basically, the design procedures included specifications, structures, magnetic circuits, rotor and stators, electrics, detailed design, and performance analysis.

Electromagnetic parameters have been the key indicators for predicting output performance. Many domestic and international scholars have been devoted into this topic. Hanselman [29], Lipo [32], Yang [33], Hwang [34, 35], Tsai [36], and Tsou [37] presented the magnetostatic analysis models. Their models can be used to analyze open-circuit fields of surface-magnet rotors, surface-inset rotors interior-magnet rotors, and axial air-gap motors. The

relationships of fluxes can be determined to calculate the Back-EMF constant and torque constant. Tsai [38] combined the equivalent magnetic method and boundary element method to describe 3-D fluxes and to calculate cogging torque. Momen [39] presented a 1-D model to calculate the flux linkage in segmented core BLDC motors. Tsai [40, 41] presented a 2-D model to calculate flux linkage distributions. Hauge, Boules, and Miller [42-44] used the Laplacian equation to determine flux distributions. Kumar [45] used a vector method to determine flux density. Tsou [46] used magnetic scalar potential to calculate the Maxwell stress to obtain cogging torque. Liu [47] considered the interaction of slot openings. Markovic [48] used a Halbach array to calculate magnetic distribution. Zhu and Howe [49-54] considered the armature reaction and slot effects.

With faster computing speed and the popularization of electromagnetic analysis software, finite-element analyses are being widely employed, not only in 2-D and 3-D electromagnetic analysis but also in computer-aided motor designs [55-63]. Currently, there are multiple versions of commercial software available on the market, such as FLUX, ANSYS/MAXWELL, MAGNET, JMAG, MOTORPRO, VECTOR FIELD, and COSMOS/EMS.

The most optimal methods are applied for considering winding types [64], structures and magnetic fields [65-70], and control current waves [71] to improve output torque.

The most efficient way to reduce cogging torque is through making structural changes [72]. The improvement methods include skewing or twisting along the axial direction on silicon steels [73] or positioning of permanent magnets [72, 74], auxiliary salient poles [75, 76], dummy slots [77, 78], rotor and stator fraction ratios [28], by changing the arc of permanent magnets [74, 79,

80] or the shape of shoes [81-85], creating asymmetry [86], altering slot openings [87] or the position of permanent magnets and slots [88], changing the width of slots and length of magnets [89], or the length-width ratios of axial air-gap motors [90].

1-2-2 Gear train design

The synthesis and analysis of PGTs have been proposed as research subjects over the past several decades. Graph theory, however, is the most common mathematical tool. Freudenstein and Buchsbaum originally introduced graph theory and Boolean algebra to represent the topological structure of a gear mechanism [91, 92]. Based on a graph representation, Tsai [93-95] then developed an algorithm for the PGT with one degree-of-freedom (DOF) and three to six links, by applying a linkage characteristic polynomial. Erdman et al. [96] proposed the topological analysis of the coincident joints of the PGT. Hsu [97-100] then presented an interactive computer program for the kinematic analysis of PGTs with any number of DOF.

The kinematic analysis by fundamental circuit method is considered to be more systematic than other approaches. Freudenstein [101] originally did a kinematic analysis of PGTs using the fundamental circuit method. Yan and Hsieh [102, 103] proposed a generalized method of kinematic analysis for all types of PGTs using generalized fundamental circuit equations and compatibility equations. The typical method to synthesize the number of gear teeth is the optimal method [104, 105]. Hsu [106] presented a relationship of speed ratio to determine all possible numbers of gear teeth.

1-2-3 Integrated device design

In 2001, Yan et al. [107] proposed an innovative concept integrating an electric motor with a mechanical PGT. By maintaining the relative angular speed between the stator and rotor, the electric motor still operated well. Then, Yan and Wu [108-113] integrated the gear elements of the PGT with a brushless DC (BLDC) motor. A feature of the integrated design is the integration of the ring gear of the PGT with the pole shoes. With a proper gear teeth design, cogging torque and torque ripple can be effectively reduced. Yan et al. [114] proposed the concept of a primary side and secondary side of an electric motor maintaining relative rotation. Using the creative mechanism design methodology, configurations of novel 3-link and 4-link integrated DC gear motors were obtained. Yan and Lin [115] presented integrated wind power generators with gear trains. Yan and Chen [116] then proposed the design of a DC commutator motor with an integrated PGT, which provided another systematic design method. Yan and Wang [117] presented an innovative cordless drill. Yan and Lee [118] worked on the integrated design with switched reluctance motors, and Wang [119] presented hybrid stepping motors with integrated planetary gear trains. Fig. 1-8 shows the research structure of Yan's research group regarding this topic.

Wu [120] proposed an inner-rotor BLDC motor integrated with a transmission. Via mechanical shifting, the motor provided three-stage speeds. Tsai et al. [121-123] invented a coaxial motor that combines two coaxial BLDC motors and a basic PGT, achieving continuously-variable speed changes. Wang presented a novel magnetic-gear PM brushless motor [124, 125]. Chau presented BLDC motors in vehicle applications [126, 127].

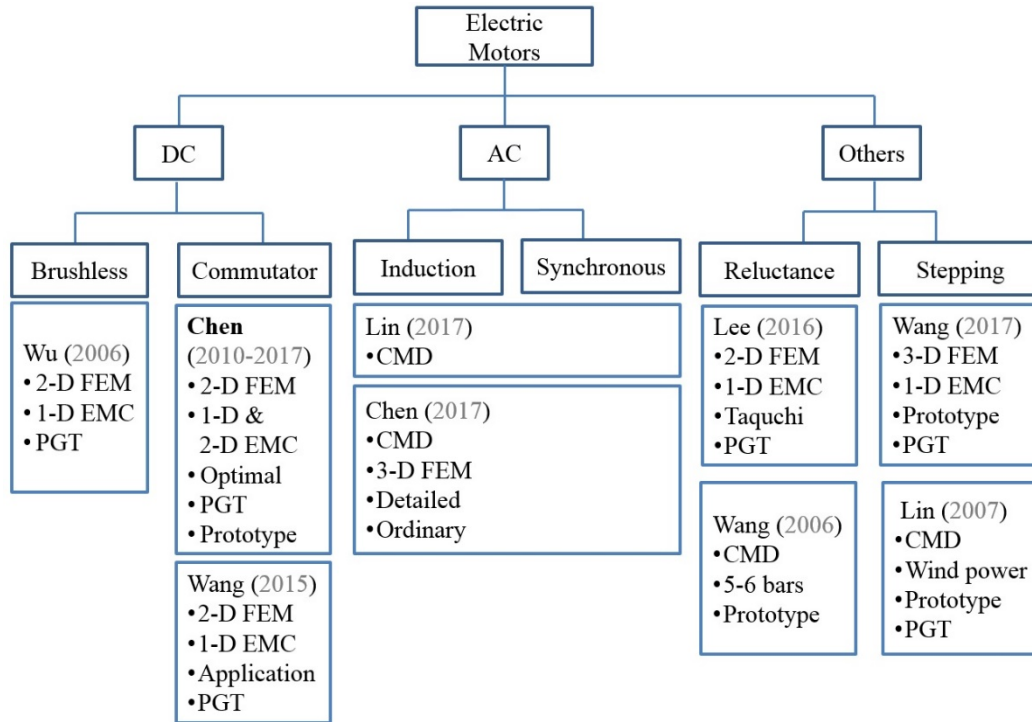


Fig. 1-8 Research structure of Yan's research group

1-3 Objectives

The goal of this study is to focus on the integration of rotating electric motors and gear mechanisms. The main objectives are summarized as follows:

1. To discuss the electromagnetic theory of electric motors, the kinematic theory of a gear mechanisms, and the integrated design theory.
2. To combine components of an existing electric motor and transmission with magnetic field design and mechanical design to develop integrated devices with better electromagnetic characteristics.
3. To investigate the effects of gear elements on both the magnetic fields and transmission abilities of the integrated device.
4. To develop a design procedure for the integrated design to guide designers with the implementation of these novel devices.

1-4 Dissertation organization

As shown in Fig. 1.2, the thesis is organized into the following seven chapters:

1. Chapter 1 is the introduction, which includes the motivation, literature review, objectives, and organization of this study.
2. Chapter 2 describes the basic theories of electric motors and gear trains. The novel integrated design concept is introduced in this chapter.
3. Chapter 3 proposes a design process with Yan's creative mechanism design methodology for the integrated devices.
4. Chapter 4 focuses on the magnetostatics analysis. 1-D and 2-D equivalent magnetic circuits are introduced and verified with FEM.
5. Chapter 5 deals with the kinematics of the integrated device and the strength of the integrated gear mechanisms.
6. Chapter 6 analyzes the effects of integrated gear teeth on electromagnetic performance.
7. Chapter 7 presents 2 design examples, and electromagnetic performances are compared with an existing motor.
8. Chapter 8 concludes the results of this study and provides suggestions for future research and design.

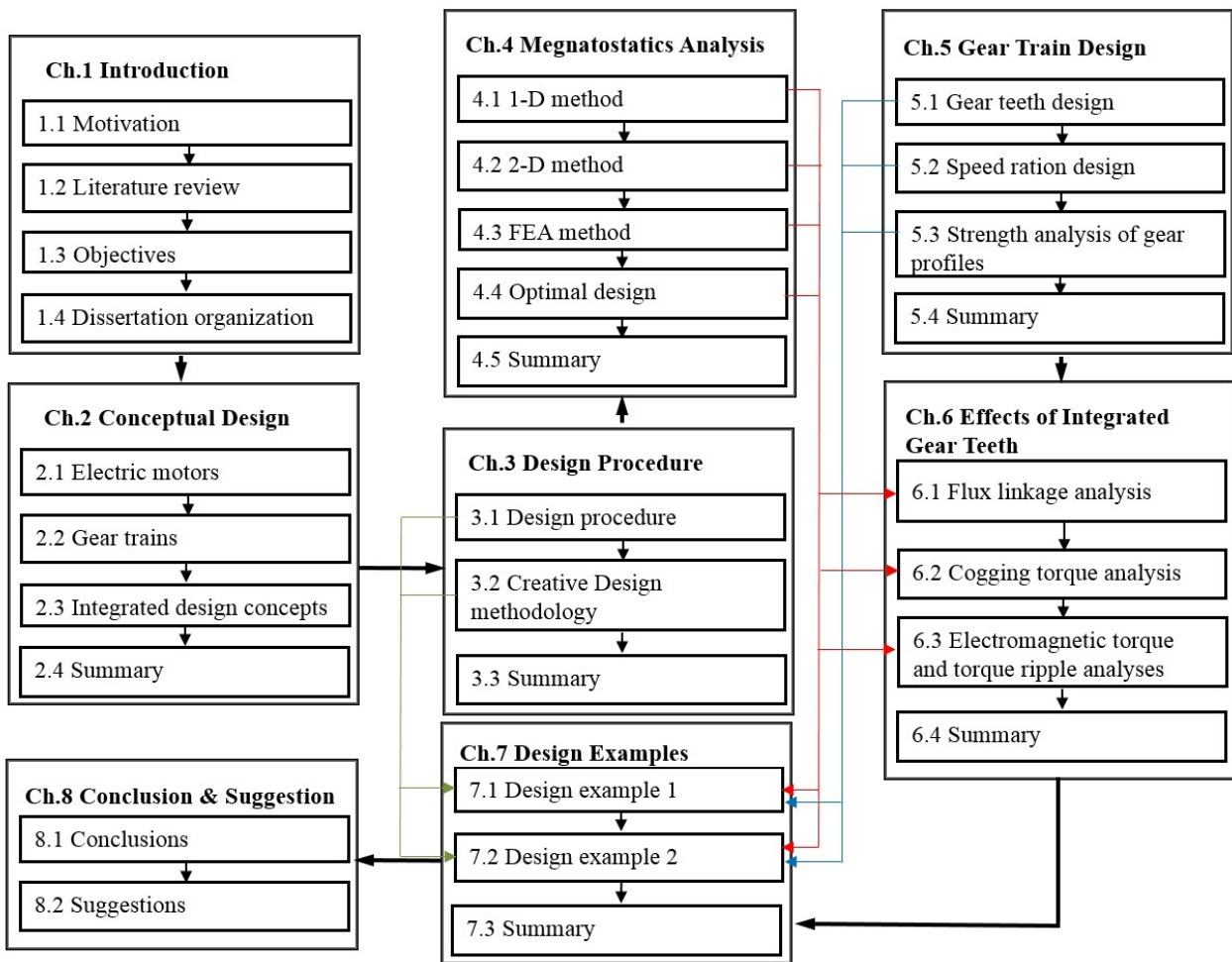


Fig. 1-9 Dissertation structure

Chapter 2 Conceptual Design

Regarding the design process, a conceptual design is indispensable. Based on an appropriate design process, feasible designs can be synthesized. In addition, thoroughly studying conventional designs can also bring about new design concepts. Therefore, in order to obtain feasible design configurations, it is necessary to analyze the characteristics of motors and gear trains, respectively. This chapter introduces the basic mechanisms and kinematic characteristics of motors and gear trains. In addition, feasible configurations are identified.

2-1 Electric motors

In modern technology, the use of electric motors is quite common. As opposed to internal combustion engines, electric motors can only be driven by electricity. Moreover, given the design of the power and control system, electric motors are easier to control than internal combustion engines. Since the invention of small motors, they have been widely used in daily necessities and precision machinery. Nowadays, electric motors are indispensable power sources in many domains.

Electric motors have a considerable number of types, such as direct current (DC) motors, induction motors, stepping motors, and linear motors. They can be classified according to their input power: some are powered by DC sources, and others are powered by alternating current (AC) sources. Generally, a rotary motor is composed of a stator and a rotor. In an electric motor, the stationary part is the stator, and the moving part is the rotor. In addition, DC motors can also be divided into permanent-magnet DC motors and excited DC motors, according to the way the magnetic field is generated. Permanent-magnet DC motors are

widely applied in small motors and electronic motors. The mechanical-commutator and electronic-commutator create the differences between DC commutator motors and brushless DC (BLDC) motors. A DC commutator motor is the earliest developed motor, which has the ability to generate torque, superior control performance, and, most importantly, is less limited. For these reasons, the application of DC commutator motors still flourishes.

As shown in Fig. 2.1, a DC commutator motor comprises a magnetic field and armature. Its permanent magnet provides a magnetic flux source, which serves as the stator; the coil winding provides EMF, which serves as the rotor. The electrical energy is converted into mechanical energy after electromagnetic induction. The stator of a DC commutator motor comprises a frame, permanent magnets, and a commutator. The permanent magnets are fixed on a frame that supports all mechanical parts.

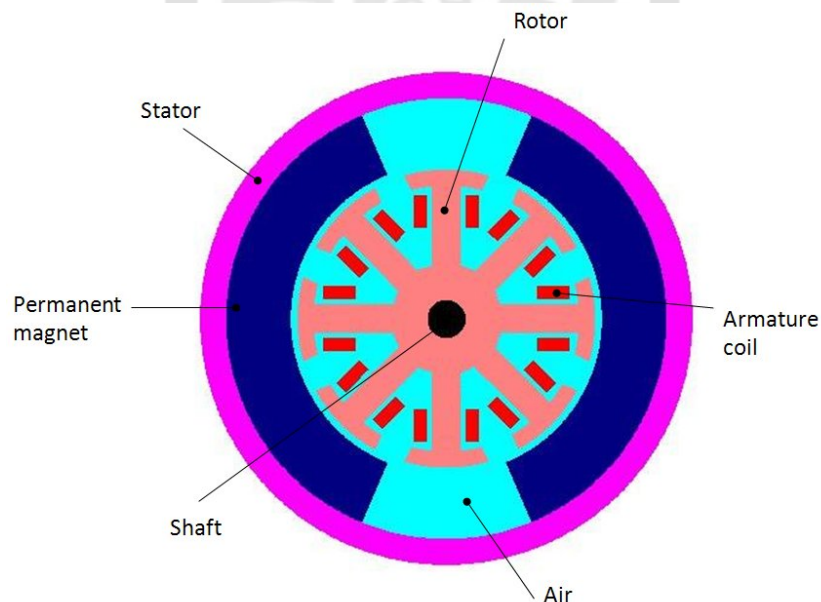


Fig. 2-1 Mechanism of a DC commutator motor

The advantage of a permanent magnet is that the magnetic field does not

change because of the external magnetic field, but rather provides a fixed magnetic field. Permanent magnets are made from hard ferromagnetic materials such as alnico and ferrite, which are subjected to special processing in a powerful magnetic field during manufacture. An alnico magnet has high flux density with low coercivity, and a ferrite magnet has low flux density with high coercivity and low cost. Hence, a ferrite magnet is used more commonly. SmCo_5 has good magnetic flux density and coercivity and is the most advanced material. Since the cost of SmCo_5 is higher than the others, it is used less commonly. A Neodymium magnet (NdFeB) can perform like SmCo_5 , but it is lower in price. Therefore, Neodymium magnets are now widely utilized in industrial applications.

Direct current is converted into an alternating current by the brushes pressing against the commutator in order to generate torque in the same direction. Currently, some brush materials include carbon, graphite, and metal fiber.

The rotor mainly consists of the commutator and the armature, which comprises the armature core and the armature winding. The armature core is formed with steel laminations, which are designed to reduce hysteresis and eddy loss. The laminations are necessarily stacked vertically to the shaft. In order to wind easily, usually there are slots although there are slotless motors. The core is part of the magnetic circuit, but in general, it must be wound with enameled wire on the slot to form the armature winding.

Usually, there are either single layer windings or double layer windings. A single layer winding means that the complete slot contains only one coil side per slot, whereas double layer winding means that there are two coil sides per slot. Basically, the armature winding of a DC motor is wound using one of two

methods: lap winding or wave winding. The difference between these two methods is exclusively owing to the end connections and commutator connections of the conductor. Frog leg winding is a combination of lap winding and wave winding in the same slot. All three of these methods can be used based on design requirements.

The theoretical foundation of electric motors is mainly based on Fleming's left-hand rule. It is claimed that whenever a current-carrying conductor is set inside a magnetic field, a force acts on the conductor in the direction vertical to both the directions of the current and the magnetic field. The magnitude of the force (F) acts on the conductor and can be expressed as follows:

$$F = I \cdot l \cdot B \quad (2-1)$$

where I (A) is the current; l (m) is the length of the wire, and B (Wb/m²) is the magnetic flux density. Its vector form can be written as:

$$\vec{F} = I(\vec{l} \times B) \quad (2-2)$$

A motor operates based on Fleming's left-hand rule. When the current flows through the commutator segments to the armature conductor, it generates the force that spins the rotor. With the commutators switching the direction of current, the rotor rotates continuously, providing the output torque.

Based on Eq. (2-1), the torque (τ) can be obtained by the following equation:

$$\tau = F \cdot r = I \cdot l \cdot B \cdot r \quad (2-3)$$

where r is the radius of the coil. In addition, without getting into theoretical substance, the torque constant, K_t , is just the slope of the torque/current curve of a motor, and is expressed as:

$$K_t = B \cdot l \cdot r \quad (2-4)$$

Eq. (2-3) can be converted to:

$$\tau = K_t \cdot I \quad (2-5)$$

As can be seen, the torque is proportional to the current.

When applying an external force on the shaft, the electric motor turns into an electrical generator. Based on Fleming's right-hand rule, the induced voltage, ε , generated in the magnetic field, B , due to a conductor moving at velocity, v , is thus given by:

$$\varepsilon = -B \cdot l \cdot v \quad (2-6)$$

while the induced voltage ε and current are in the opposite direction.

Back electromotive force (Back-EMF, E_b) is frequently used to refer to the voltage that occurs in electric motors when there is a relative movement between the armature and the magnetic field caused by the permanent magnets. Based on Faraday's law, the voltage, V , is proportional to the magnetic field, B , the length of the wire, l , in the armature, and the rotating speed, ω , of the motor. Therefore, the Back-EMF is proportional to the rotating speed, as follows:

$$E_b = K_E \omega \quad (2-7)$$

where K_E is the Back-EMF constant.

A commutator DC motor has a set of windings wound on an armature which is mounted on a rotating shaft. The shaft carries the commutator, a rotary electrical switch that reverses the current flow in the rotor windings when the shaft rotates. Thereby, every commutator DC motor has alternating current flowing through its windings. The current flows through brushes that contact the

commutator, and the brushes connect an external source of electric power to the rotating armature. After the armature starts to rotate, the torque becomes zero the moment the armature becomes horizontally aligned. At this point, the commutator reverses the direction of current through the coil, reversing the magnetic field and causing the armature to continue to rotate.

2-2 Gear trains

To providing a smooth transmitting rotation, gear trains are now broadly used in many industry categories, such as automobiles, machine tools, cranes, and small instruments and apparatuses.

Both electric motors and internal combustion engines are common power sources. Generally, power sources can generate maximum power under high rotational speeds. Therefore, speed reducers are a prerequisite for general machines for reducing the rotational speed.

Depending on whether the center of the gear shaft is fixed or not, gear trains can be divided into ordinary gear trains and planetary gear trains [128, 129]. Ordinary gear trains contain fixed axes, which are relative to the frame for all gears comprising the train. Planetary gear trains contain one or more axes rotating around another axis. In other words, a planetary gear train has at least one axis unfixed relative to the frame. As shown in Fig. 2-2(a), a planetary gear train consists of a ground link (member 1), a sun gear (member 2), a carrier (member 3), a ring gear (member 4), and a planet gear (member 5). The sun gear is adjacent to the planet gear with an external gear pair, while the planet gear is adjacent to the ring gear with an internal gear pair. The carrier is adjacent to the sun gear and planet gear with revolute pairs.

In a planetary gear train with n gears, T_S , T_P , and T_R denote the number of teeth in the sun gear, the planet gear, and the ring gear, respectively. The center axle and main axle coincide with each other. In order to make the ring gear, sun gear, and the orbits of the planet gear concentric, the concentric condition must be as follows:

$$T_R = T_S + 2T_P \quad (2-8)$$

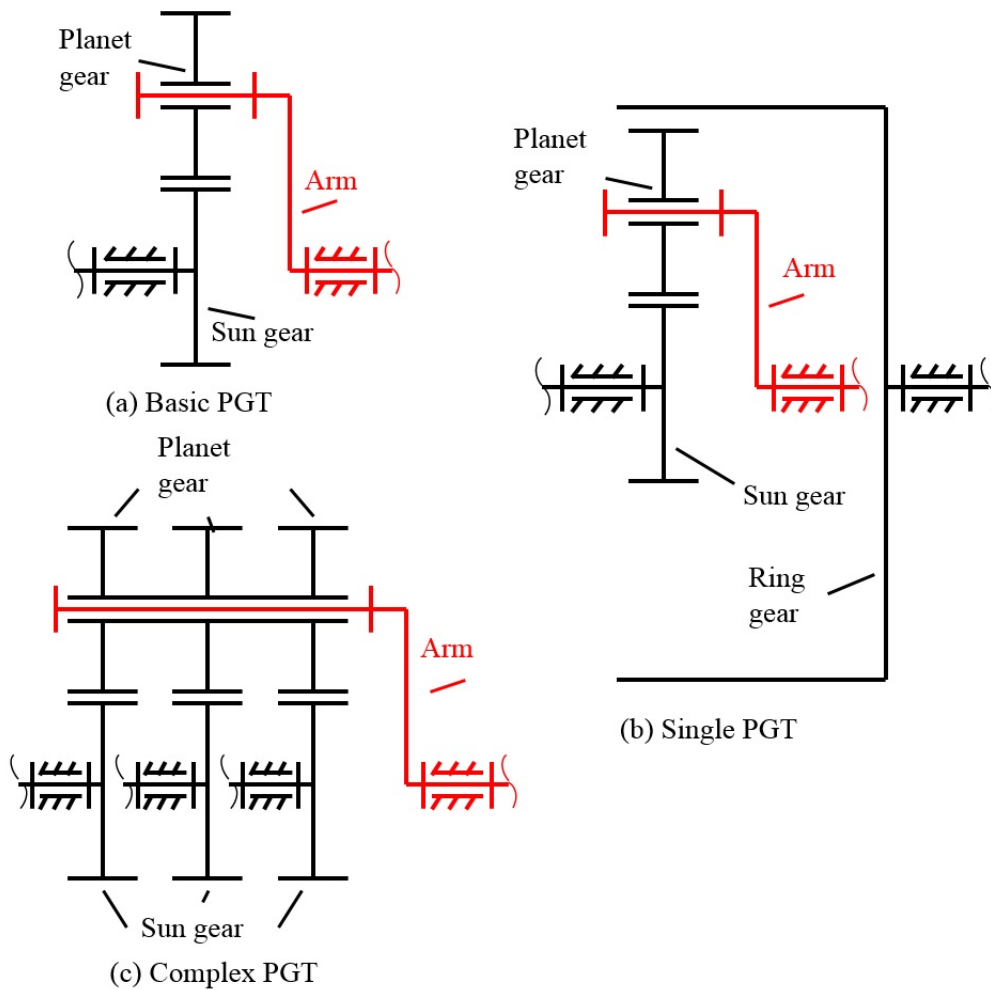


Fig. 2-2 Planetary gear trains

In order to maintain the workspace of the system, the planet gears are usually assembled symmetrically surrounding the sun gear, so the gears should follow the following assembly condition:

$$\frac{T_S + T_R}{n} = \text{integer} \quad (2-9)$$

In order to prevent collisions between gears, there must be a space between them. The following conjugate condition should be followed:

$$T_P + 2 < (T_S + T_P) \sin \frac{180^\circ}{n} \quad (2-10)$$

The PGT is able to operate smoothly only when the system satisfies Eqs. (2-8), (2-9), and (2-10).

The purpose of kinematic design and an analysis of PGT is to determine the velocity ratio and the angular velocity of the PGT. In this study, the principle of a fundamental circuit is applied [101]. Based on the principles of relative motion, the relationships between gears and rotational speed are determined. The simultaneous solutions of all the mathematical relationships are used to define the velocity ratios and the angular velocities.

A PGT has a fundamental circuit (i, j, k) in which gear i and gear j are the two gears incident to the gear pair, and carrier k is the transfer link. Let ω_i , ω_j , and ω_k be the angular velocities of member i , j , and k , respectively. The relative angular velocity of gear i to carrier k is:

$$\omega_{ik} = \omega_i - \omega_k \quad (2-11)$$

The relative angular velocity of gear j to carrier k is:

$$\omega_{jk} = \omega_j - \omega_k \quad (2-12)$$

Furthermore, let r_v be the velocity ratio of gear i to gear j assuming that both gears are external gears; then, the velocity ratio r_v is:

$$r_v = \frac{\omega_{jk}}{\omega_{ik}} = -\frac{T_i}{T_j} \quad (2-13)$$

where T_i and T_j are the number of teeth in gear i and gear j , respectively. The negative sign means that the two gears rotate in opposing directions. In other words, if gear i and gear j are an external gear and an internal gear, respectively, the velocity ratio r_v becomes:

$$r_v = \frac{\omega_{jk}}{\omega_{ik}} = +\frac{T_i}{T_j} \quad (2-14)$$

where the positive sign means that the two gears rotate in the same direction. Eqs. (2-13) and (2-14) can be rewritten for the fundamental circuit equation as:

$$r_v \omega_i - \omega_j - (r_v - 1) \omega_k = 0 \quad (2-15)$$

The velocity ratio can be obtained by Eq. (2-15). There are n independent fundamental circuit equations if there are n gears in a gear train.

Fig. 2-2(b) shows a simple planetary gear train. Gear 2 is the sun gear with number of teeth T_2 and velocity ω_2 ; gear 3 is a planet gear with number of teeth T_3 and velocity ω_3 ; gear 4 is a ring gear with number of teeth T_4 and velocity ω_4 , and link 5 is the carrier with velocity ω_5 . The fundamental circuit equations of the PGT are:

$$r_{v1} \omega_2 - \omega_3 + (r_{v1} - 1) \omega_5 = 0 \quad (2-16)$$

$$r_{v2} \omega_4 - \omega_3 + (r_{v2} - 1) \omega_5 = 0 \quad (2-17)$$

where $r_{v1} = -T_2/T_3$, and $r_{v2} = +T_4/T_3$. The velocity ratio r_v can be derived as follows: if gear 2 is the driving gear with known velocity, and gear 4 is fixed such that $\omega_4 = 0$:

$$r_v = \frac{\omega_5}{\omega_2} = \frac{T_2}{T_2+T_4} \quad (2-18)$$

2-3 Integrated design concepts

The conceptual design of integrating DC commutator motors with gear trains involves producing a preliminary solution with desired functions that satisfy both design requirements and constraints. The design requirements and constraints are the essential prerequisites of the design task associated with the novel device. This section summarizes the design requirements and constraints that the new design should encompass from both structural and functional viewpoints. Subject to the design requirements and constraints, feasible design concepts are developed by combining one of the planetary gear trains of the reducer within interior-rotor DC commutator motor.

According to the kinematic structural characteristics of basic planetary gear trains, three coaxial links are designated as the input link, output link, and fixed link, respectively, in order to obtain a constant velocity ratio. The links must be connected to the rotor, output shaft, and frame of the DC commutator motor for the purpose of transmission. For the sake of compactness, one of the admissible methods is to integrate the gear components within the motor elements. In fact, this can be achieved by setting the gear teeth on the circumference of the rotor. From a functional point of view, adding gear teeth to the rotor serves not only to support the function of transmitting but also to improve the magnetostatic field of the motor. Additionally, to simplify the components as well as minimize manufacturing costs, the integrated design of the planetary gear train and motor should not contain any additional elements or mechanisms.

By applying a PGT and a DC commutator motor as an integrated device as

an example, the design requirements and constraints are summarized as follows:

- R1. The fixed link of the PGT must be connected to the stator of the DC commutator motor.
- R2. The input link of the PGT must be connected to the rotor of the DC commutator motor.
- R3. The output link of the PGT must be combined with the output shaft of the integrated device.
- R4. The gear teeth must be integrated on the rotor of the DC commutator motor facing the permanent magnets.
- R5. With the exception of the PGT and the DC commutator motor, no additional mechanisms are employed in the integrated device.

The design concepts should follow the design requirements mentioned above in order to achieve the desired functions. The design constraints are more flexible and can be changed according to designers' decisions. Two design constraints for the integrated device are identified and summarized as follows:

- C1. Because the ring gear of the basic PGT is a fixed link, it is more suitable to integrate it with the stator of the DC commutator motor.
- C2. To simplify the design process, the gear teeth integrated on the rotor are the exterior type and on the stator, they are the interior type.

The design requirements R1-R5 are fixed to guarantee that the results have the desired functions. The design constraints C1 and C2 are flexible and can be varied according to engineers' decisions. From R1 to R4, the gear profiles are applied on the rotor of the DC commutator motor as the sun gear of the PGT. Based on C1, the gear profiles are applied on the stator of the DC commutator motor as the ring gear of the PGT. The arm of the PGT is the output shaft of the

integrated device. The integrated design should meet requirement R5 and constraint C2. Fig. 2-3 shows an exploded view of the design concept.

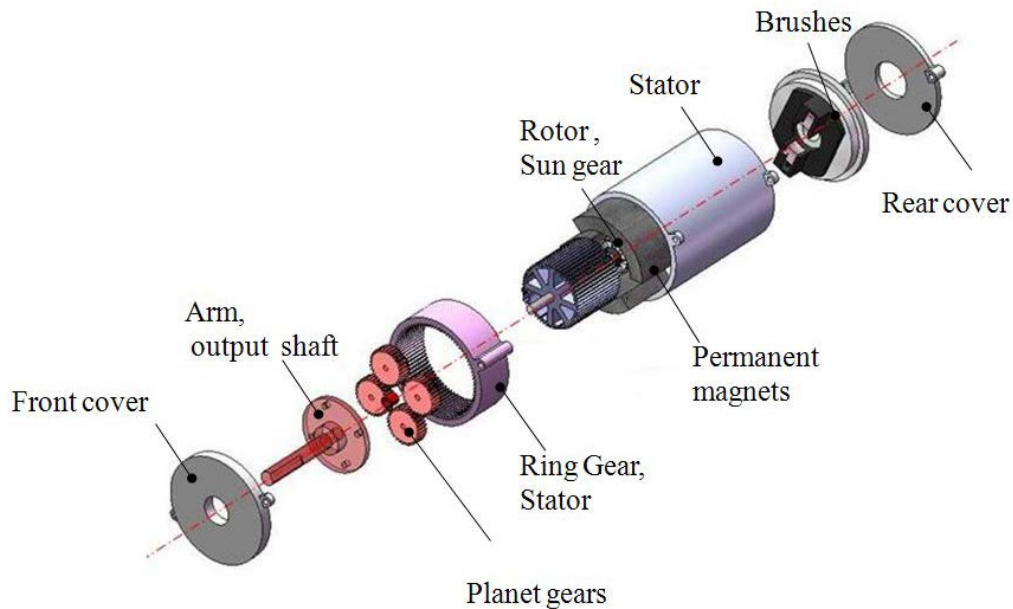


Fig. 2-3 Integrated design concept

For the purpose of dynamic balancing and loading capacity, there are two or more planet gears in a planetary gear train reducer. The design concept of integrated teeth with the rotor is shown in Fig. 2-4. The gear teeth integrated to the rotor comprise a spur gear, and the slot openings are retained for winding. Additionally, the distance between the addendum circle and the inner radius of the magnets is the width of the air gap. Because the manufacturing of the teeth profile is difficult, applying a stacked silicon sheet can solve this problem.

In contrast to conventional designs, the proposed concepts have the following qualitative features:

1. The integrated device eliminates the use of couplings, the gearbox casing, and bolts or fasteners, which makes the entire device more compact, lightweight, and easier to maintain.

2. The output shaft of the PGT and relational shaft of the motor are coaxial, while the balanced planet gears are also employed. This may contribute to better dynamic balance characteristics and reduce possible noises and vibration.
3. The integrated device reduces the axial direction spaces required for installation. It also shrinks the length of the power flow path and decreases the mechanical losses that occur due to the combined components.
4. The gear teeth integrated on the rotor act as dummy slots [77, 78] to effectively reduce the cogging torque and torque ripple of the motor.

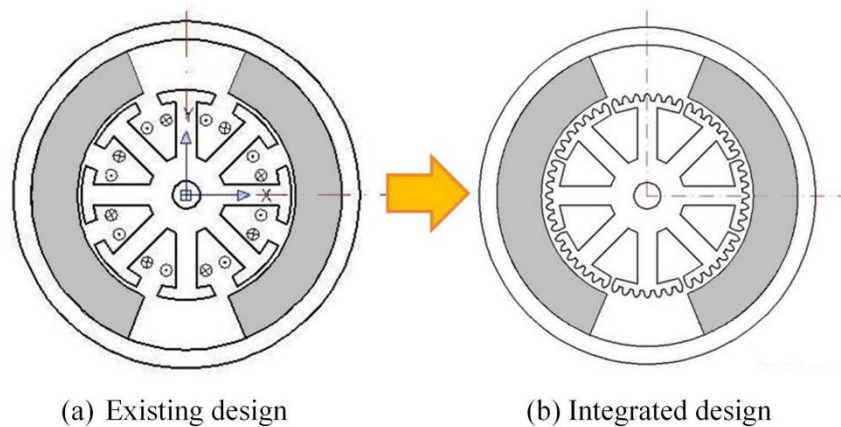


Fig. 2-4 Cross-section of the integrated gear teeth

2-4 Summary

In order to obtain innovative design configurations that meet design requirements, a conceptual design is an indispensable step. Investigating the properties of an existing design can generate new design concepts. The summaries of this chapter are as follows:

1. Through theoretical studies of motors and gear trains, new design concepts are stimulated to provide a theoretical foundation for the integrated device.
2. Via the analysis of existing designs, the design requirements and constraints

of the integrated device are summarized, thus making the integrated device achieve the desired functions.

3. The design concepts of the integrated device are obtained subject to the design requirements and constraints. In this study, the integrated design not only meets the demand of power transmission but also improves motor characteristics.



Chapter 3 Design Procedure

In this chapter, a design procedure is provided to systematically generate feasible integrated devices, along with the integrated design concept. [130]

3-1 Design procedure

The design procedure shown in Fig. 3-1 includes the following 9 steps:

- Step 1. Select one existing design to analyze the specifications and characteristics that meet design requirements. If no existing design is available, go to step 2 to list the required design specifications.
- Step 2. Summarize the design specifications of the integrated device.
- Step 3. Determine the fixed parameters of the integrated device.
- Step 4. Conceptual design of integrated devices: in this step, the creative mechanism design methodology is applied [114].
- Step 5. Detailed design of the stator and rotor of the electric motor.
- Step 6. Magnetic design of the permanent-magnet rotating machines.
- Step 7. Identification and strength analysis of gear profiles. The material properties and scales of gears are applied to a finite-element analysis (FEA), where the strength of the gear profiles is evaluated to ensure the transmission capabilities.
- Step 8. Kinematic design of gear mechanisms. Its purpose is to determine the velocity ratio and the angular velocity of the gear mechanism.
- Step 9. Arrive at feasible integrated devices.

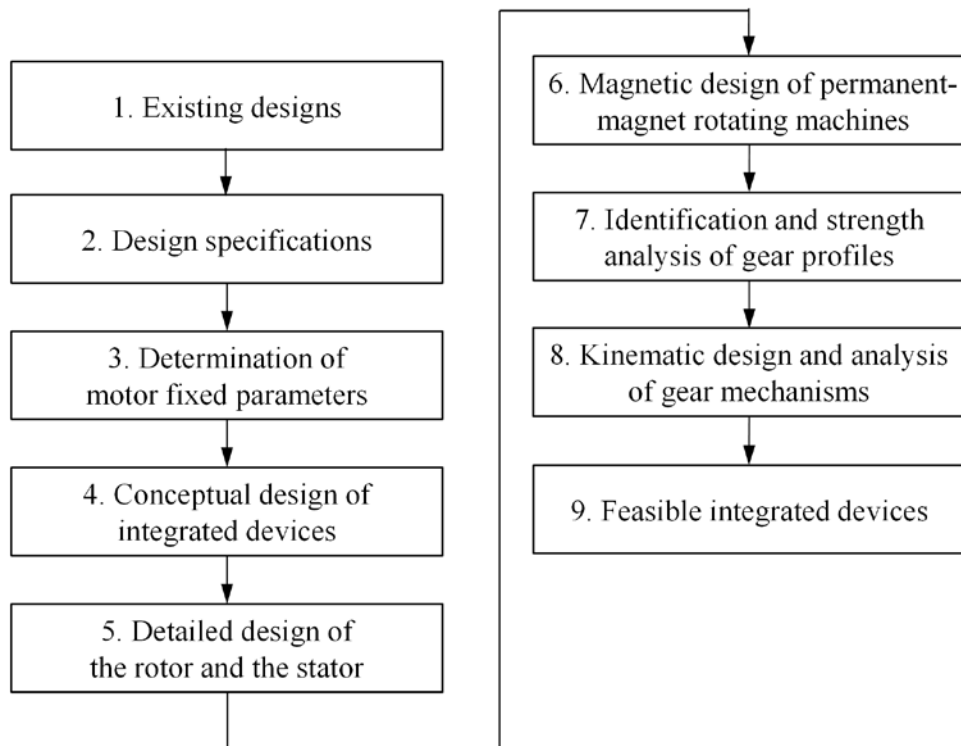


Fig. 3-1 Integrated design procedure

First of all, designers can choose one existing design to analyze the specifications and characteristics that meet the design requirements if there is one existing design to use for the integrated design procedure. If not, designers can go direct to step 2 for a totally new design, subject to the design specifications. Based on the configurations of electric motors and the kinematic structure of gear mechanisms, the feasible design concepts are generated, and fundamental theories are applied, subject to the design requirements and constraints.

The following two steps are intended to conclude the design specifications and determinate the fixed parameters of the electric motors. Designers must choose a proper type of electric motor. Table 3-1 lists the fixed parameters in this study.

Table 3-1 Fixed parameters

Parameters	Symbols
Rated speed (rpm)	ω_R
Number of phases	N_{ph}
Number of magnet poles	P
Number of armature slots	S
Air gap length (mm)	g
Radius of shaft (mm)	R_s
Inner radius of stator (mm)	R_{si}
Outer radius of stator (mm)	R_{so}
Number of coils per armature tooth (turn)	N_c
Stack length (mm)	L
Rated conduct current (A)	I
Magnet remanence (T)	B_r
Magnet relative permeability	μ
Allowed steel flux density (T)	B_a

In an integration device design, there are lot of unknown design variables. To simplify the design process, designers can choose several fixed parameters and then design the remaining variables. In the integrated device design process, it is important to define the variables. Based on the specifications in step 2, the output torque, the rated current, the magnetic materials, and the assembly spaces can be fixed or can remain the same as those in the existing design. However, it is necessary to state that the fixed parameters can be set flexibly by designers.

The fourth step is the conceptual design of the integrated devices. In this step, the creative design methodology is applied [114], and designers must conclude the design requirements and constraints to systematically generate feasible design concepts.

The fifth step is obtaining the detailed design of the stator and the rotor of

the electric motor. Based on the design requirements and constraints, a detailed design of the rotor and the stator can be obtained. By applying the material properties and scales to the finite-element analysis, the strength of gear profiles can be evaluated to ensure transmission capabilities.

It's important to analyze the influences of gear profiles implemented into the magnetic fields as well as the transmission capabilities of magnetic materials in the gear mechanisms. It has been shown that gear teeth integrated on the rotor act as dummy slots [77, 78] to effectively reduce the cogging torque and torque ripple of the motor. With the aid of the FEA, the maximum stress and displacements under the acting torque are calculated in step 6.

In step 6, a 1-D equivalent magnetic circuit method is applied as a tool that assists in the design of the magnetic field and can be used to analyze the performance of the integrated device. They can also be verified using a finite-element analysis [32, 77] to ensure that the design results concur with the desired design performance. The average flux density within the air-gap, which is expressed in terms of the magnetic material properties and motor dimensions, is obtained. The mathematic expression of the motor characteristics can be used in the optimal design process.

When the topological structure and kinematic design of the gear mechanisms are obtained in steps 7 and 8, designers can obtain feasible integrated devices. The design methods for gear trains, gear profiles, number of gear teeth, and the gear strength are also introduced. Finally, a feasible integrated device can be determined.

The design procedure is actually an iterative process. Designers must check all of the steps to comply with the listed specifications. If any step results in

unsuitable output performance, designers must go back to the previous step to revise the concept until the specification is met.

3-2 Creative design methodology

The purpose of this study is to synthesis all possible integrated devices with electric motors and gear trains to meet the design specifications, requirements, and constraints. In this procedure, Yan's creative mechanism design methodology is modified [114], and three-link and four-link gear mechanisms are chosen as part of the conceptual design.

3-2-1 Graph representations

The use of graphs on the mechanism synthesis can simplify the complex structures of mechanisms and present the topological structures and kinematic characteristics. Table 3-2 lists the graph representations of members in gear trains.

Graph representations of electric motors can simplify the integrated design procedure. The main components of an electric motor are the stator and the rotor. They can be treated as two members with a constant relative velocity that keep the motor rotating. Theoretically, the rotor and the stator can be assigned as moving members. Graphic representations of motors are provided in Table 3-3.

For some cases with two motors working as the inputs, i.e. the design has two degrees of freedom, and the stators are on the same link, where there are two situations: the rotors are coaxial and nonaxial, as shown in Table 3-4.

Moreover, the combinations of the types of rotors/stators and the types of armatures and air-gaps are represented graphically in Table 3-5.

Table 3-2 Graphic representations of members of gear trains



Representation	Member
---	Gear pair
—	Revolute pair
	Revolute pair (triangle)
	Revolute pair (quadrangle)
○	Moving link
⊙	Fixed link
→○	Moving internal gear
---○	Moving external gear
→⊙	Fixed internal gear
---⊙	Fixed external gear

Table 3-3 Graph representations of members in motors

Representation	Member
—	Revolute pair
□	Rotor
△	Stator
△—□	Fixed and moving members
□—□	Relative moving members

Table 3-4 Graph representations of members with two inputs


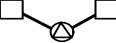
Representation	Member
	Coaxial
	Nonaxial

Table 3-5 Graphic representations of armature direction and air-gap direction

Armature direction	Air-gap direction		
	Radial		Axial
Radial	<p>I-Cr-Gr</p> <p>Cr-Gr</p>	<p>E-Cr-Gr</p> <p>Cr-Gr</p>	<p>A-Cr-Ga</p> <p>Cr-Ga</p>
Axial	<p>I-Ca-Gr</p> <p>Ca-Gr</p>	<p>E-Ca-Gr</p> <p>Ca-Gr</p>	<p>A-Ca-Ga</p> <p>Ca-Ga</p>

Permanent magnets
 Coil winding
 Armature

3-2-2 Creative design methodology

The conceptual design of integrated devices must be resolved to meet the design specifications. In this step, designers must complete the design requirements and constraints for the design concept. To generate design concepts systematically, the creative design methodology is applied. The design procedure is shown in Fig. 3-2. Through analyzing the structure of the target device mechanism, the structural characteristics are derived, including the number of members and joints in the device. The second step is to identify the atlas of generalized chains subject to arriving at the structural characteristics by applying the number synthesis algorithm. Assigning specific types of members and joints in the atlas of generalized chains, subject to the required design constraints, is called specialization. The last step is to obtain all feasible designs

from the specialized chains with particular identities, according to the motion and functional requirements of the device.

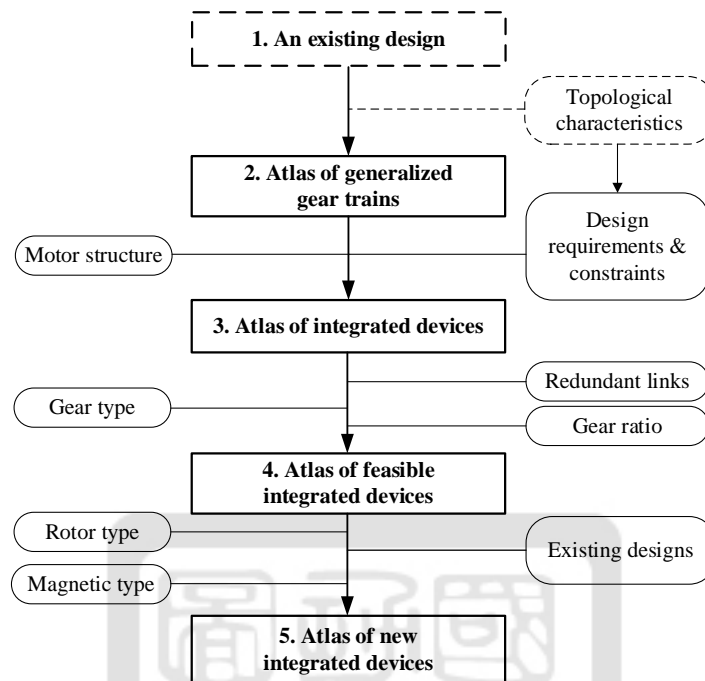


Fig. 3-2 Creative design methodology

Step 1: Analyze the existing design

First of all, designers can choose an existing design to arrive at the design requirements and constraints. If there is no existing design, designers can go direct to step 2 for a totally new design that conforms with the design specifications. For an existing AC motor, there are no design requirements, for which the design constraints are listed as follows:

- C1. The output link must not be the fixed link.
- C2. The fixed link and the output link must be connected by a revolute pair or polygonal revolute pair.
- C3. The stator and the rotor must not be assigned to the fixed link and the output link at the same time.

- C4. The stator and the rotor must be connected by a revolute pair or a polygonal revolute pair.
- C5. The stator should be assigned as the fixed link.
- C6. Only internal rotors are used.
- C7. The number of teeth should be integer multiple of the number of slots. The teeth root should be removed as the slot openings to wind the coil windings for automatic manufacturing purpose.
- C8. The radius of the addendum/dedendum circle of the gear profiles should be the same as or close to the radius of the rotor/stator to maintain the radius of the air-gap.
- C9. The widely used AGMA standard 20° pressure angle involute spur gear profile is used.
- C10. The commonly used JIS B 1701 gear modulus is selected.

Step 2: Atlas of feasible gear trains

In this step, all the atlases of gear trains that meet the design requirements and constraints are synthesized. Each member is labeled, and the fixed link and output link for the gear trains are assigned. To synthesize all possible atlases of gear trains, the fixed link and output link must be assigned in the first step. Based on design constraints C1 and C2, there is only 1 graph that meets the design constraints for a three-link gear train and 3 graphs that meet the design constraints for a four-link gear train, as shown in Fig. 3-3. After labeling each member and assigning the fixed link and output link, there are 2 atlases of feasible three-link gear trains, as shown in Fig. 3-4.

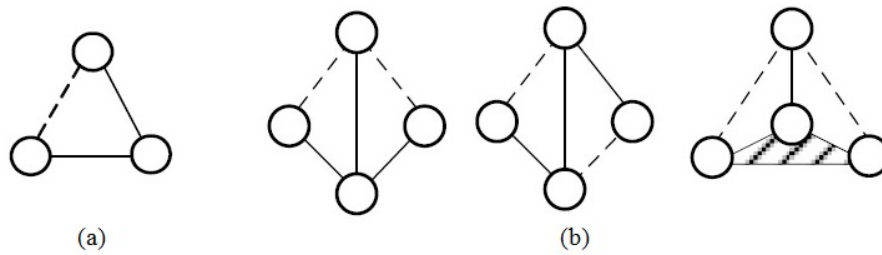


Fig. 3-3 Graphs of (a) three-link and (b) four-link gear trains

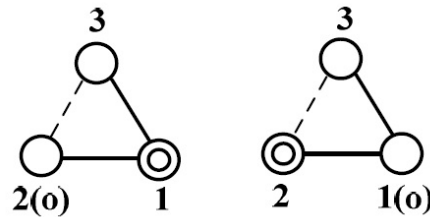


Fig. 3-4 Atlas of feasible three-link gear trains

Step 3: Atlas of integrated devices

In this step, the rotor and the stator of the motor are assigned to obtain the atlas of the integrated design that complies with the design requirements and constraints.

Based on the characteristics of AC motors, the design constraints of the rotor and stator assignment are C3 and C4. An AC induction motor is an asynchronous motor, so the electric current in the rotor must produce torque that is obtained by electromagnetic induction from the magnetic field of the stator winding. The rotor and the stator have a constant relative velocity to keep the motor rotating. Theoretically, the rotor and the stator can be assigned as moving members, and then the output angular velocity will be defined by their relative velocity. To avoid any unpredictable effects and to simplify the design, constraint C5 should be considered. There is only one result for the three-link gear train that meets the design constraints, as shown in Fig. 3-5.

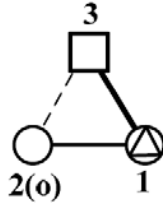


Fig. 3-5 Atlas of feasible three-link integrated device

Step 4: Atlas of feasible integrated devices

In this step, all the atlases of integrated design are analyzed to remove the redundant links, and the internal gears are assigned to analyze the gear ratio. By removing all the incompatible integrated devices, the atlases of feasible integrated devices are obtained. For three-link gear trains, there is only one fundamental loop with three members. There are no redundant links in three-link gear trains.

Step 5: Atlas of new integrated devices

By assigning the type of rotor and the type of armature, along with removing the existing designs, the atlas of new integrated devices is obtained. In this study, most AC induction motors use internal rotors, and this yields the constraint C6.

By following the design procedure, the three-link gear mechanism results in one feasible new design concept, as shown in Fig. 3-6 (a), and the four-link gear mechanism has six feasible new design concepts, as shown in Fig. 3-6 (b)-(g).

3-3 Summary

For the integrated device, the integrated design procedure is important. A summary of the procedure is as follows:

1. A design procedure is introduced to generate integrated devices systematically, along with the integrated design concept.

- The use of graphs for the mechanism synthesis can simplify the complex structures of mechanisms and present the topological structures and kinematic characteristics clearly.

Yan's creative mechanism design methodology is applied in this chapter. The three-link gear mechanism results in one feasible new design concept, and the four-link gear mechanism results in six feasible new design concepts.

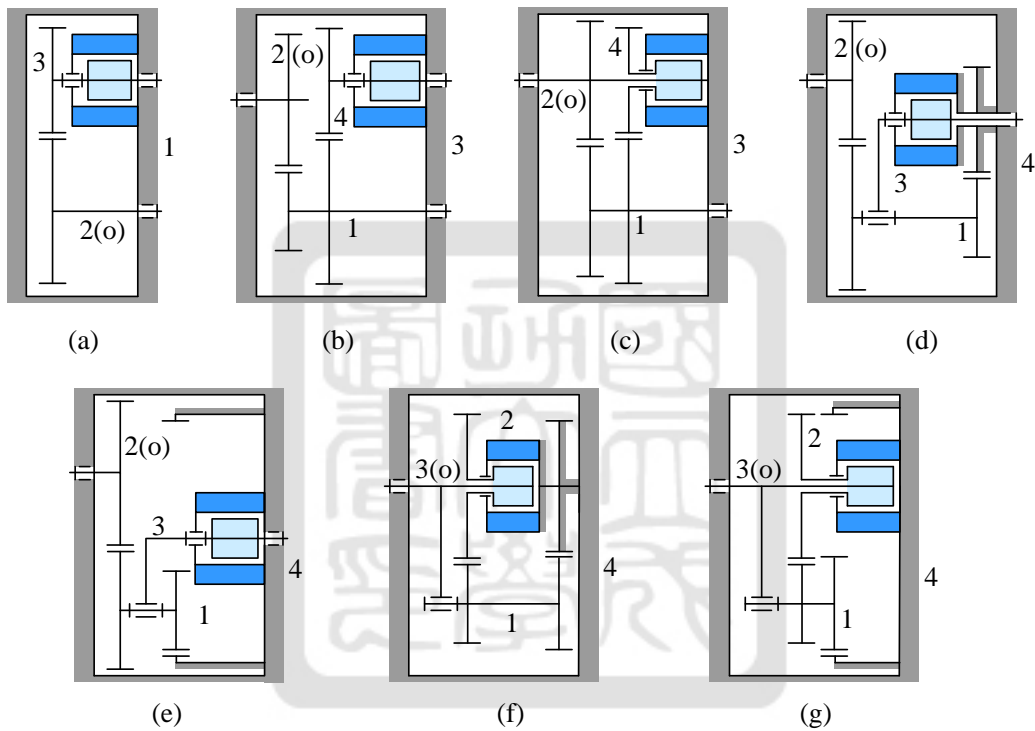


Fig. 3-6 Atlases of feasible integrated AC induction motor with three-link and four-link gear trains

Chapter 4 Magnetostatics Analysis

In order to predict the motor performance before fabricating a physical prototype, the magnetic field analysis of an electric motor is a major concern for motor designers. In general, there are two major approaches for the magnetic field approximations: the equivalent magnetic circuit analysis and the FEA [29]. There are two typical types of equivalent magnetic analysis methods, including one-dimensional (1-D) [32] and two-dimensional (2-D) [131, 132] methods. The 1-D equivalent magnetic circuit method with lumped circuit parameters is a suitable, fast tool for the preliminary design of an electric motor. However, it is not possible to analytically express the distribution of the flux density within the air-gap. The 2-D equivalent magnetic method is based on a 2-D magnetic field and is used to investigate the influence of design parameters, including the direction of magnetization, the number of magnet poles, the magnet arc angle, etc., on the amount of magnetic flux and the flux density distribution, which affects the electromagnetic torque of an electric motor. In addition to analytical techniques, numerical methods for magnetic field computation, such as the finite-difference method, the boundary-element method, and the finite-element method, also provide accurate means of determining the flux density distribution.

4-1 1-D method

The 1-D equivalent magnetic circuit method is an analytical technique used to predict the open-circuit magnetostatic field of electric motors. The magnetic model can account for the leakage flux paths around the magnets [32].

A linear translational model of a DC commutator motor is shown in Fig.

4-1. By observing the model, it can be seen that all the fluxes are provided by the permanent magnets. The fluxes can be divided into the air gap flux Φ_g and the leakage flux. The air gap flux Φ_g is the main source for an electric motor. The fluxes go through the air gap and connect to the coil windings to provide the main magnetic force for the electromagnetic reaction. The other fluxes that don't connect with the coil windings are leakage fluxes. In general, the leakage fluxes can be divided into a magnet to rotor flux Φ_{mr} and a magnet to magnet flux Φ_{mm} . The leakage flux is one of the important specifications by which to predict the average flux density and the output torque of electric motors.

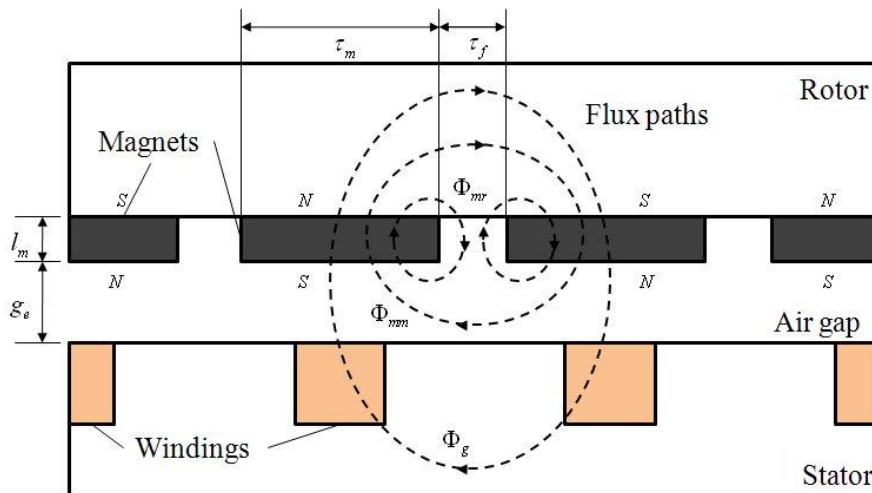


Fig. 4-1 Topology of the linear translational motor

To simplify the analytical model, there are three assumptions as follows:

1. There is no saturation in the steel region.
2. The magnetic intensity produced by the windings is negligible.
3. The stator and rotor back iron have infinite permeability.

Based on the concept of the Norton equivalent circuit, the permanent magnet can be treated as a power source parallel to an inner reluctant. Similar to the Ohm's law in an electric circuit analysis, the equivalent magnetic circuit

model of a PM electric motor is shown in Fig. 4-2. This equivalent magnetic circuit is combined with two 1/2 PM models, one 1/2 rotor, and the stator. The $\Phi_r/2$ is the flux source; the $\Phi_g/2$ is the air-gap flux; the $\Phi_m/2$ is the flux that goes through the magnet; the R_r and R_s are the reluctance of the rotor and stator; R_g is the air gap reluctance; R_{mo} is the inner reluctance of the magnet, and R_{mm} and R_{mr} are the reluctance model of magnet to rotor flux and magnet to magnet flux, respectively.

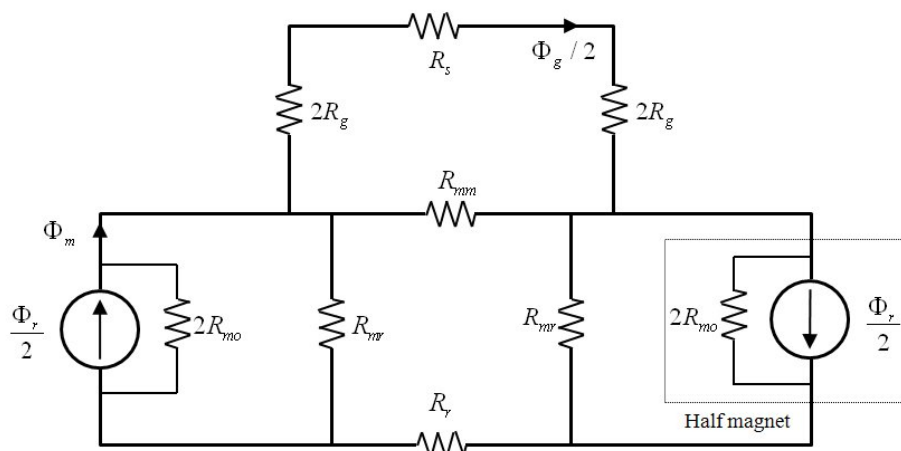


Fig. 4-2 Equivalent magnetic circuit

The R_r and R_s equal 0 by the assumption, and the circuit can be simplified as shown in Fig 4-3. By applying the concept of the Norton equivalent, the simplest circuit can be determined as shown in Fig. 4-4.

The R_m can be derived as:

$$R_m = \frac{R_{mo}}{1 + 2\eta + 4\lambda} \quad (4-1)$$

where

$$\eta = R_{mo} / R_{mr} \quad (4-2)$$

$$\lambda = R_{mo} / R_{mm} \quad (4-3)$$

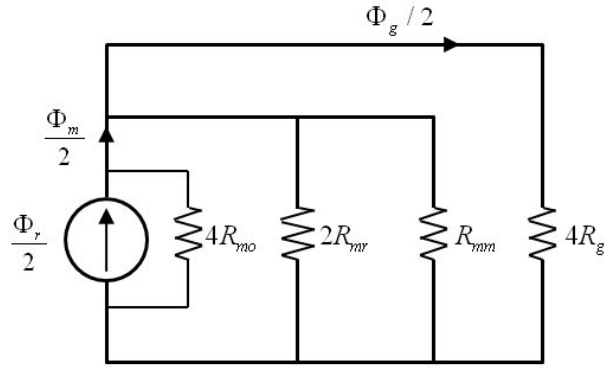


Fig. 4-3 Simplified circuit

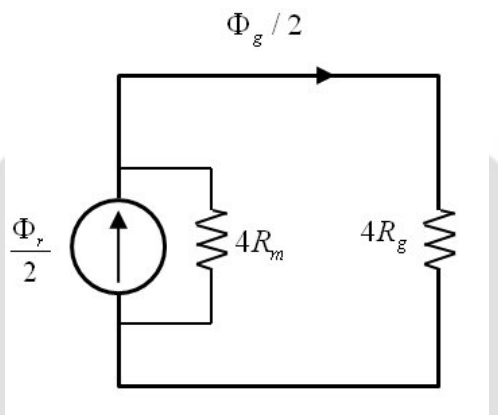


Fig. 4-4 Simplest circuit

The relationship of Φ_g is:

$$\Phi_g = \frac{R_m \Phi_r}{R_m + R_g} = \frac{R_{mo}}{R_{mo} + R_g (1 + 2\eta + 4\lambda)} \Phi_r \quad (4-4)$$

Φ_m is :

$$\Phi_m = \frac{R_{mo} + R_g (2\eta + 4\lambda)}{R_{mo} + R_g (1 + 2\eta + 4\lambda)} \Phi_r \quad (4-5)$$

and Φ_r is :

$$\Phi_r = A_m B_r \quad (4-6)$$

where A_m is the cross-section area the flux passed, and B_r is the residual flux density.

By taking the air-gap flux, magnet-to-magnet leakage flux, and magnet-to-stator leakage flux into account, the equivalent magnetic circuit of the flux loop can be set up, and the average flux density within the air-gap $B_{g,ave}$ is obtained [32] as:

$$B_{g,ave} = \frac{A_m / A_g}{1 + (R_g / R_{mo})(1 + 2\eta + 4\lambda)} B_r \quad (4-7)$$

where A_m / A_g is the ratio of the flux passing area of the magnet to that of the air-gap; B_r is the magnet residual flux density; R_g is the reluctance of a magnet; η is the reluctance ratio of a magnet pole to the magnet-to-rotor leakage flux, and λ is the reluctance ratio of a magnet pole to the magnet-to-magnet leakage flux. These factors can be further expressed in terms of magnetic material properties and motor dimensions as follows:

$$A_m = \tau_m L \quad (4-8)$$

$$A_g = (\tau_m + \tau_f) L \quad (4-9)$$

$$R_{mo} = \frac{l_m}{\mu_0 \mu_r A_m} \quad (4-10)$$

$$\eta = \frac{l_m}{\mu_r \pi \tau_m} \ln \left[1 + \frac{\pi \min(g_e, \tau_f / 2)}{l_m} \right] \quad (4-11)$$

$$\lambda = \frac{l_m}{\mu_0 \pi \tau_m} \ln \left(1 + \frac{\pi g_e}{\tau_f} \right) \quad (4-12)$$

$$g_e = K_c g \quad (4-13)$$

where L is the stack length; τ_m is the magnet width; τ_f is the length of two magnets; l_m is the magnet height; μ_r is the relative permeability of the magnet;

K_c is the Carter's coefficient [29], which is obtained to model the permeance in the presence of slotting and gear-teeth, and g_e is the effective air-gap length. Substituting Eqs. (4-8)-(4-13) into Eq.(4-7), the average air-gap flux density of a DC commutator motor can be obtained.

Fig. 4-5 shows the cross-section and geometric parameters of an existing DC commutator motor as the benchmark in this study [20]. The corresponding values of the magnet properties and geometrical dimensions are listed in Table 3-1, and the analytical results based on the 1-D equivalent magnetic circuit method are listed in Table 3-2. The AGMA stub gear-teeth with a 20° pressure angle and 56 teeth are integrated uniformly on the rotor. The result shows that by applying the Carter's coefficient to obtain the effective air-gap, designers can more easily analyze the effect of gear-teeth on the average air-gap flux density.

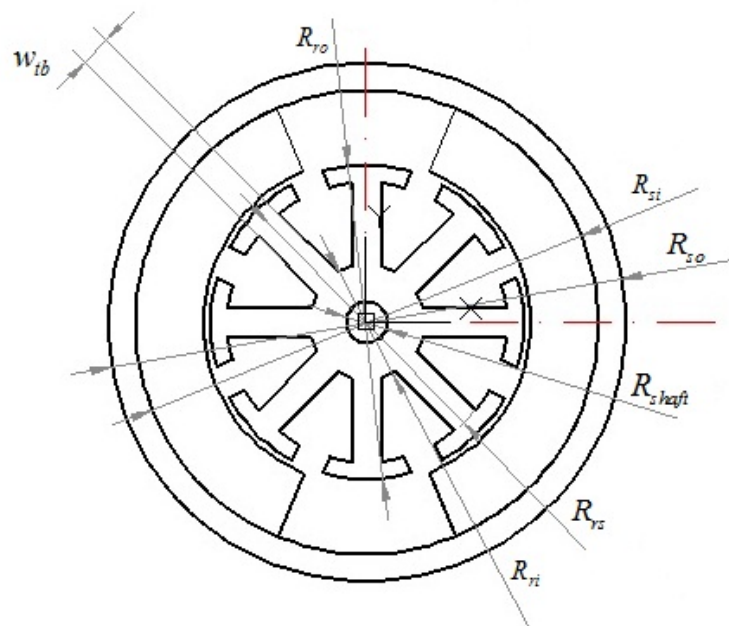


Fig. 4-5 Geometric parameters of a DC commutator motor

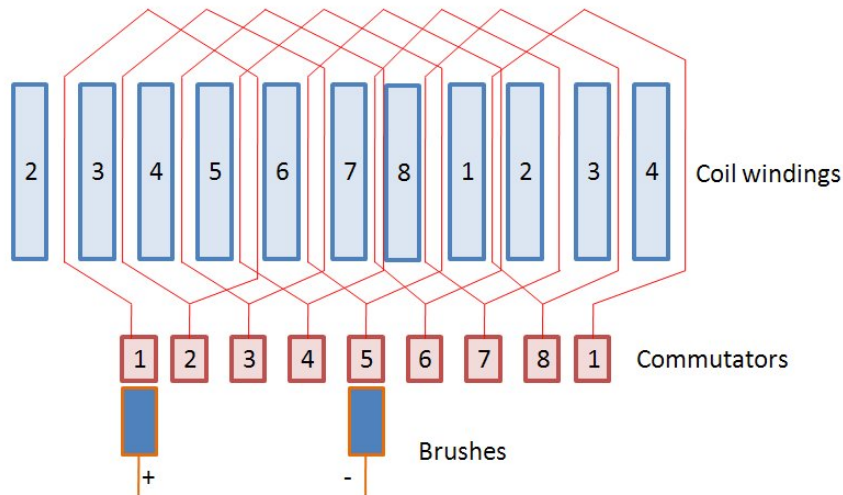


Fig. 4-6 Linear translation of coil windings

Table 4-1 Specifications of a DC commutator motor

Items	Symbols	Values
Number of phases	N_{ph}	1
Number of magnet poles	P	2
Number of armature slots	S	8
Air gap length (mm)	g	0.5
Radius of shaft (mm)	R_{shaft}	1.5
Inner radius of rotor (mm)	R_{ri}	4.25
Radius of rotor shoe (mm)	R_{rs}	10.25
Outer radius of rotor (mm)	R_{ro}	11.5
Inner radius of stator (mm)	R_{si}	17
Outer radius of stator (mm)	R_{so}	19
Tooth width of rotor (mm)	W_{tb}	2.2
Number of coils per armature tooth (turn)	N_c	60
Stack length (mm)	L	16
Rated conduct current (A)	I	2
Remanence (T)	B_r	0.12
Relative permeability	μ_r	0.9645
Magnet thickness (mm)	l_m	5
Magnet arc(degree)	θ_m	135

Table 4-2 Results of the 1-D equivalent magnetic circuit method

Items	Symbols	Existing	Gear-teeth
Magnet width (mm)	τ_m	68.330	
Length of two adjacent magnets (mm)	τ_f	22.777	
Effective air gap length (mm)	g_e	0.951	1.7
Reluctance ratio of a magnet pole to the magnet-to-stator leakage flux	η	0.0113	0.0172
Reluctance ratio of a magnet pole to the magnet-to-magnet leakage flux	λ	0.003	0.005
Average magnetic flux densities within the air gap (T)	$B_{g,ave}(T)$	0.076	0.068

4-2 2-D method

For the 2-D equivalent magnetic circuit method, a DC commutator motor is separated into a number of nodes to form an equivalent circuit. Since the magnetostatic field generated by permanent magnets is symmetrical, motor designers do not need to analyze the entire magnetic field of an electric motor [132]. However, if there are obvious slot structures on the motor rotor, especially if the slot-pole ratio is a fraction, designers must analyze at least one pole pair in order to avoid possible errors. In general, a DC commutator motor can be divided into five main parts in the radial direction: the rotor irons, the rotor teeth, the air-gap, the permanent magnets, and the stator irons. Then, the motor is divided into N parts in the circumferential direction, i.e., there are $5N$ nodes in the motor, as shown in Fig. 4-7. The accuracy of the simulation result is directly proportional to the number of nodes.

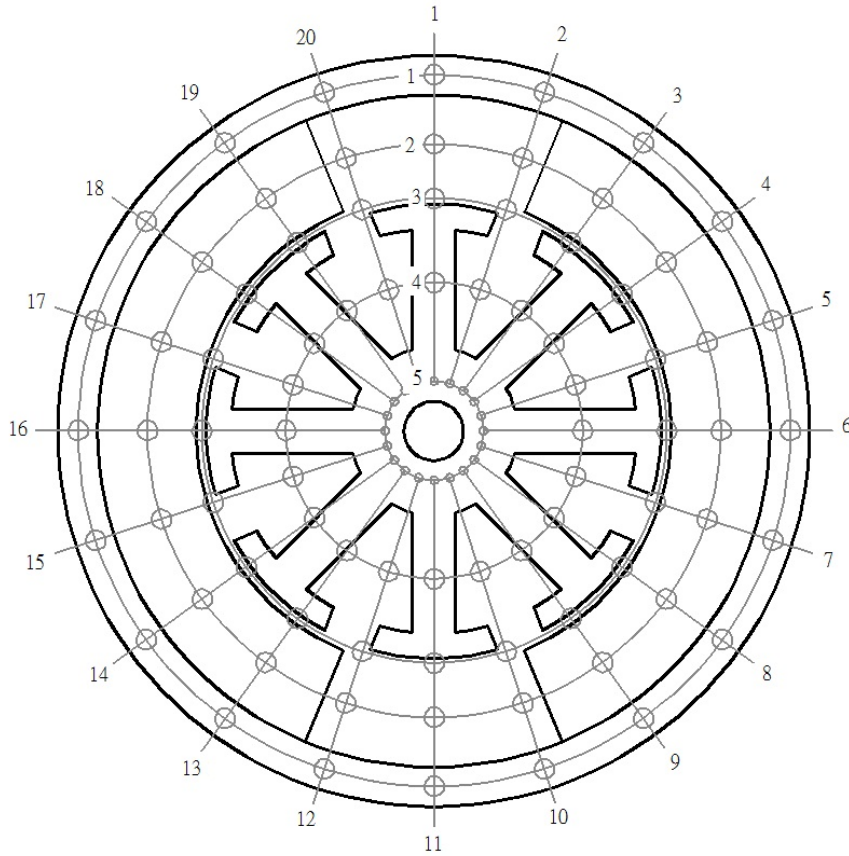


Fig. 4-7 Division of a DC commutator motor

In the analysis process, the motor scales and the characteristics of magnetic materials should be specified in order to obtain the permeance and magnetomotive force of each node. Basically, the permeance is the reciprocal of reluctance, which can be expressed as:

$$R = \frac{l}{\mu A} = \frac{l}{\mu_0 \mu_r A} \quad (4-14)$$

where μ is the permeability of the magnetic material; μ_0 is the permeability of vacuum; μ_r is the relative permeability of the magnetic material; l is the length of the magnetic material, and A is the cross section of the magnetic material. The permeance in circumferential direction, Q , and radial direction, P , as shown in Fig. 4-8 can be expressed as [110]:

$$dQ = \frac{\mu L dx}{(r_i + x)\theta_m} \quad (4-15)$$

$$Q = \int_{r_i}^{r_i+l_m} dQ = \frac{\mu_r \mu_0 L}{\theta_m} \int_{r_i}^{r_i+l_m} \frac{1}{r_i + x} dx = \frac{\mu_r \mu_0 L}{\theta_m} \ln\left(1 + \frac{l_m}{r_i}\right) \quad (4-16)$$

$$dR = \frac{dl}{\mu A} = \frac{dr}{\mu r \theta_m L} \quad (4-17)$$

$$R = \int_{r_i}^{r_i+l_m} dR = \int_{r_i}^{r_i+l_m} \frac{dr}{\mu_r \mu_0 \theta_m L r} = \frac{\ln\left(1 + \frac{l_m}{r_i}\right)}{\mu_r \mu_0 \theta_m L} \quad (4-18)$$

$$P = \frac{1}{R} = \frac{\mu_r \mu_0 \theta_m L}{\ln\left(1 + \frac{l_m}{r_i}\right)} \quad (4-19)$$

where θ_m is the arc angle of the magnetic material; l_m is the thickness of the magnetic material; r_i is the inner radius of the magnetic material, and L is the length of the magnet in the axial direction.

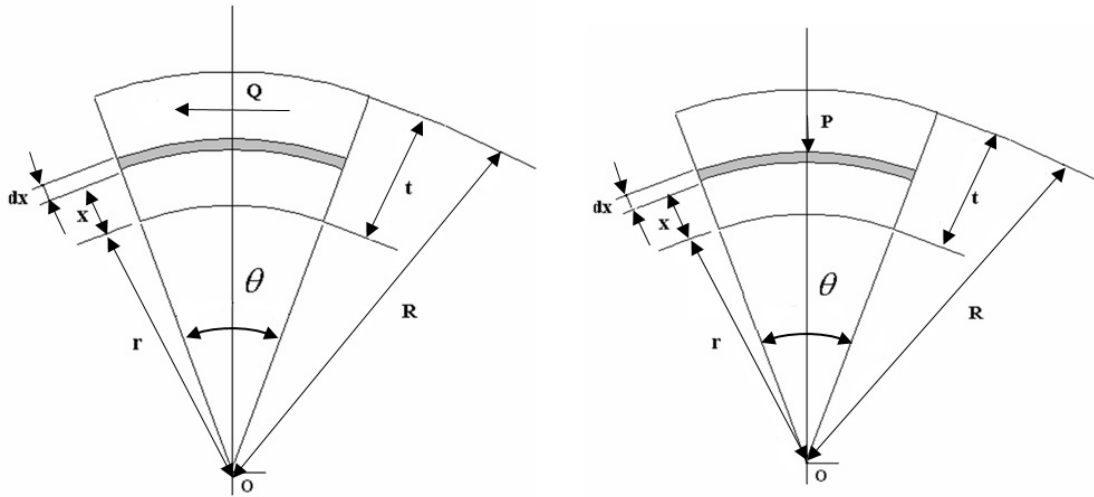


Fig. 4-8 The permeance in the circumferential and radial directions

The magnetomotive force E of a linear demagnetization magnet is:

$$E = H_c \cdot l = \frac{B_r}{\mu} \cdot l \quad (4-20)$$

where H_c is the coercivity of the magnet. In addition, the magnetomotive force in the radial direction, $E_{i,j}$, and the circumferential direction, $F_{i,j}$, can be expressed as:

$$E_{i,j} = \frac{l_m}{2} \cdot [H_c \cdot \cos \theta_i] \quad (4-21)$$

$$F_{i,j} = l_f \cdot [H_c \cdot \sin \theta_i] \quad (4-22)$$

Since the sum of magnetic fluxes flowing into a node is equal to the sum of magnetic fluxes flowing out of that node, as shown in Fig. 4-9, the following equations can be obtained:

$$\phi_{i-1,j} + \phi_{i+1,j} + \phi_{i,j-1} + \phi_{i,j+1} = 0 \quad (4-23)$$

$$\phi_{i-1,j} = Q_{i-1,j} \cdot (U_{i-1,j} - U_{i,j} + F_{i-1,j}) \quad (4-24)$$

$$\phi_{i+1,j} = Q_{i,j} \cdot (U_{i+1,j} - U_{i,j} - F_{i,j}) \quad (4-25)$$

$$\phi_{i,j-1} = P_{i,j-1} \cdot (U_{i,j-1} - U_{i,j} - E_{i,j-1}) \quad (4-26)$$

$$\phi_{i,j+1} = P_{i,j} \cdot (U_{i,j+1} - U_{i,j} + E_{i,j}) \quad (4-27)$$

where $\phi_{i,j}$ is the flux flowing into the node, and $U_{i,j}$ presents the magnetic potential of a node. Substituting Eqs.(4-24)-(4-27) into Eq.(4-23) yields:

$$Q_{i-1,j} \cdot (U_{i-1,j} - U_{i,j} + F_{i-1,j}) + Q_{i,j} \cdot (U_{i+1,j} - U_{i,j} - F_{i,j}) + P_{i,j-1} \cdot (U_{i,j-1} - U_{i,j} - E_{i,j-1}) + P_{i,j} \cdot (U_{i,j+1} - U_{i,j} + E_{i,j}) = 0 \quad (4-28)$$

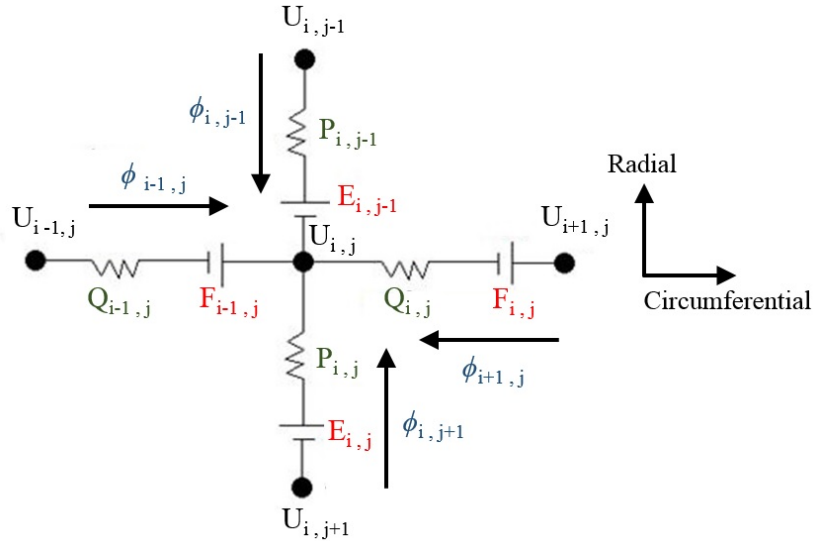


Fig. 4-9 The concept of fluxes flowing into a node

From Eq.(4-28), designers can obtain 5N linear equations with 5N unknowns of the magnetic potential. For example, Fig. 4-10 shows a 3x3 equivalent magnetic circuit net with only magnetomotive force in the radial direction, which means the magnets are axially magnetized.

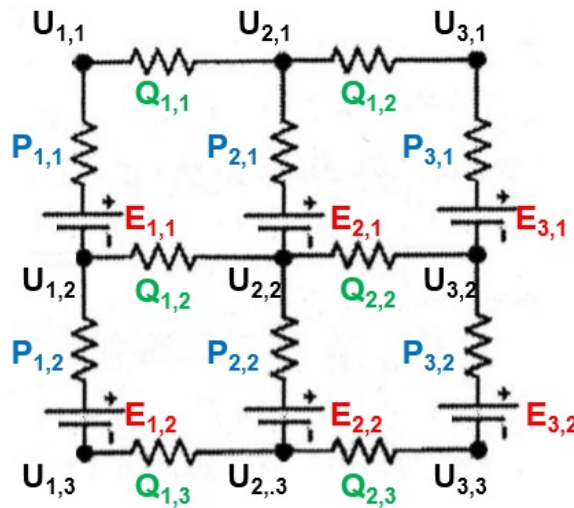


Fig. 4-10 A 3x3 equivalent magnetic circuit net

By applying Eq.(4-28) into the model, the linear equation can be obtained in the form $AX=B$, and the coefficient matrices can be written as:

$$X = \begin{bmatrix} U_{1,1} \\ U_{1,2} \\ U_{1,3} \\ U_{2,1} \\ U_{2,2} \\ U_{2,3} \\ U_{3,1} \\ U_{3,2} \\ U_{3,3} \end{bmatrix}, B = \begin{bmatrix} -P_{1,1}E_{1,1} \\ P_{1,1}E_{1,1} - P_{1,2}E_{1,2} \\ P_{1,2}E_{1,2} \\ -P_{2,1}E_{2,1} \\ P_{2,1}E_{2,1} - P_{2,2}E_{2,2} \\ -P_{2,2}E_{2,2} \\ -P_{3,1}E_{3,1} \\ P_{3,1}E_{3,1} - P_{3,2}E_{3,2} \\ -P_{3,2}E_{3,2} \end{bmatrix} \quad (4-29)$$

$$A = \begin{bmatrix} -P_{1,1} - Q_{1,1} & P_{1,1} & 0 & Q_{1,1} & 0 & 0 & 0 & 0 & 0 & 0 \\ P_{1,1} & -P_{1,1} - P_{1,2} & P_{1,2} & 0 & Q_{1,2} & 0 & 0 & 0 & 0 & 0 \\ 0 & P_{1,2} & -P_{1,2} - Q_{1,3} & 0 & 0 & Q_{1,3} & 0 & 0 & 0 & 0 \\ Q_{1,1} & 0 & 0 & -Q_{1,1} - Q_{2,1} & P_{2,1} & 0 & Q_{2,1} & 0 & 0 & 0 \\ 0 & Q_{1,2} & 0 & P_{2,1} & -Q_{1,2} - P_{2,1} & P_{2,2} & 0 & Q_{2,2} & 0 & 0 \\ 0 & 0 & Q_{1,3} & 0 & P_{2,2} & -Q_{1,3} - P_{2,2} & 0 & 0 & 0 & Q_{2,3} \\ 0 & 0 & 0 & Q_{2,1} & 0 & -Q_{2,3} & -Q_{2,1} - P_{3,1} & P_{3,1} & 0 & 0 \\ 0 & 0 & 0 & 0 & Q_{2,2} & 0 & P_{3,1} & -Q_{2,2} - P_{3,1} & P_{3,2} & 0 \\ 0 & 0 & 0 & 0 & 0 & Q_{2,3} & 0 & -P_{3,2} & P_{3,2} & -Q_{2,3} - P_{3,2} \end{bmatrix} \quad (4-30)$$

where the X matrix represents the unknown magnetic potentials of each node; the B matrix represents the relationship of magnetomotive force and permeance between each node, and the A matrix represents the permeance relationship between the nodes. The general form of Eq.(4-28) can be written as:

$$X = \begin{bmatrix} U_{1,1} \\ U_{1,2} \\ \vdots \\ U_{i,j-1} \\ U_{i,j} \end{bmatrix}, B = \begin{bmatrix} -P_{1,1}E_{1,1} \\ \vdots \\ -P_{i,j-2}E_{i,j-2} \\ P_{i,j-2}E_{i,j-2} - P_{i,j-1}E_{i,j-1} \\ P_{i,j-1}E_{i,j-1} \end{bmatrix} \quad (4-31)$$

By observing Eq.(4-30), matrix A is a symmetric matrix. The upper triangle and lower triangle elements are the circumferential and radial direction permeance positions related to all the nodes. The summation of each row/column is equal to zero, which represents the Kirchoff's circuit law, and the diagonal elements can be obtained. The general form of matrix A depends on the main parts separated by designers. In this study, Carter's coefficient [29] is applied to model the permeance in the presence of a slot and gear-teeth space.

By solving the linear equations of the model, designers can obtain the magnetic potentials of all the nodes. Substituting all the magnetic potentials into Eqs.(4-24)-(4-27), the magnetic flux in any node and the flux density at any region can be determined, as shown in Fig. 4-11. In this case, the number of nodes is set at 6000, and the convergence is verified.

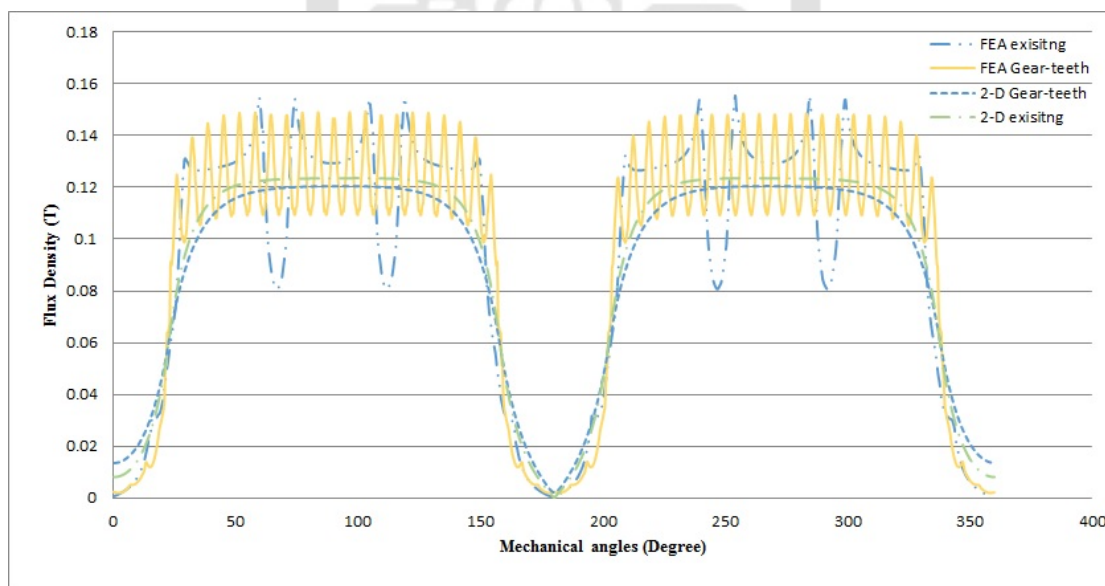


Fig. 4-11 Flux density comparison of the FEA result and the 2-D method

4-3 FEA method

The finite-element analysis method is widely employed not only for a variety of physical problems but also in the simulation of electromagnetic field

analyses. There are a number of related software packages that can be used: Ansys/Maxwell, Flux, IES, Magnet, etc. These software packages allow motor designers to build a motor through a simple model of the electromagnetic field by setting the parameters. Moreover, the desired physical quantities with a specific level of accuracy can be obtained without understanding the FEA method or electromagnetic theory. The principle of the FEA method is to cut a continuous physical field into many small elements with meshes and to provide an approximate solution for each mesh. Finally, the result is calculated by superposition. In order to get a more accurate result, the number of meshes in the physical field is required. However, a greater number of meshes leads to a slower solution speed. This is a shortcoming of the FEA method.

ANSYS/Maxwell is employed in this study. This electromagnetic field simulation software is used for engineering tasks related to designing and analyzing a 2-D or 3-D electromagnetic field, which contain a number of models, including magnetostatic, transient, eddy current, etc. To solve the problem of a magnetostatic field with a variety of sources, the magnetostatic analysis model is applied in order to obtain important physical quantities, such as magnetic flux, flux densities, output torque, etc. In the case of an axisymmetric motor, the 2-D magnetic field is considered.

The main concept of solving the magnetostatic field according to Ampère's law is:

$$\nabla \times \vec{H} = \vec{J} \quad (4-32)$$

where \vec{J} is the current density, and \vec{H} is the magnetic field intensity. While $\vec{H} = \vec{B} / \mu_r \mu_0$, after substituting the value, Eq. (4-29) can be rewritten as:

$$\nabla \times \frac{\vec{B}}{\mu_r \mu_0} = \vec{J} \quad (4-33)$$

where \vec{B} is the magnetic flux density; μ_0 is the permeability of free space, and μ_r is the relative permeability of the material. Furthermore, Ampère's law implies that:

$$\nabla \cdot \vec{B} = 0 \quad (4-34)$$

Therefore, the basic equation can be derived as follows after substituting the value $\vec{B} = \nabla \times \vec{A}_p$ to Eq. (4-32):

$$\nabla \times \frac{\nabla \times \vec{A}_p}{\mu_r \mu_0} = \vec{J} \quad (4-35)$$

where \vec{A}_p is the magnetic potential energy. The magnetic flux and flux densities can be obtained by solving the above equations.

Fig. 4-12 shows the mesh model with the specifications of a DC commutator motor, as listed in Table 4-1. In addition, the silicon steel is type 50CS1300 made by the China Steel Corporation, for which the B-H curve is shown in Fig. 4-13 [133].

Fig. 4-14 shows a simulation result of flux linkage, where the cycles are 360° , and the phase difference of each set of the coil is 45° . Fig. 4-15 shows the first derivative of the flux linkage waveforms, which means that a change occurred in the amount of flux linkage at different rotor positions, where the cycles are also 360° .

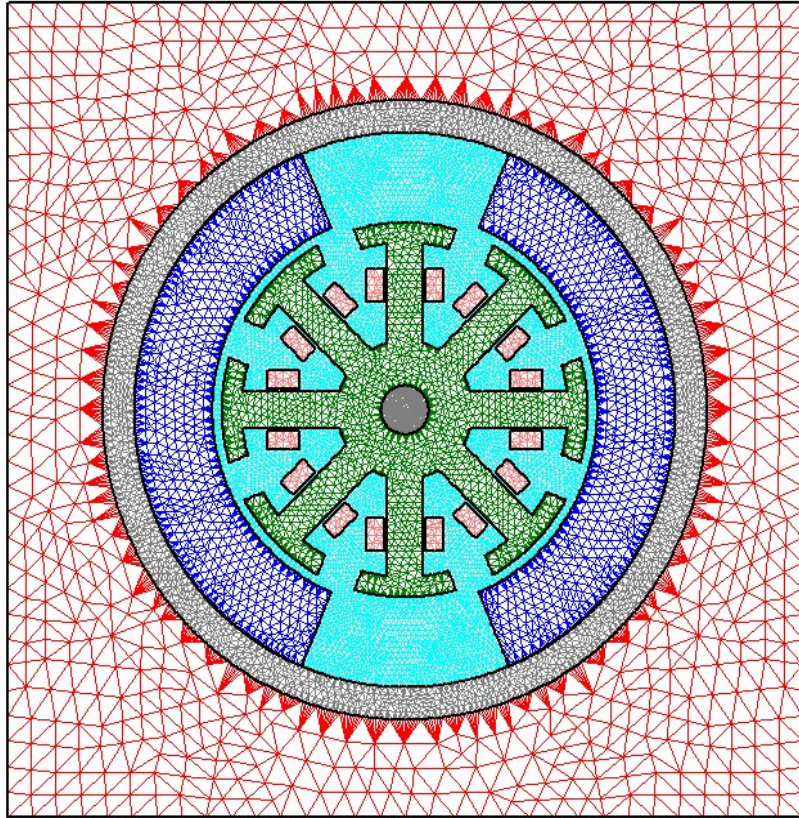


Fig. 4-12 Mesh model

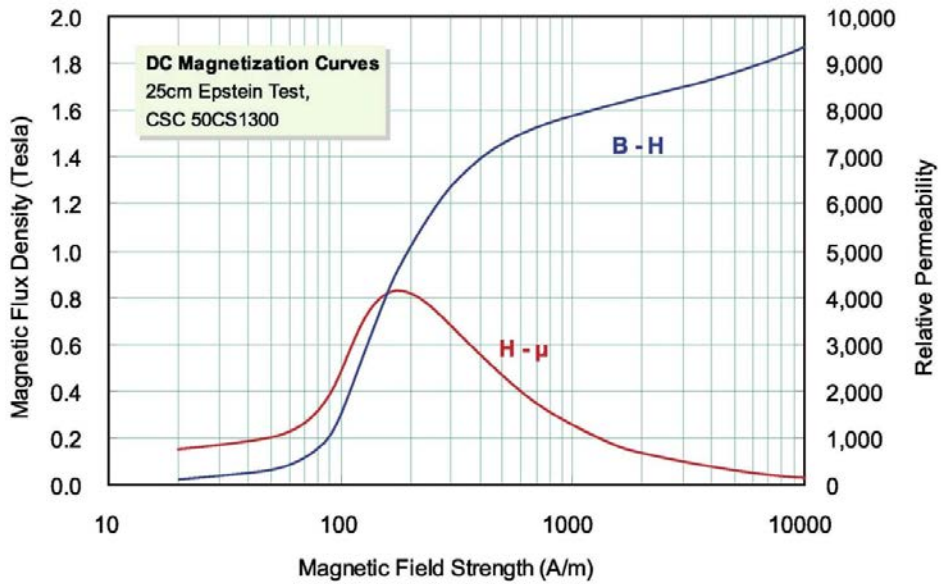


Fig. 4-13 B-H curve of silicon steel type 50CS1300 [133]

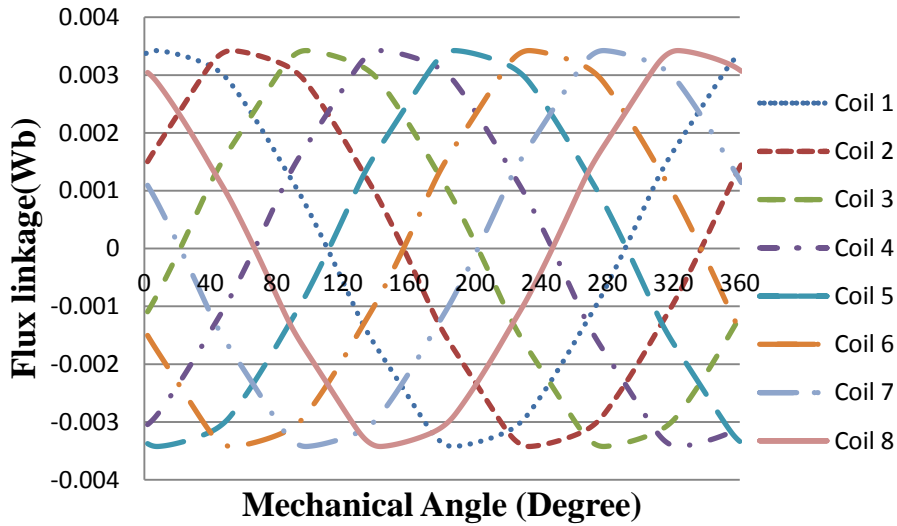


Fig. 4-14 Flux linkage result

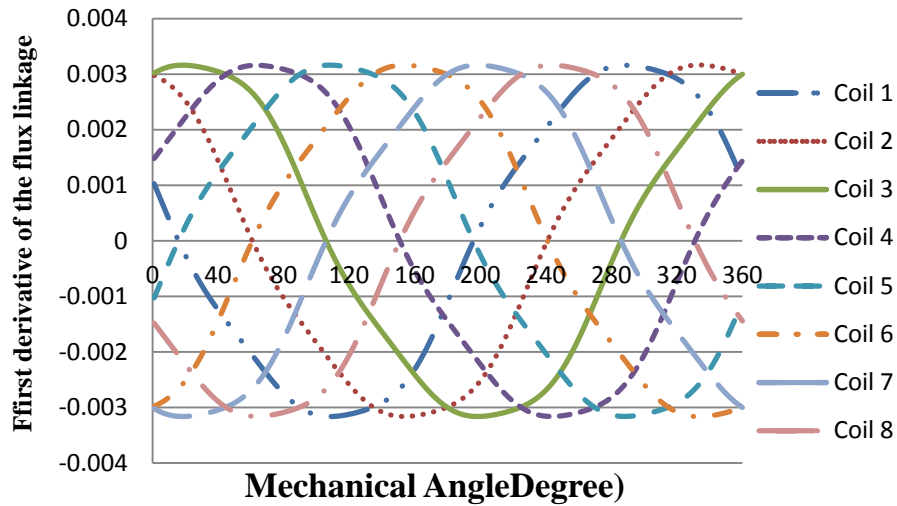


Fig. 4-15 The first derivative of the flux linkage result

Fig. 4-16 shows the magnetic flux density distribution of the existing motor, which reveals the maximum magnetic flux density to be around 1.27T. Since the saturation flux of the material is 1.6 T, the motor has no magnetic saturation.

Fig. 4-17 shows the average air-gap flux density of the existing motor, in which the average air-gap flux density is 0.0948T. The opening arc of the magnets is 135°, which causes these peaks to become zero. Moreover, decreases and oscillations in the flux density are created by the slot openings.

Fig. 4-18 shows the output torque waveforms of the existing motor, in which the average torque is 0.12 *kg-cm*, and the torque ripple is 16.97%. The torque ripple is defined as:

$$\text{Torque ripple} = \frac{\max(\text{torque}) - \min(\text{torque})}{\text{average torque}} \times 100\% \quad (4-36)$$

The torque waveforms are provided by 8 sets of coils, in which the cycles are 45°. In particular, through the first derivative of the flux linkage waveforms, the trend of the torque can be seen. Theoretically, the oscillations are relatively small due to the shorter cycle and appropriate design of the slots and winding ways.

Generally, FEM is considered to provide the most accurate results. As long as the mesh is cut properly, and the number of meshes is great enough, accurate results are achievable. However, the processing time of FEM is usually longer than is the case using other methods. In this case, completing the analysis takes about an hour using an Intel i7 CPU PC.

In order to make a quantitative comparison with the analytical results, an FEA is applied to assist in numerically calculating the magnetostatic field of a DC commutator motor. In this study, the ANSYS/Maxwell 2D field simulator is employed for the field analysis. Fig. 4-11 shows the distribution of the air-gap flux density of the FEA results of the integrated device and existing design compared with the 2-D method. The average value of the air-gap flux density from 0 to 180 degrees is 0.0736T and 0.0948T with parallel and axial magnetization-type permanent magnets, respectively.

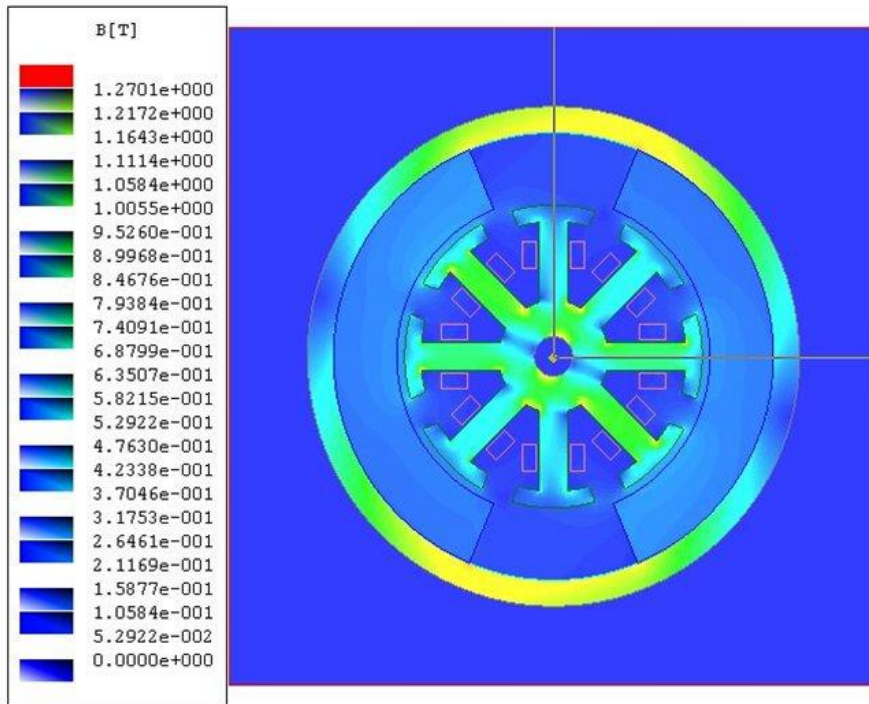


Fig. 4-16 Magnetic flux density distribution

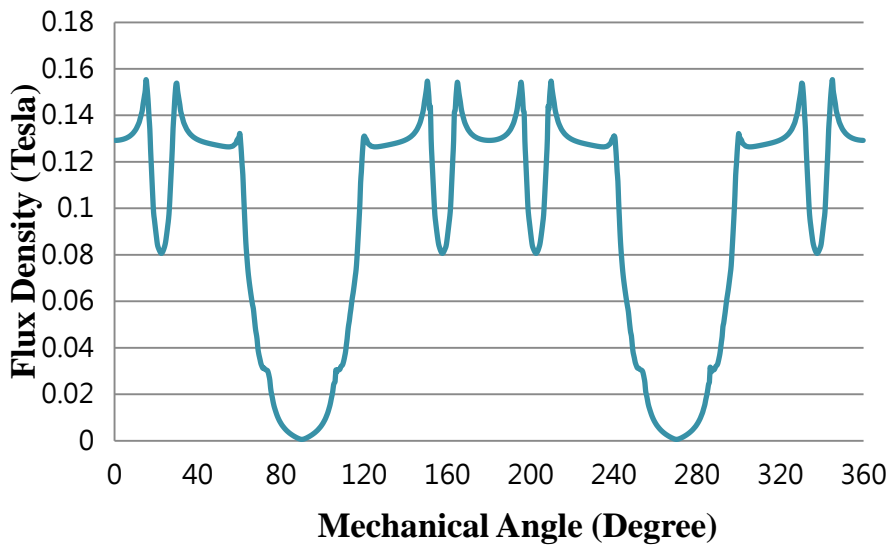


Fig. 4-17 Average air-gap flux density

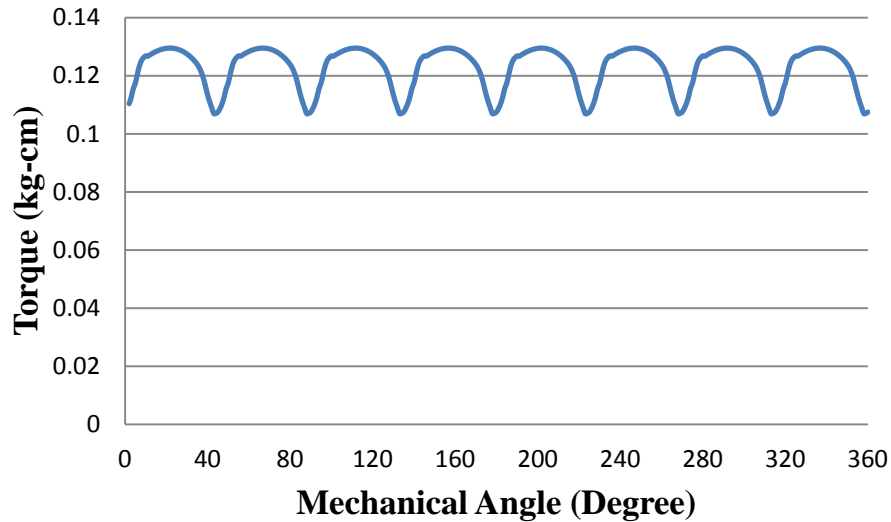


Fig. 4-18 Output torque waveform

The major differences between the 1-D and 2-D equivalent magnetic circuit methods is that the 1-D method only shows the average value of the air-gap flux density, and the 2-D method illustrates the distribution of the air-gap flux density. In addition, the magnetization of the permanent magnet can be treated only as the parallel magnetization type when using the 1-D method. However, the 2-D method deals with not only parallel and radial magnetization types, but also other magnetization types, such as a Halbach array. For motor designers, the 2-D equivalent magnetic circuit method can obtain more information about the magnetic field, especially the detailed changes in the motor dimensions and permanent magnet properties.

By comparing the analytical results with the FEA results, the differences in the air-gap flux density are 3.21% and 3.06% for the 1-D and 2-D methods, respectively. For the air-gap flux density waveform, the difference between the 2-D equivalent magnetic circuit method and the FEA is due to the slot and gear-teeth effect. The 1-D and 2-D equivalent magnetic circuit methods provide fast and accurate results related to designing and analyzing the electric

characteristics of electric motors, and the FEA provides more accurate results for detailed designs.

4-4 Optimal design

For motor designers, there are lots of design variables to be chosen for designing a motor. Optimal design provides an approach for designers to get better design configurations with appropriate design models. The equivalent magnetic circuit method mentioned above is related to the field distribution, magnetic material properties, and machine dimensions, which can act as the mathematical model of the motors in the optimal design method, and the main motor dimensions can be obtained.

Since the torque is greatly affected by the flux density produced by the magnets, the air-gap density is chosen as the objective function and the design constraint is identical volume of the permanent magnets. And, the mathematical expression is:

$$\begin{aligned} & \min(-\max(\text{flux density of the air gap})) \\ & \text{subject to } h_1: \text{volumes of magnets remain the same} \end{aligned} \quad (4-37)$$

Substituting Eqs.(4-24)-(4-27) into Eq.(4-37), designers can set the variables with the arc and width of the permanent magnets. There is another constraint to remain the original inner radius of the stator to make the least change. And, the initial values of permanent magnet arc can be any value between 0 to 180 degrees.

Using the gradient method to solve the optimal problem, the detail motor dimensions are easily found. For a nonlinear problem, the optimal equation can be expressed as:

$$\min_x f(x), \text{ such that } \begin{cases} c(x) \leq 0 \\ ceq(x) = 0 \\ A \cdot x \leq b \\ Aeq \cdot x = beq \\ lb \leq x \leq ub \end{cases} \quad (4-38)$$

where b and beq are vectors, A and Aeq are matrices, $c(x)$ and $ceq(x)$ are functions that return vectors, and $f(x)$ is a function that returns a scalar.

The variable expressions are:

$$\begin{aligned} R_{mt} &= 17 \times 10^{-3} \\ r_{mt} &= x(1) \times 10^{-3} \\ arc &= x(2) \end{aligned} \quad (4-39)$$

where $x(1)$ and $x(2)$ are the inner radius and the opening arc of the permanent magnets. The nonlinear constraint can be expressed as:

$$R_{mt}^2 \times arc - r_{mt}^2 \times arc - V_{magnet} = 0 \quad (4-40)$$

After elapsing 30921.02 seconds (8.59 hours), the optimal results are shown in Table 4-3 and Fig. 4-19. The result shows that the original design is the optimal one.

Table 4-3 Results of optimal design

	Radius of magnet(mm)	Opening arc(°)
Original design	12	135
Optimal design	11.99	134.66
Difference	0.125%	0.25 %

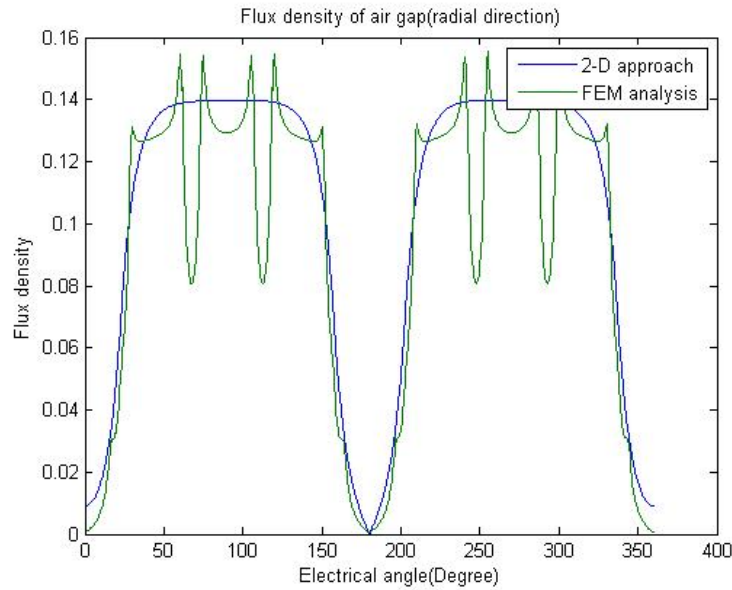


Fig. 4-19 Flux densities of the optimal design

4-5 Summary

A summary of this chapter is as follows:

1. The 1-D and 2-D equivalent magnetic circuit methods used to analyze the magnetostatic field of a DC commutator motor are applied and verified using the FEA.
2. The Carter's coefficient is obtained to model the permeance in the presence of slotting and gear-teeth.
3. By comparing the analytical results with the FEA results, the differences in the air-gap flux density are found to be 3.21% and 3.06% for the 1-D and 2-D methods, respectively.
4. The major difference between these two methods is that the 1-D method only shows the average air-gap flux density; however, the 2-D method presents the distribution of the air-gap flux density.
5. The flux linkages, the first derivative of the flux linkage, cogging torques, electromagnetic torques, and torque ripples of two sets of gear-teeth

integrated on the rotor are analyzed to verify the effects of gear profiles.

6. The result shows that gear-teeth integrated on the motor can act as dummy slots, which was found to reduce the cogging torque and torque ripple by 92.02% and 50.14 %, respectively.



Chapter 5. Gear Train Design

The overall design concept of this work involves adding teeth to the rotor as the sun gear of the PGT as the input. On the account of geometric restrictions, the teeth design is a non-negligible part of the design. It is important to analyze the transmission capabilities of the magnetic materials in the gear mechanisms. The design methods for the gear train, gear profiles, number of gear teeth, and the gear strength are introduced in this chapter.

5-1 Gear teeth design

In the design process, both of the number of poles, P , and slots, S , of the DC commutator motor are fixed parameters, while the design parameter is the number of teeth. Accordingly, the design constraints regarding the number of teeth are as follows:

1. The number of teeth should be an integer multiple of the number of slots. Due to the manufacturing process, there should be slot openings on the rotor to wind the coil windings. The designer thus must remove the teeth roots to form the slot openings. The number of slots is set as a fixed parameter, and the number of teeth should be an integer multiple of the number of slots.
2. The radius of the addendum circle of the gear profiles should be the same as or close to the radius of the rotor. The air-gap length is an important design variable that can affect the output performance of the motor. To maintain the radius of the air-gap, the radius of the addendum circle of the gear profiles should be the same as or close to that of the rotor.
3. The widely used AGMA standard 20° pressure angle involute spur gear profile is used to simplify the manufacturing process. Table 5-1 lists the

standard ratios of metric involute gear teeth.

Table 5-1 S tandard ratios of metric involute gear teeth

Addendum	0.8000 m
Dedendum	1.0000 m
Clearance	0.2000 m
Work depth	1.6000 m
Whole depth	1.8000 m
Tooth thickness	1.5708 m

4. The commonly used JIS B 1701 gear modulus is selected and listed in Table 5-2.

Table 5-2 Standard modulus of involute gears

JIS Standard Value of Module					
Series1	Series2	Series3	Series1	Series2	Series3
--	0.15	--	2.5	2.75	--
0.2	0.25	--	3.0	--	3.25
0.3	0.35	--	--	3.5	3.75
0.4	0.45	--	4	4.5	--
0.5	0.55	0.65	5	5.5	--
0.6	0.7	--	6	--	6.5
--	0.75	--	--	7	--
0.8	0.9	--	8	9	--
1.0	--	--	10	11	--
1.25	--	--	12	14	--
1.5	1.75	--	16	18	--
2.0	2.25	--	20	22	--

The stator also must conform to the design constraints. The radius of the dedendum circle of gear profiles cannot be larger than the outer radius of the

stator. The stator acts as the ring gear and the frame of the integrated design. The gear profiles that are integrated on the stator are of the interior type. If the radius of the dedendum circle is larger than the outer radius of the stator, the gear profiles will be incomplete.

Based on the above constraints, an AGMA standard 20° pressure angle involute spur gear profile with module 0.4 and 56 teeth is applied to the rotor, and the same gear profile with 82 teeth is applied to the stator. The diameters of the addendum circles are provided in Table 5-3.

Table 5-3 Diameter of the addendum circles

	8	16	24	32	40	48	56	64	72
0.2	1.92	3.52	5.12	6.72	8.32	9.92	11.52	13.12	14.72
0.3	2.88	5.28	7.68	10.08	12.48	14.88	17.28	19.68	22.08
0.4	3.84	7.04	10.24	13.44	16.64	19.84	23.04	26.24	29.44
0.5	4.8	8.8	12.8	16.8	20.8	24.8	28.8	32.8	36.8
0.6	5.76	10.56	15.36	20.16	24.96	29.76	34.56	39.36	44.16
0.8	7.68	14.08	20.48	26.88	33.28	39.68	46.08	52.48	58.88
1	9.6	17.6	25.6	33.6	41.6	49.6	57.6	65.6	73.6
1.25	12	22	32	42	52	62	72	82	92
1.5	14.4	26.4	38.4	50.4	62.4	74.4	86.4	98.4	110.4
2	19.2	35.2	51.2	67.2	83.2	99.2	115.2	131.2	147.2

5-2 Speed ratio design

A simple PGT with two degrees of freedom requires two independent inputs. For the simple PGT shown in Fig. 2-3, after identifying the input link, the output link and the fixed link, there are 6 different combinations, as listed in Table 5-4.

It is known that different speed ratios can be generated by different settings based on Table 5-4. In this table, Case 1, Case 4, and Case 6 can produce speed

acceleration, while Case 2, Case 3, and Case 5 can produce speed reduction. Furthermore, Case 3 is a PGT with a fixed carrier, which causes it to degenerate into an ordinary gear train and operate in the opposite direction. Table 5-4 reveals that Case 5 is the most efficient reduction among these six combinations.

Table 5-4 Combinations of a simple PGT

Case	Fixed link	Input link	Output link	Speed ratio	Range
1	Sun gear	Arm	Ring gear	$(T_2+T_4)/T_4$	SR>1
2	Sun gear	Ring gear	Arm	$T_4/(T_2+T_4)$	SR<1
3	Arm	Sun gear	Ring gear	$-T_2/T_4$	SR <1
4	Arm	Ring gear	Sun gear	$-T_4/T_2$	SR >1
5	Ring gear	Sun gear	Arm	$T_2/(T_2+T_4)$	SR<1
6	Ring gear	Arm	Sun gear	$(T_2+T_4)/T_2$	SR>1

*SR=Speed ratio = output/input

An existing 2-pole/8-slot DC commutator motor and a two-stage reduction PGT (Fig. 5-1) consists of a sun gear (member 2), a sun gear integrated with a carrier (member 4), two ring gears with the same number of teeth (member 1' and 1''), two sets of planet gears (members 3 and 5), and the output shaft (member 6). Each of members 3 and 5 employs three planet gears to mesh with the ring gear for the purpose of providing better balancing of gear tooth loads and inertia forces. The number of teeth of member 2 is 56; the number of teeth of members 1' and 1'' are set as 82 in step 5. Planet gear member 3 has 13 teeth by applying the geometric constraint. The velocity ratio of the output shaft and the input sun gear for the first stage PGT is 0.406. If the required velocity ratio is 0.08, the designer can apply the simple PGT unit series to achieve the

required velocity ratio as follows:

$$r_v = \frac{\omega_7}{\omega_2} = \frac{T_2}{T_2 + T_{1'}} \times \frac{T_4}{T_4 + T_{1''}} \quad (5-1)$$

where $T_{1'} = T_{1''}$ is 82 teeth; T_2 is 56 teeth, and T_4 is 20 teeth, and this is the integer solution of the second stage sun gear. The velocity ratio is 0.0796. The planet gear of the second stage PGT T_5 can be derived as 31 teeth.

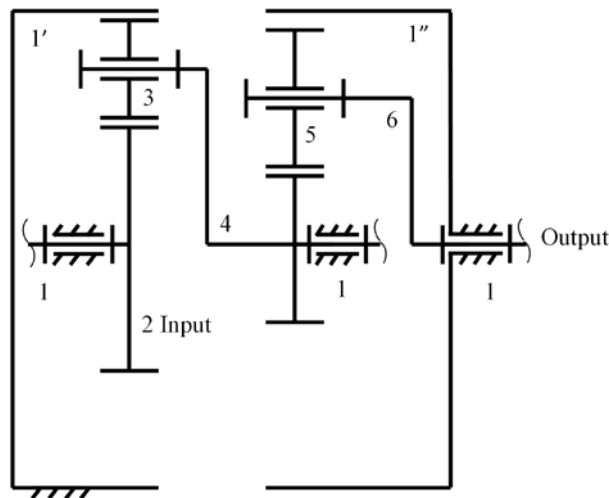


Fig. 5-1 A two-stage planetary gear train

5-3 Strength analysis of gear profiles

The design concept involves integrating the gear profiles on the rotor of a DC commutator motor as the sun gear of the PGT. The iron core is stacked using a silicon steel sheet, and it is hollow so as to leave the winding space. In the gear view, it is a hollow spur gear. It is also important to analyze the strength of gear profiles that may be capable of torque transmission to avoid a failure situation.

The force acting on the gear during the torque transmission process can be determined. In the torque transmission process, the force acts along the line of action. If the force is F_p , and the base circle velocity is V_b , the power H_p can be determined as:

$$H_p = F_p \cdot V_b \quad (5-2)$$

The base circle velocity V_b can be expressed as

$$V_b = \pi \cdot n \cdot d_b = \pi \cdot n \cdot d \cdot \cos \phi \quad (5-3)$$

where d_b is the base circle diameter; d is the pitch circle diameter; ϕ is the pressure angle, and n is the gear's rotational speed. The pitch circle velocity V can be expressed as:

$$V = \pi \cdot V_g \cdot d \quad (5-4)$$

Substituting Eqs.(5-3) and (5-4) into eq. (5-2),

$$H_p = F_p \cdot \pi \cdot V_g \cdot d \cdot \cos \phi = F_p \cdot V \cdot \cos \phi = F_t \cdot V \quad (5-5)$$

where $F_t = F_p \cos \phi$ is the tangential component of force F_p .

Due to manufacturing tolerances, the actual F_p is larger than ideal loading. The extra force, which is called dynamic loading F_d is,

$$F_d = \frac{2e}{t} \sqrt{k \cdot m_e} \quad (5-6)$$

The actual force F is,

$$F = F_p + F_d \quad (5-7)$$

where t is the contact time; k is the equivalent elastic coefficient; m_e is the equivalent mass, and e is the summation of the manufacturing tolerances. The AGMA standard includes the accuracy level, and the manufacturing tolerances can be determined.

If the number of teeth of driving gear i is T_i with ω_i rpm, the contact time t is:

$$t = \frac{60}{T_i \omega_i} \quad (5-8)$$

The loading F_d can be derived as:

$$F_d = \frac{T_i \omega_i e}{30} \sqrt{k \cdot m_e t} \quad (5-9)$$

Fig. 5-2 shows the equivalent elastic system of two meshed gears, and the equivalent elastic coefficient can be derived as:

$$k = \frac{b}{9} \cdot \frac{E_1 E_2}{E_1 + E_2} \quad (5-10)$$

where E_1 and E_2 are the Young's modulus of gear 1 and 2, respectively, and b is the gear width.

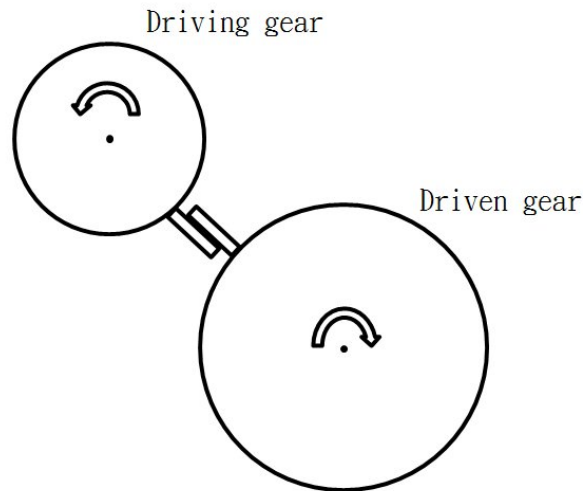


Fig. 5-2 Equivalent elastic system of two meshed gears

The equivalent mass m_e is:

$$m_e = \frac{m_1' m_2'}{m_1' + m_2'} \quad (5-11)$$

where m_1' and m_2' are the equivalent mass concentrated to the pitch circle.

If it is a solid gear, the moment of inertia I is:

$$I_m = \frac{\pi b \rho}{2} r_p^4 \quad (5-12)$$

where r_p is the pitch circle radius, and ρ is the density.

The moment of inertia concentrated to pitch circle I_m is:

$$I_m = m' r_p^2 \quad (5-13)$$

$I=I_m$ yields

$$m' = \frac{\pi b \rho}{2} r_p^2 \quad (5-14)$$

If it is a hollow gear, the moment of inertia I_H is:

$$I_H = \frac{\pi b \rho}{2} (r_p^4 - r_i^4) \quad (5-15)$$

The equivalent mass m_H' is

$$m_H' = \frac{\pi b \rho}{2 r_p^2} (r_p^4 - r_i^4) \quad (5-16)$$

For the 56 teeth rotor with basic parameters listed in Table 5-5, the loading results can be determined, as shown in Table 5-6. By applying the FEM software, the result is shown in Fig. 5-3. The maximum stress of the gear profile implemented on the magnetic materials is 7.94 MPa, and the material yielding stress is 312 MPa. The strength of the gear is thus determined to be capable of torque transmission.

Table 5-5 Parameters of the sun gear

Items	Values
Output torque (kg-cm)	0.1
Rotation speed (rpm)	6500
Number of teeth	56
Module	0.4
Density (kg/m ³)	7850
Gear type	Hollow
Outer radius (m)	0.011
Inner radius (m)	0.010
Thickness (m)	0.005
Manufacture error (mm)	0.06
Young's modulus (GPa)	200
Poisson's ratio	0.3

Table 5-6 Results of gear loading

Items	Values
Equivalent elasticity coefficient	5.56×10^8
Equivalent mass (kg)	4.00×10^{-3}
Theoretical load (N)	89.29
Dynamic load (N)	686.20

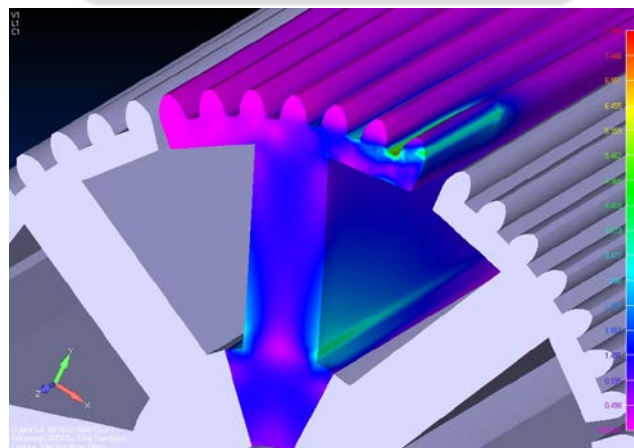


Fig. 5-3 Stress analysis of the gear mechanism

5-4 Summary

For the integrated device, the tooth design impacts not only the transmission but also the electromagnetic characteristics. The teeth added to the rotor structurally and functionally limit the motor. A summary of this chapter is as follows:

1. The number of teeth added to the rotor is set as a design variable, and the corresponding design constraints are concluded.
2. The planetary gear teeth and ring gear teeth are related to the sun gear teeth. The number of teeth for the transmission is derived, where $T_1 = T_1''$ is 82 teeth; T_2 is 56 teeth, and T_4 is 20 teeth, and this is the integer solution of the second stage sun gear. The velocity ratio is 0.0796. The planet gear of the second stage PGT T_5 can be derived as 31 teeth.
3. The dynamic loading is derived as 686.2 N.
4. The maximum stress of the gear profile implemented on the magnetic materials is 7.94 MPa, and the material yielding stress is 312 MPa. The strength of the gear makes it capable of torque transmission.

Chapter 6 Effects of Integrated Gear Teeth

In order to verify if the magnetic characteristics of the integrated device conform with the design requirements, it is important to analyze the affection of the gear-teeth profile integrated on the rotor. In this study, the flux linkages, the first derivative of the flux linkage, the cogging torque, and the electromagnetic torque are analyzed to compare the existing design with the integrated devices.

6-1 Flux linkage analysis

Table 6-1 lists design parameters of a 2-pole/8-slot DC commutator motor with integrated gear-teeth. Based on the parameters, simulation models can be built to analyze the flux linkage and the first derivative of the flux linkage, as shown in Fig. 6-1 and Fig. 6-2, respectively. These figures indicate that the flux linkage has some phase-lag, but it doesn't affect the output values. The first derivative of the flux linkage shows the same trend. Basically, the affection of the integrated gear-teeth on the flux linkage and the first derivative of the flux linkage can be ignored, and the magnetic characteristics remain the same.

Table 6-1 Parameters of the integrated device

Case	T	m	A (mm)	D (mm)	w (mm)	w_0 (mm)	R_{ro} (mm)	g (mm)	l_m (mm)	θ_m ($^\circ$)	L (mm)
Existing	--	--	--	--	--	--	11.5	0.5	5	135	16
2	24	0.9	1.44	1.8	1.41	0.96	11.52	0.5	5	135	16
3	56	0.4	0.64	0.8	0.63	0.56	11.25	0.5	5	135	16

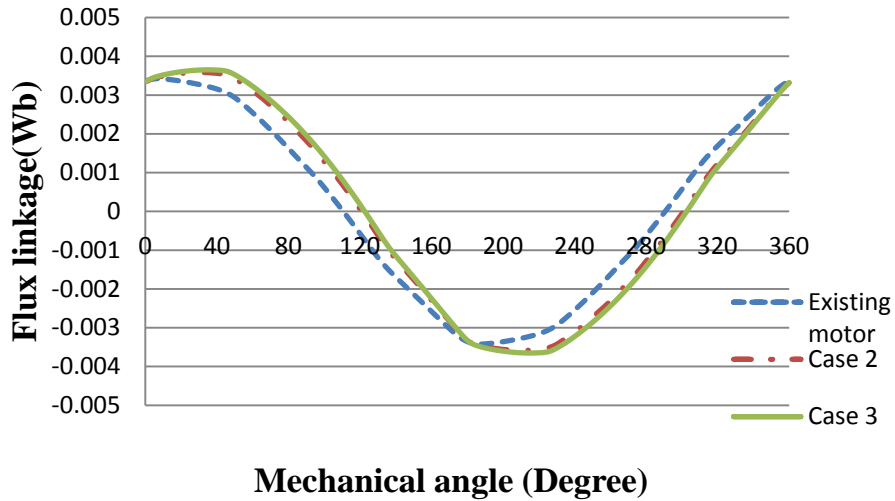


Fig. 6-1 Flux linkage comparison

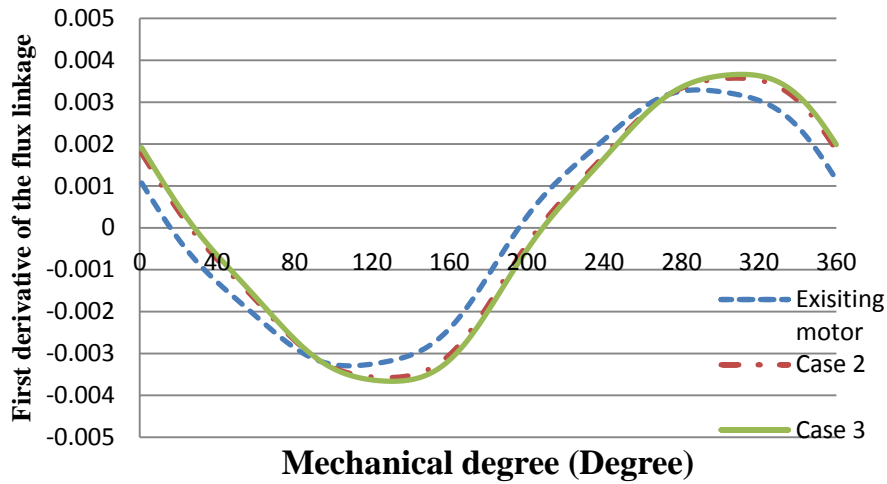


Fig. 6-2 The first derivative of the flux linkage comparison

6-2 Cogging torque analysis

The permanent magnets will produce a fixed magnetic field and interact with the rotor irons. The required torque to turn the motor shaft without excitation is called cogging torque. It is an oscillatory torque that always induces vibration, noise, resonance, and torque ripple. Since the cogging torque is greatly affected by the configuration of the rotor, the prediction of cogging torque for the integrated devices is proposed in this study.

Cogging torque is the torque due to the interaction between the permanent

magnets of the stator and the rotor core in a DC motor. Based on the virtual work principle, the cogging torque $T_c(\theta)$ is expressed as:

$$T_c(\theta) = \frac{-\partial E_g(\theta)}{\partial \theta} \quad (6-1)$$

where θ is the rotating angle of the rotor relative to the stator, and $E_g(\theta)$ is the magnetic energy stored in the air gap. In addition, the electromagnetic energy of the air gap per volume $\Delta E_g(\theta)$ is expressed as:

$$\Delta E_g(\theta) = \frac{1}{2\mu_0} B_g^2(\theta, \phi) \cdot dv \quad (6-2)$$

where μ_0 is the permeability of air; ϕ is the arbitrary angle in the air gap, and $B_g(\theta, \phi)$ represents the flux density of the air gap. Therefore, the electromagnetic energy in the air gap is:

$$E_g(\theta) = \int_0^{2\pi} \frac{1}{2\mu_0} B_g^2(\theta, \phi) v(\phi) d\phi \quad (6-3)$$

where $v(\phi)$ represents the function of volume indicating the length of the air gap, which is generally a constant.

In order to show the impact of the gear tooth and gear space on the cogging torque, as shown in Fig. 6-3, the position of the tooth space α_m is defined using a step function as:

$$u(x - \alpha_m) = \begin{cases} 1, & \text{when } |x - \alpha_m| \leq w/2 \\ 0, & \text{when } |x - \alpha_m| > w/2 \end{cases} \quad (6-4)$$

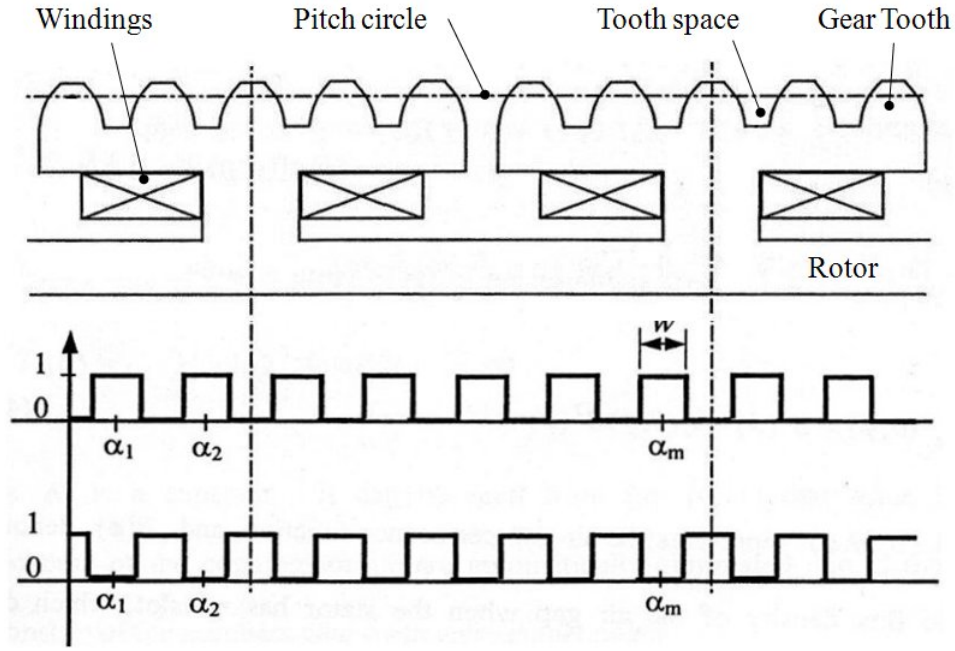


Fig. 6-3 Representation of the presence of the tooth spaces and the corresponding permeance function

where w is the width of the tooth space along the pitch circle of the sun gear.

Therefore, the presence of the tooth on the sun gear is:

$$u_i(\theta, \phi) = \sum_{m=1}^T u\left(\phi - \theta - \frac{2\pi}{T}m\right) \quad (6-5)$$

where T is the number of teeth integrated on the rotor.

To simplify the analysis process, the permeance of the air gap is assumed to be a simple unit function, which is reciprocal to the step function. Hence, the flux density of the air gap is expressed as:

$$B_g(\theta, \phi) = [1 - u_i(\theta, \phi)]B(\phi) \quad (6-6)$$

$$B_g^2(\theta, \phi) = B^2(\phi) - u_i(\theta, \phi)B^2(\phi) \quad (6-7)$$

where $1 - u_i(\theta, \phi)$ is the permeance function of the air gap, and $B(\phi)$ is the flux density of the air gap when there is no slot on the rotor, which represents

the distribution of the residual flux density of the permanent magnets.

Since the waveform of the residual flux density is an odd function, which has a fundamental cycle equal to $4\pi/P$ in mechanical angle, it can be expanded using a Fourier series as follows:

$$B(\phi) = \sum_{n=1}^{\infty} B_n \sin\left(\frac{nP\phi}{2}\right) \quad (6-8)$$

$$B^2(\phi) = A_0 + \sum_{n=1}^{\infty} A_n \cos(nP\phi) \quad (6-9)$$

where P is the number of poles; A_0 is the DC component of $B^2(\phi)$, and A_n and B_n are respectively the coefficients of the n -th harmonic components of $B(\phi)$ and $B^2(\phi)$.

Based on the mean value theorem, the following equation is derived:

$$\int_0^{2\pi} B^2(\phi) u_i(\theta, \phi) d\phi = w \cdot \sum_{m=1}^T B^2\left(\theta + \frac{2\pi}{T}m\right) \quad (6-10)$$

Substituting Eqs. (6-3), (6-7), (6-9), and (6-10) into Eq. (6-1) yields:

$$T_c(\theta) = K \cdot \sum_{n=1}^{\infty} n A_n \sum_{m=1}^T \sin nP\left(\theta + \frac{2\pi}{T}m\right) \quad (6-11)$$

where K is a constant.

Due to the particular relationship of the numbers of gear teeth and the magnet poles, the harmonic components of the cogging torque are automatically eliminated as:

$$\sum_{m=1}^T \sin nP\left(\theta + \frac{2\pi}{T}m\right) = 0, \text{ when } \frac{nP}{T} \notin N \quad (6-12)$$

The n -th harmonic components that cause the cogging torque are given by:

$$T_n = i \frac{T}{gcd(P, T)}, i = 1, 2, 3, \dots \quad (6-13)$$

where $gcd(P, T)$ is the greatest common divisor of the number of magnet poles P and the number of integrated gear-teeth T . It is apparent that the order of the harmonic components that dominate the cogging torque is directly related to the number of gear teeth on the rotor and the number of magnet poles.

The space between two slots S_p is $S_p = 360^\circ / S$, and S is the number of slots. The number of cogging torque pulse T_{cn} where the magnets rotate one S_p is:

$$T_{cn} = \frac{S_p}{\theta_s} = \frac{lcm(S, P)}{S} \quad (6-14)$$

where $lcm(S, P)$ is the least common multiplier of P and S , and θ_s is the period of the stable equilibrium in mechanical degrees.

Hence, the cogging torque will perform periodicity in different motor positions. The relationships can be expressed as:

$$\theta_s = \frac{360^\circ}{lcm(S, P)} \quad (6-15)$$

The number of gear-teeth on the rotor and the number of magnet poles are two important cogging torque design parameters. This is why electric motors with fractional slot-to-pole ratios are frequently employed by experienced motor designers to reduce the cogging torque. The fractional slot-to-pole ratios have higher orders of dominant harmonic cogging torque components. The magnitude of the harmonic component usually decreases in accordance with the increase in the order number. The strategy for reducing the cogging torque is to make the dominant harmonic components have a higher order number.

Table 6-2 lists the components of an existing 2-pole/8-slot permanent magnet DC commutator motor. By integrating different numbers of gear-teeth, the number of slots is replaced by the number of teeth. The gear teeth act as dummy slots in the magnetic field, which can increase the order number of the dominant harmonic components. In this study, the AGMA stub gear-teeth with a 20° pressure angle are integrated on the rotor of the DC commutator motor. The number of gear-teeth in the 2nd case is 24, and the number of teeth in the 3rd case is 56.

Table 6-2 The n-th harmonic components generate the cogging torque

Case	P	S	T	T/P	gcd(P,T)	T _n
Existing	2	8	--	4	2	4i
2	2	8	24	12	2	12i
3	2	8	56	28	2	28i

To compare the gear-teeth effect on the cogging torque, the FEA is applied to simulate the cogging torque, as shown in Fig. 6-4. The simulation shows that the 3rd case has the smallest cogging torque, where the period is 4.29°. The cogging torque of the 2nd case is also smaller than the existing design, where the period is 15°. The peak value of each case is listed in Table 6-3, which shows that the cogging torques are greatly reduced by 92.02% in the 3rd case and 20.10% in the 2nd case, respectively. The results show the gear-teeth integrated on the rotor of the motor act as dummy slots, which reduce the cogging torque efficiently.

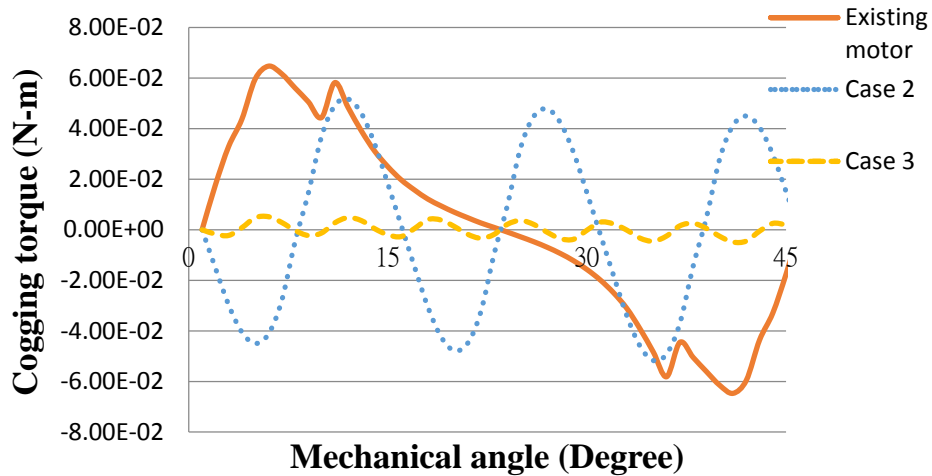


Fig. 6-4 Cogging torque comparison

Table 6-3 Cogging torque comparison

Case	Peak value (N-m)	Difference (%)
Existing design	0.065	--
2	0.052	-20.10
3	0.005	-92.02

$$\text{Difference} = (\text{Case-Existing design})/\text{Existing design}$$

6-3 Electromagnetic torque and torque ripple analyses

The electromagnetic torque is the most important aspect of motor performance. It provides the power source to the machine required to make it work. The value and stability of the electromagnetic torque will affect the output performance of the electric motor. The electromagnetic torque of an electric motor is related to the torque constant and the input current. Since the torque constant is related to the configuration of motor, the input current and the flux density of the magnet are the important parameters that affect the electromagnetic torque. In integrated devices, the gear teeth on the rotor will increase the air gap length, which will reduce the electromagnetic torque. If the gear teeth greatly reduce the electromagnetic torque, the concept can't be applied

on the motor.

To compare the electromagnetic torque, the FEA is applied to simulate the 3 cases, as shown in Table 6-4 and Fig. 6-5, which shows that the electromagnetic torque is reduced by the effect of the slot opening and also the gear teeth. In the 2nd case, the torque is reduced by the gear teeth with a 15° period. In the 3rd case, the period is smaller, so the electromagnetic torque is stable. Table 6-4 provides a comparison of these 3 cases. The average electromagnetic torque of these 3 cases don't reveal large differences. Due to the reduction in the slot opening, the electromagnetic torques for the 2nd and the 3rd cases are a bit larger than the those in the existing design. By analyzing the standard deviation and torque ripple, it can be seen that integrating the appropriate number of gear-teeth on the rotor can reduce the torque ripple, and the electromagnetic torque can thus remain the same. In the 3rd case, the torque ripple is reduced by 50.14 %. The integrated design presented in this work can be employed in high driving torque and/or low rotational speed applications, such as cordless power tools, electric vehicles and scooters, powered mobility transporters, and factory conveying equipment.

Table 6-4 Electromagnetic and torque ripple analyses

Case	Existing motor	2	3
Average torque (kg-cm)	0.120	0.122	0.126
Max torque value (kg-cm)	0.127	0.133	0.130
Min torque value (kg-cm)	0.106	0.111	0.120
Standard deviation	0.007	0.006	0.003
Torque ripple (%)	17.57	18.68	8.76

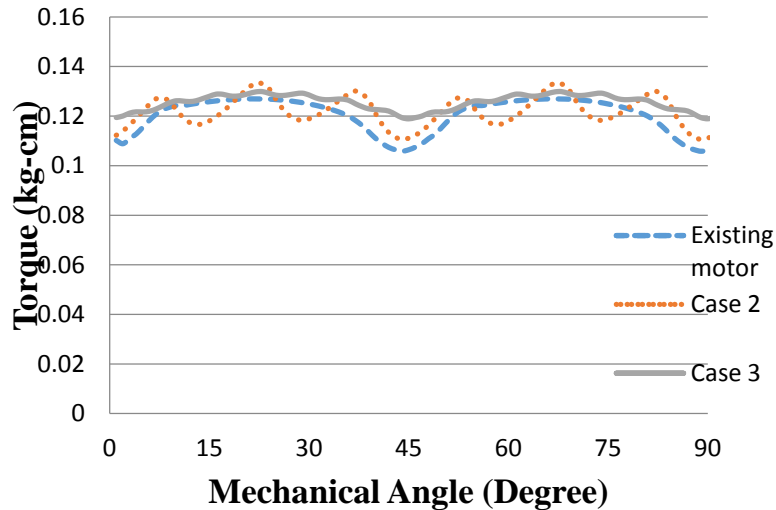


Fig. 6-5 Electromagnetic torque comparison

6-4 Summary

It is important to analyze the affection of gear-teeth profile integrated on the rotor. This chapter is summarized as follows:

1. The flux linkages and the first derivative of the flux linkage are analyzed to compare the existing design with the integrated devices. The affection of the integrated gear-teeth on the flux linkage and the first derivative of the flux linkage can be ignored, and the magnetic characteristics remain the same.
2. Two gear profiles with a feasible number of teeth integrated on the rotor are provided for the purpose of effectively reducing the cogging torque. The cogging torques are greatly reduced by 92.02% in the 3rd case and 20.10% in the 2nd case, respectively. The results show that the gear-teeth integrated on the rotor of the motor act as dummy slots, which reduces the cogging torque efficiently.
3. By analyzing the standard deviation and torque ripple, it can be observed that the electromagnetic torque can remain the same.

Chapter 7 Design Examples

Based on the above discussion, the objective of this work is to present a design procedure for the integration of rotating electric motors and gear mechanisms. An existing DC commutator motor and an existing AC induction motor are shown as examples to illustrate this process step by step. The design specifications, parameters, and conceptual design process are shown in detail.

7-1 Design example 1

A DC commutator motor is thus used as an example. The first step of the integrated design procedure is to define the design specifications of the integrated device. Finding and examining existing designs that have the desired functions can help designers determine the characteristics of an integrated device. It is very important for the designer to list all the quantitative values of the desired functions, such as output torques, input currents, and the sizes of the integrated devices. Table 7-11 lists the design specifications of a 2-pole/8-slot DC commutator motor with an ordinary gear train as the benchmark [20].

There are many design variables in the integrated device design. In order to simplify the design process, designers can choose fixed parameters and optimize the rest of the variables. Based on the specifications in step 2, the output torque, rated current, magnetic materials, and assembly spaces can be fixed or left the same as those in the existing design. Table 2 lists the fixed parameters that are chosen in this study; however, it should be noted that these fixed parameters could be different.

Table 7-1 Design specifications of the integrated device

	Items	Values
Rated conditions	Rated speed of the motor	6500 rpm
	Rated voltage	DC 24V
	Reduction ratio of the reducer	1:12.5
Magnet material properties	Material of magnets	Ferrite
	Direction of magnetization	Radial
	Remanence	0.12 T
	Coercivity	99007.74 A/m
	Relative permeability	0.9645
Steel material properties	Steel material	50CS1300
	Saturated flux density	1.6 T

Table 7-2 Fixed parameters of the integrated device

Parameters	Symbols	Values
Rated speed (rpm)	ω_R	6500 rpm
Number of phases	N_{ph}	1
Number of magnet poles	P	2
Number of armature slots	S	8
Air gap length (mm)	g	0.5 mm
Radius of shaft (mm)	R_s	1.5 mm
Inner radius of stator (mm)	R_{si}	17 mm
Outer radius of stator (mm)	R_{so}	19 mm
Number of coils per armature tooth (turn)	N_c	60
Stack length (mm)	L	16 mm
Rated conduct current (A)	I	2 A
Magnet remanence (T)	B_r	0.12 T
Magnet relative permeability	μ	0.9645
Allowed steel flux density (T)	B_a	1.6 T

Based on the configurations of permanent-magnet rotating electric machines and the kinematic structure of the gear mechanism, feasible design concepts and fundamental theories are generated and applied subject to the concluded design requirements and constraints. The designer can then generate the design concept systematically by applying these requirements and constraints. The design concept for this example is the same as that shown in Fig. 2-4.

The detailed design of the rotor and stator can be obtained based on the design requirements, constraints, fixed parameters, and known variables. The stack length of the rotor/stator, slot opening width, gear profiles, and number of teeth are determined in this step. In the design procedure, the number of poles P and the number of slots S are fixed parameters, and the design constraints are as follows:

1. For the 2-pole/8-slot DC commutator motor, the number of teeth should be a multiple of 8.
2. For the 2-pole/8-slot DC commutator motor, the radius of the addendum circle should be close to 23mm.
3. The widely used AGMA standard 20° pressure angle involute spur gear profile is used to simplify the manufacturing process.
4. The commonly used JIS B 1701 gear modulus is selected.

The stator also must address the design constraints. The radius of the dedendum circle of gear profiles cannot be larger than the outer radius of the stator. The stator acts as the ring gear and the frame of the integrated design. The gear profiles that are integrated on the stator are of the interior type. If the radius of the dedendum circle is larger than the outer radius of the stator, the gear profiles will be incomplete.

Based on the above constraints, an AGMA standard 20° pressure angle involute spur gear profile with module 0.4 and 56 teeth is applied to the rotor, and the same gear profile with 82 teeth is applied to the stator.

The ANSOFT/Maxwell 2D field simulator is employed in the field analysis. The parameters of the model are listed in Table 7-3. Since the characteristics of a DC commutator motor in the axial direction are the same, a 2D simulation is chosen instead of a 3D simulation. Fig. 7-1 shows the mesh model of integrated design. Fig. 7-2 shows the flux linkage of each set of coil windings. Fig. 7-3 shows the flux density distribution of the entire motor. Fig. 7-4 shows the distribution of the air-gap flux density. The average value of the air-gap flux density from 0 to 180 degrees is 0.0736 and 0.0948 Tesla with parallel and radial magnetization-type permanent magnets, respectively.

Table 7-3 FEA parameters of the integrated device

T	m	A (mm)	D (mm)	w (mm)	w_0 (mm)	R_{ro} (mm)	g (mm)	l_m (mm)	θ_m (°)	L (mm)
56	0.4	0.64	0.8	0.63	0.56	11.25	0.5	5	135	16

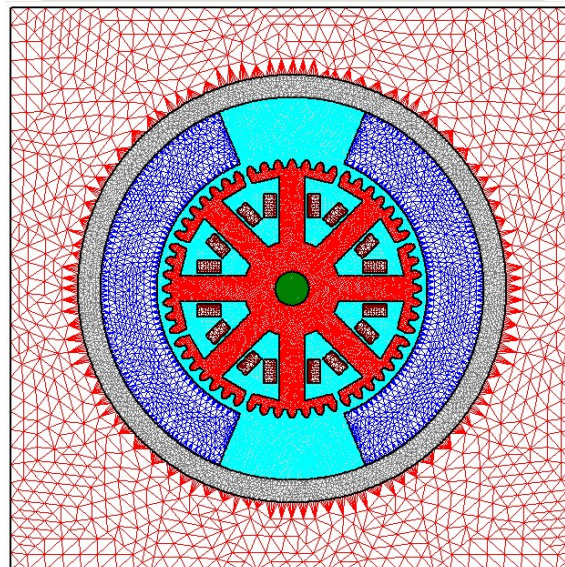


Fig. 7-1 Mesh model of the integrated design

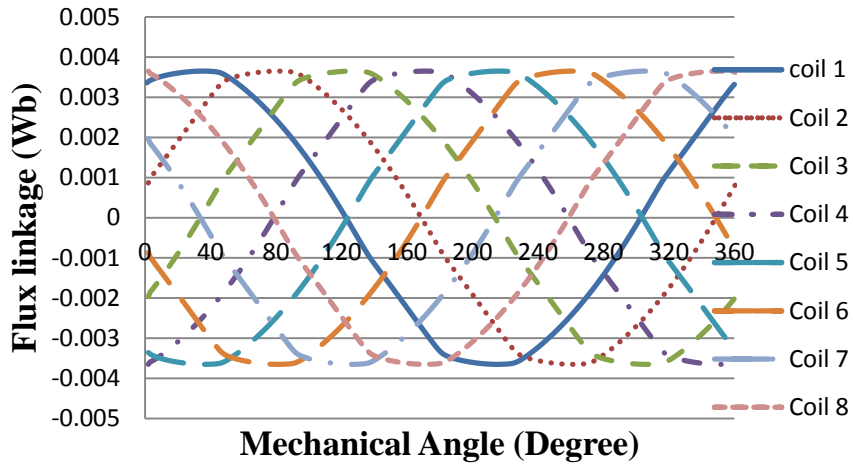


Fig. 7-2 Flux linkages of the coil windings

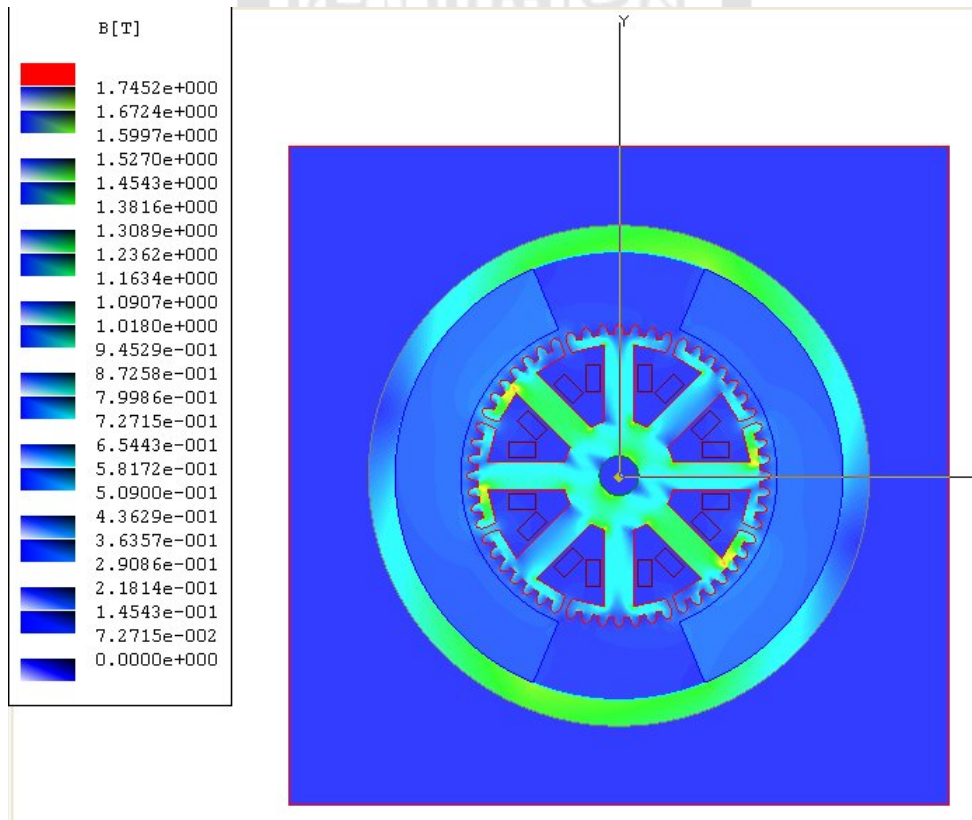


Fig. 7-3 Flux distribution of the integrated device

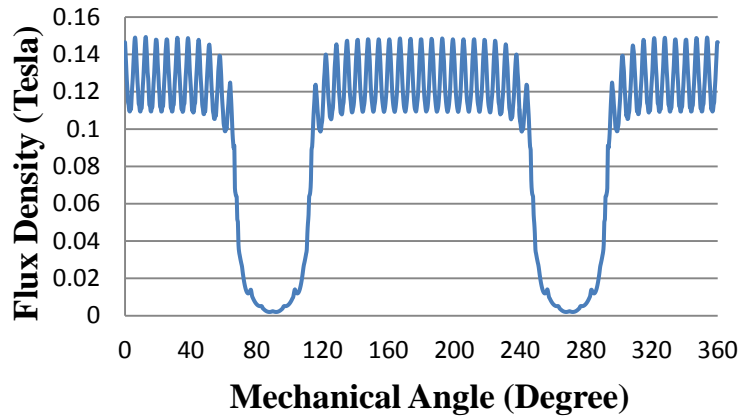


Fig. 7-4 Air gap flux distribution of the integrated device

The results for cogging torque and electromagnetic torque are shown in Table 7-4, Fig. 7-5, and Fig 7-6. Theoretically, the cogging torque is equal to the variation in the energy within a motor as the rotor rotates. The reduction in the cogging torque for the proposed motor configuration is effectively achieved by designing the number of gear teeth and magnet poles with fractional tooth-to-pole ratios and also by making the dominant harmonic components have a higher order number. With this design, the gear teeth integrated on the rotor act as dummy slots [77, 78], thus effectively reducing the cogging torque and torque ripple of the motor.

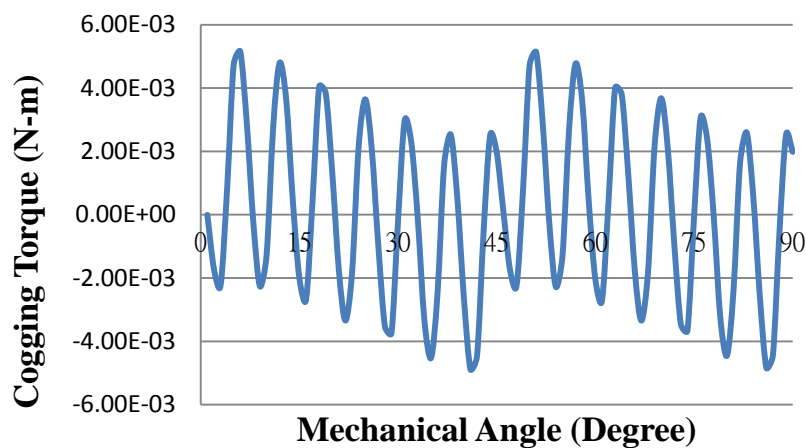


Fig. 7-5 Cogging torque of the integrated device

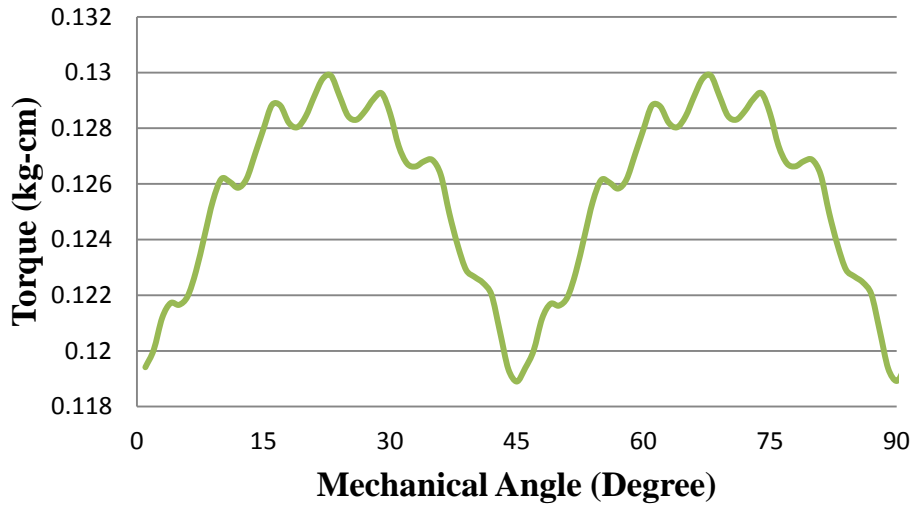


Fig. 7-6 Electromagnetic torque of the integrated device

Table 7-4 Results of the magnetostatic analysis

Air gap density (Tesla)	Cogging torque (N-m)	Average torque (kg-cm)	Torque ripple (%)
0.09542	0.00516	0.126	8.76

There are many design variables that must be determined when designing a motor. The use of an optimal design can enable designers to obtain better design configurations with appropriate design models. The equivalent magnetic circuit method mentioned above is related to the magnetic field distribution, magnetic material properties, and machine dimensions. Since the output torque is greatly affected by the air-gap flux density produced by the magnets, the air-gap flux density is chosen as the objective function, and the design constraint is set as an identical volume of permanent magnets. The variables are the arc and width of the permanent magnet. The detailed motor dimensions can be easily found using the Matlab software `fmincon` function, which is based on the gradient method. The optimal value of the permanent magnet arc is 134.66° . The maximum air-gap flux density is 0.09542 T.

For the 56 teeth rotor with basic parameters listed in Table 5-5, the loading results can be determined as shown in Table 5-6. By applying the FEM software, the result is shown in Fig. 5-3. The maximum stress of the gear profile implemented on the magnetic materials is 7.94 MPa, and the material yielding stress is 312 MPa. The strength of the gear is shown to capable of torque transmission.

An existing 2-pole/8-slot DC commutator motor and a two-stage reduction PGT consists of a sun gear (member 2), a sun gear integrated with a carrier (member 4), two ring gears with the same number of teeth (member 1' and 1''), two sets of planet gears (members 3 and 5), and the output shaft (member 6). Each of members 3 and 5 employs three planet gears to mesh with the ring gear for the purpose of providing better balancing of gear tooth loads and inertia forces. The number of teeth of member 2 is known to be 56; the number of teeth of members 1' and 1'' are set as 82 in step 5. The planet gear member 3 has 13 teeth by applying the geometric constraint. The velocity ratio for both the output shaft and the input sun gear for the first stage PGT is 0.406. If the required velocity ratio is 0.08, the designer can apply the simple PGT unit series to achieve the required velocity ratio. $T_{1'} = T_{1''}$ is 82 teeth; T_2 is 56 teeth, and T_4 is 20 teeth, and this is the integer solution of the second stage sun gear. The velocity ratio is 0.0796. The planet gear of the second stage PGT T_5 can be derived as 31 teeth.

The feasible integrated device that is derived using the integrated design procedure outlined above is presented in Fig. 7-7 and Fig. 7-8. According to the structural characteristics, the PGT is coaxial with the rotor and stator of the DC commutator motor by a common axis. All three of them can be employed as the

input, output, and ground terminals for the transmission. In this concept, the sun gear (member 2) is the input terminal with integrated exterior gear profiles on the slots of the rotor. The ring gear (members 1' and 1'') is the ground terminal, which is connected to the stator of the motor. The carrier (member 5) is the output terminal, which is the same member as the output shaft. This kinematic structure of the PGT produces the maximum speed reduction. Each slot opening of the rotor is formed by removing the bottom land of the sun gear, which enables the copper conductors to set into the slot areas and also does not affect the conjugate gear meshing relation.

The integrated device eliminates the use of couplings, the gearbox casing, and bolts or fasteners, which makes the entire device more compact, lightweight, and easier for maintenance. The output shaft of the PGT and the rotational shaft of the motor are coaxial, while balanced planet gears are also employed. The integrated device reduces the spaces in the axial direction needed for installation. The gear teeth integrated on the rotor act as dummy slots to effectively reduce the cogging torque and torque ripple of the motor. The performance of the integrated device is shown in Table 7-5. These results show that the proposed integrated device performs better than the existing design, reducing the cogging torque by 92.02% and the torque ripple by 50.14%. Moreover, the machine volume of the integrated device is smaller than the existing design due to the compact space arrangement, especially in the axial direction. For the same rate of output torque, the proposed design enhances the torque density by 16.66%, which is defined as the torque capacity per unit volume. A prototype structure is built and shown as Fig. 7-9

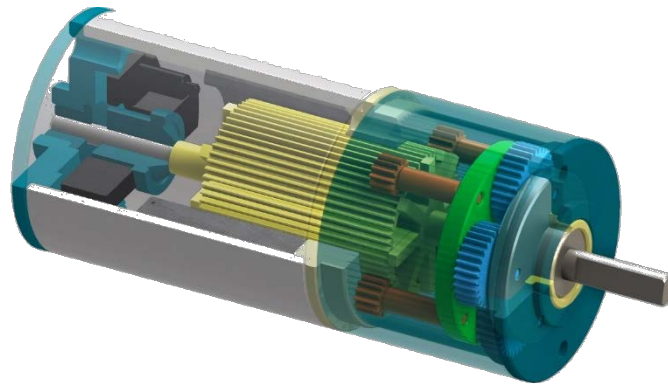


Fig. 7-7 Configuration of the proposed integrated design.

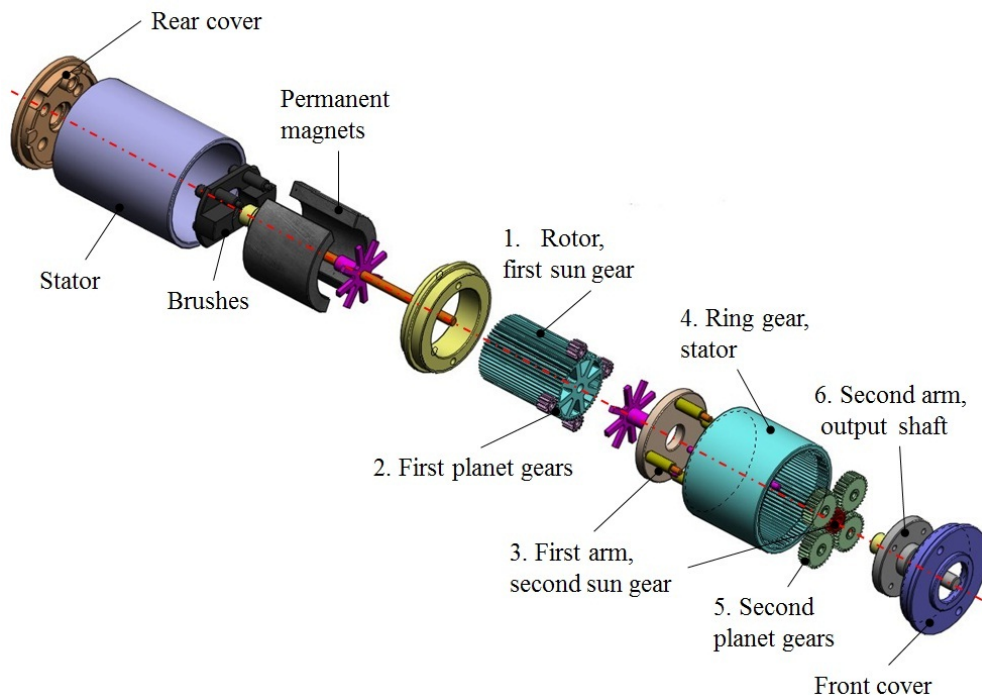


Fig. 7-8 Explosion drawing of the proposed integrated design.

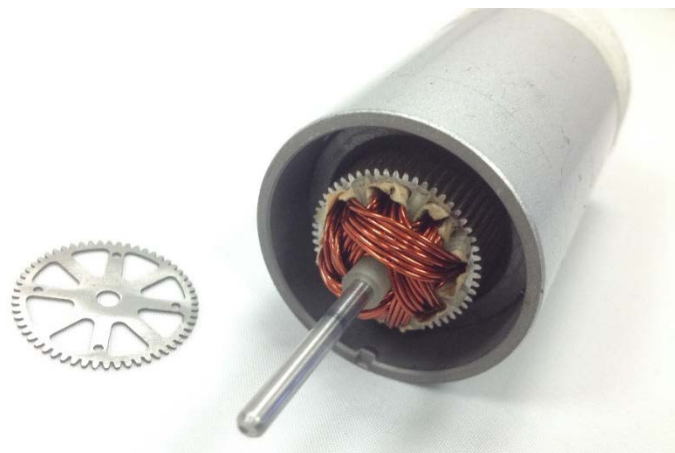


Fig. 7-9 Prototype structure

Table 7-5 Comparison of the performance of the integrated device

Case	Air gap density (Tesla)	Cogging torque (N-m)	Average torque (kg-cm)	Torque ripple (%)	Axial length (mm)	Machine Volume (m ³)	Torque density (N-m/m ³)
Existing motor	0.0948	0.0647	0.120	17.57	104	1.18x10 ⁻³	1246.31
New design	0.09542	0.00516	0.126	8.76	94	1.07 x10 ⁻³	1453.94
Improvement	0.65%	92.02%	5%	50.14%	9.62%	9.58%	16.66%

*Improvement=|(New design-Existing motor)/Existing motor |*100%

7-2 Design example 2

An existing AC induction motor is used for the gear train design. By following the design procedure discussed in Section 3-2, the three-link gear mechanism results in one feasible new design concept, as shown in Fig. 3-6 (a), and the four-link gear mechanism results in six feasible new design concepts, as shown in Fig. 3-6 (b)-(g). Fig. 7-10 shows the cross-section of the design concept provided in Fig. 3-6(b).

To integrate an AC induction motor with the gear trains, the design strategy must share a designated part without extra transmitting elements. Gear profiles are integrated on the rotor/stator of an AC induction motor. In order to verify the magnetic characteristics of the integrated device to meet the design requirements, it is important to analyze the affection of the teeth profile integrated on the rotor/stator. The FEA is applied to assist in numerically calculating the characteristics of the existing AC induction motor and integrated device. In this study, the ANSOFT/Maxwell 3D field simulator is employed for the field analysis, and the flux linkages, the induced voltages, the current, and the electromagnetic torque are analyzed to compare the existing design and the integrated devices.

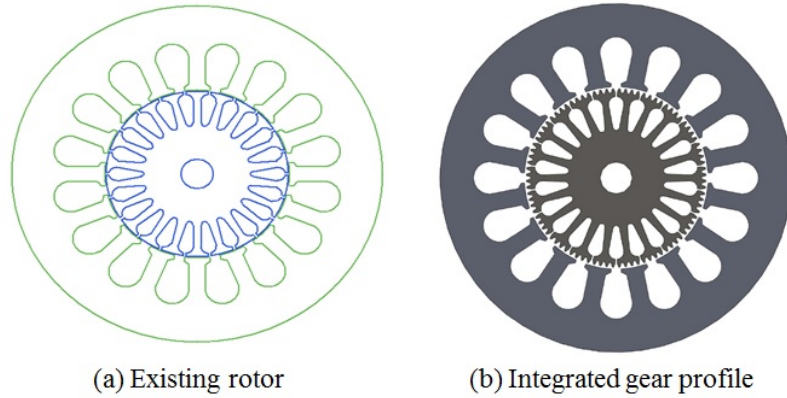


Fig. 7-10 The cross-section of the gear profile integrated on the rotor

Table 7-6 lists the parameters of the existing AC induction motor, which will be the benchmark in this example. Based on the parameters, the simulation model can be built to analyze the magnetic characteristics, as shown in Fig. 7-11. Fig. 7-12 and Fig. 7-13 provide a comparison of the induced voltages and the current analysis of the existing AC induction motor and the integrated device. Basically, the affection of the integrated gear teeth on the induced voltages and the current can be ignored.

Fig. 7-14 provides a comparison of the flux linkage between the existing AC induction motor and the integrated device. It shows that the flux linkages have some differences in terms of the peak values, but this does not affect the output values. Basically, the affection of the integrated gear teeth on the flux linkage can be ignored, which means that the design constraints and the magnetic characteristics remain the same.

Table 7-6 Parameters of the AC induction motor

Items	Symbols	Values
Number of phases	N_{ph}	1
Number of poles	P	4
Number of slots on the rotor	S_r	22
Number of slots on the stator	S_s	16
Air gap length (mm)	g	0.45
Radius of shaft (mm)	R_{shaft}	4
Inner radius of rotor (mm)	R_{ri}	4
Outer radius of rotor (mm)	R_{ro}	21.6
Inner radius of stator (mm)	R_{si}	22.05
Outer radius of stator (mm)	R_{so}	43.9
Skew width of rotor (mm)	W_{tb}	2
Number of conductors per layer	N_c	360
Stack length (mm)	L	16.2
Speed (rpm)	V	1600
Rated output power (W)	W	150
Rated Voltage (V)	V	110
Frequency (Hz)	f	60

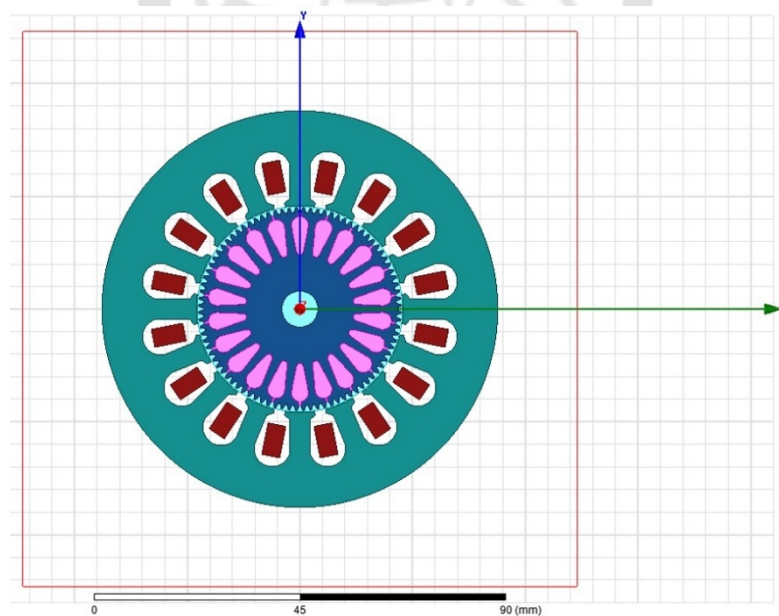


Fig. 7-11 FEA model of the integrated device

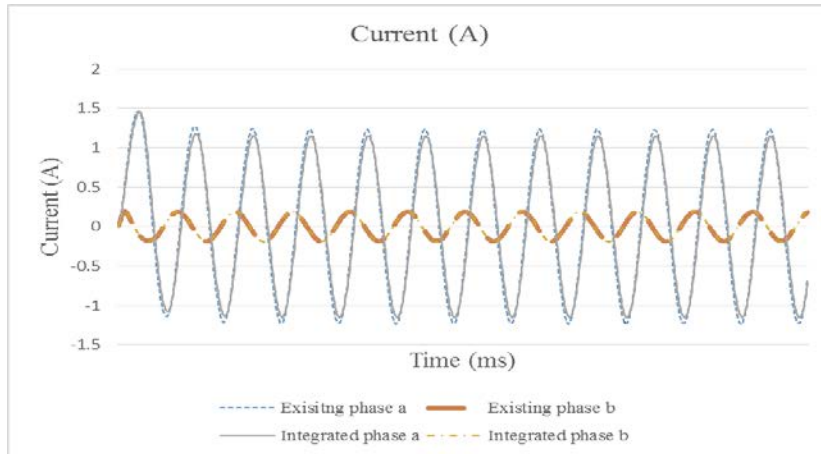


Fig. 7-12 Comparison of the current

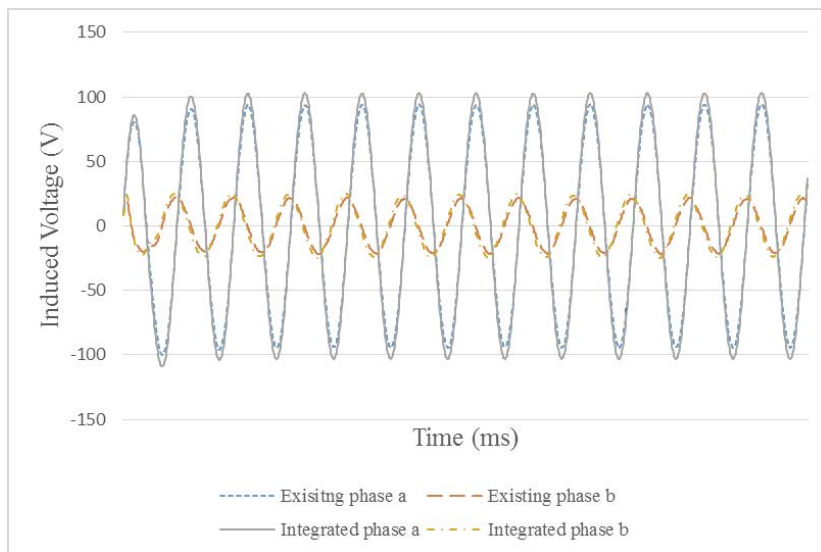


Fig. 7-13 Comparison of the induced voltage

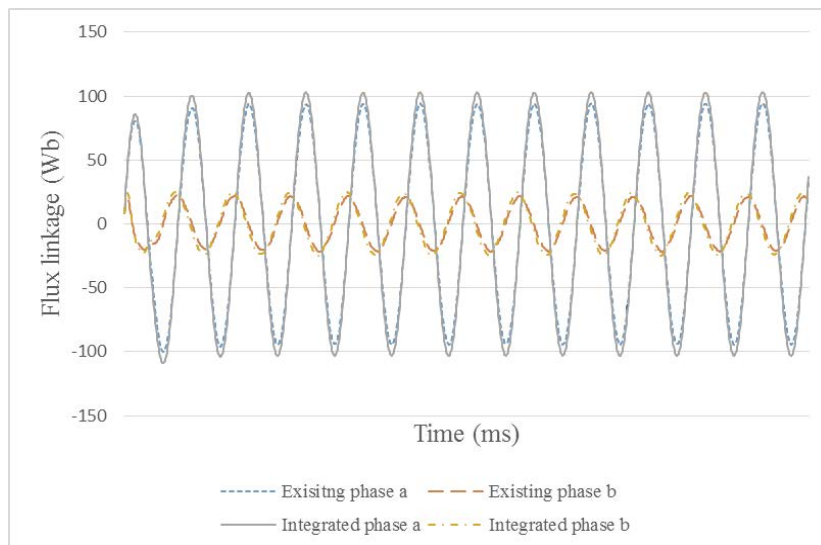


Fig. 7-14 Comparison of the flux linkages

To integrate the gear profile on the above design concepts, design constraints C7-C10 are considered for the purpose of manufacturing. In this work, the rotor radius of the AC induction motor is 43.2mm. The gear profile with module 0.5 and 88 teeth meets the design constraints. Fig. 7-15 shows the 3D model of the gear train, for which the required reduction ratio is 6.8. Fig. 7-16 shows the 3D model of the integrated device.

By applying the finite-element analysis, the strength of the gear profiles can be evaluated to ensure transmission capabilities. The parameters of the gear train are listed in Table 7-7, and the loading results for the gear train are shown in Table 7-8. The results of the FEA are shown in Fig. 7-17. The maximum stress of the gear is 98.32 MPa, and the yielding stress is 312 MPa. The strength of the gear is thus capable of transmission.

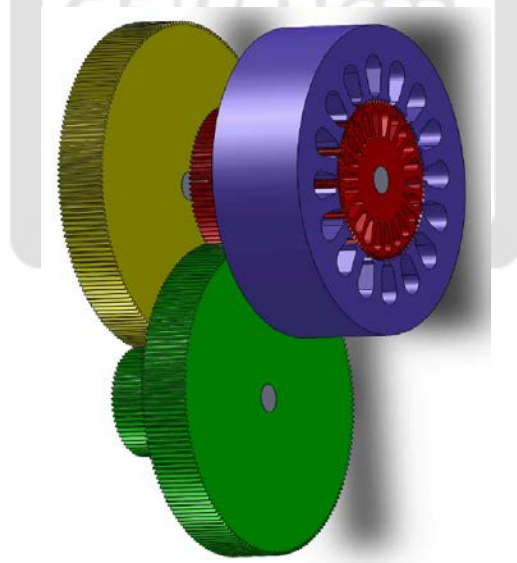


Fig. 7-15 A feasible gear train design

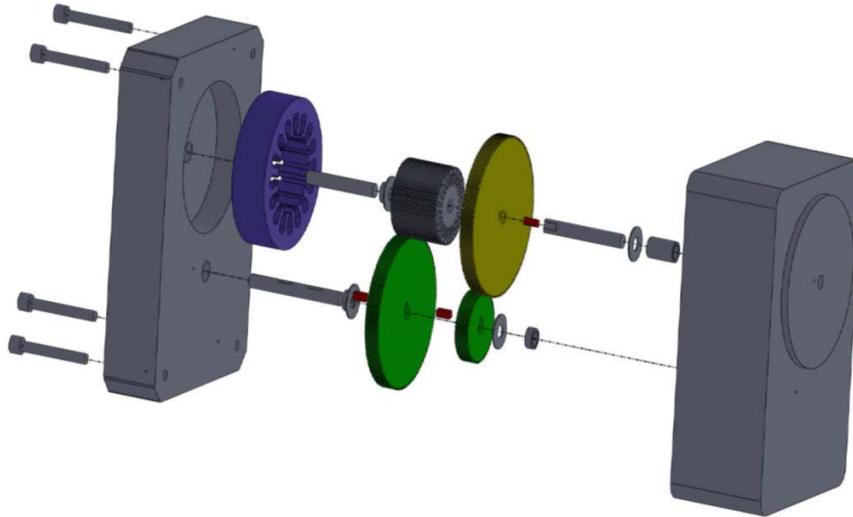


Fig. 7-16 3D model of the concept in Fig. 3-6 (b)

Table 7-7 Parameters of the gear train

Items	Values
Torque (mN-m)	55.3
Rotation speed (rpm)	1600
Number of teeth	88
Module	0.5
Density (kg/m ³)	7850
Gear type	Hollow
Outer radius (m)	0.022
Inner radius (m)	0.004
Thickness (m)	0.005
Manufacture error (mm)	0.06
Young's modulus (GPa)	200
Poisson's ratio	0.3

Table 7-8 Loading results of the gear train

Items	Values
Equivalent elasticity coefficient	5.56×10^8
Equivalent mass (kg)	5.91×10^{-3}
Theoretical load (N)	2.51
Dynamic load (N)	322.64

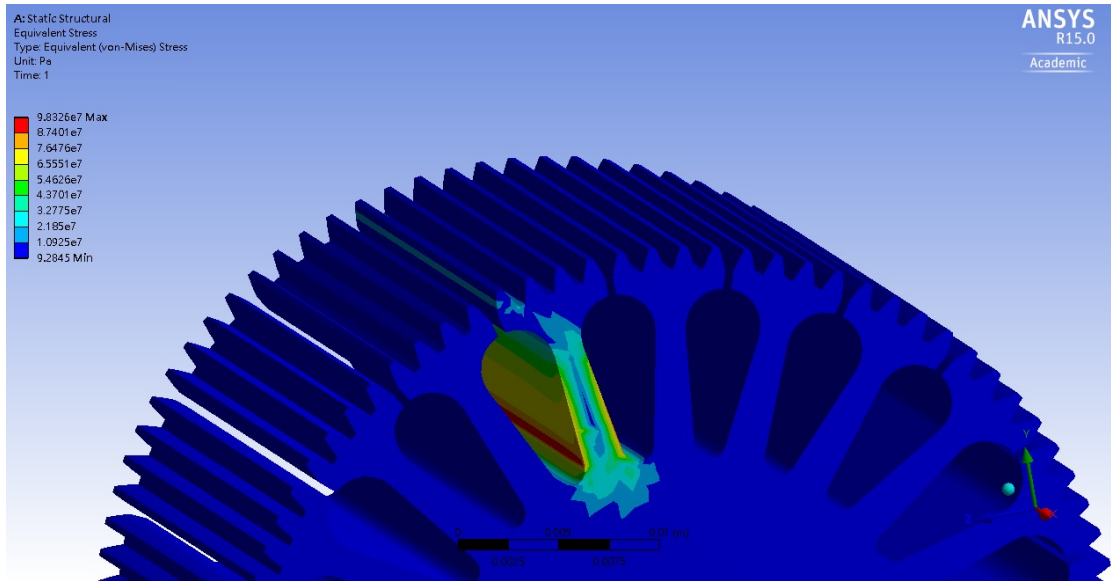


Fig. 7-17 FEA gear strength results

The electromagnetic torque provides the power source for work. The output performance of the motor is affected by the stability of the electromagnetic torque. In the integrated devices, the gear teeth on the rotor increase the air gap length, which reduces the output torque. Fig. 7-18 and Table 7-9 provide a comparison of the performance between the existing AC induction motor and the integrated device. The average torque is reduced by 8.96% as expected. The torque ripple is reduced by 14.23%, and the torque density, which is the output torque per unit volume, is increased by 1.75%. The results show that although the average torque is reduced, the integrated device can provide more stable and efficient output torque than other options.

Table 7-9 Comparison of the output performance

	Average Torque (mN/m)	Torque Ripple (%)	Axial length (mm)	Machine Volume (m ³)	Torque density (mN-m/m ³)
Existing design	60.74	197.35	113	6.84x10-4	88801.17
Integrated device	55.3	169.27	101	6.12x10-4	90359.48
Improvements (%)	-8.96	-14.23	10.62	10.53	1.75

*Improvement=|(New design-Existing motor)/Existing motor |*100%

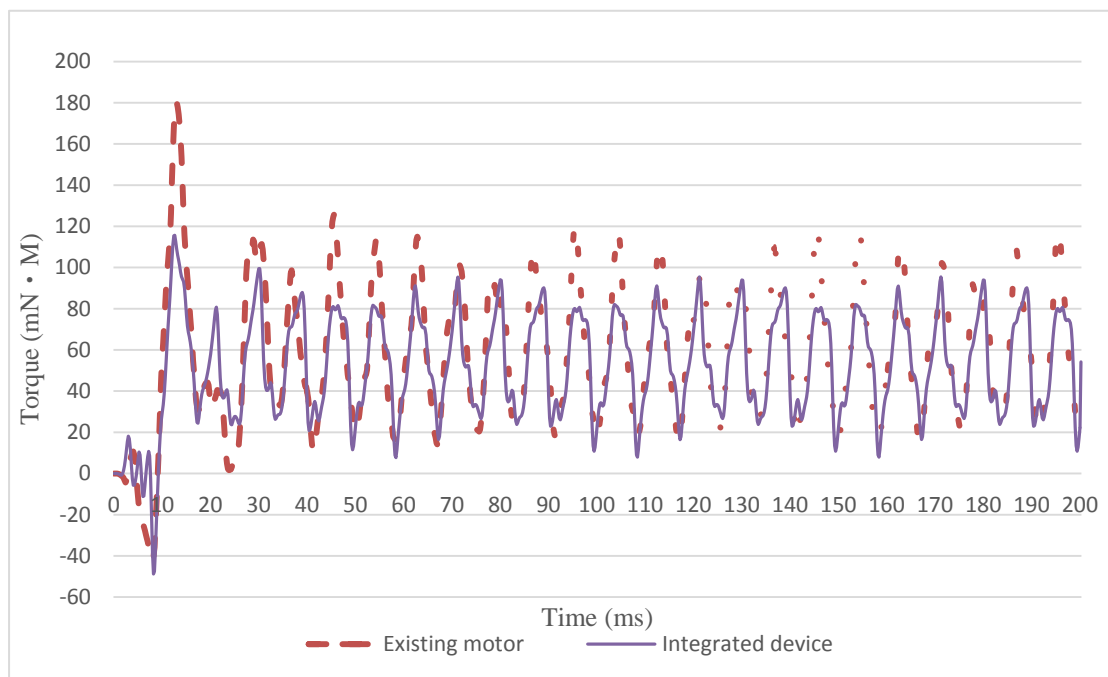


Fig. 7-18 Comparison of the electromagnetic torque

7-3 Summary

Through the systematic design procedure, two configurations of the integrated devices are obtained, for which a summary is as follows:

1. A feasible design concept for the integrated design of permanent-magnet rotating electric motors with gear mechanisms is synthesized, and design requirements and constraints are determined.

2. The feasible numbers of gear teeth to effectively reduce the cogging torque and torque ripple are presented. The results show that the proposed integrated device performs better than the existing design by reducing the cogging torque by 92.02% and the torque ripple by 50.14%.
3. The proposed design also enhances the torque density by 16.66% for the same rate of output torque.
4. An AC induction motor and gear trains are applied as an example.
5. The 3D model of the designed gear train is developed, for which the required reduction ratio is 6.8.
6. The strength of the gear is analyzed in which the maximum stress is 98.32 MPa, and the yielding stress is 312 MPa. This shows the gear train is capable of transmission.
7. The integrated gear profiles have no effect on the flux linkage, the induced voltages, or the current.
8. The torque of the integrated design is reduced by 8.96% when the torque ripple is reduced by 14.23%. The torque density is increased by 1.75%, which indicates that the integrated device provides more stable and efficient output torque.

Chapter 8 Conclusions and Suggestions

This study presents a design procedure for the integrated design of electric motors with gear mechanisms. A feasible design concept is synthesized subject to the derived design requirements and constraints. The 1-D and 2-D equivalent magnetic circuit methods for analyzing the magnetostatic field of a DC commutator motor are applied and verified using an FEA. The flux linkages, the first derivative of the flux linkage, cogging torques, electromagnetic torques, and torque ripples of two sets of gear-teeth integrated on the rotor are analyzed to verify the effects of gear profiles. The design methods used for the gear mechanism are also introduced in this work. The feasible numbers of gear teeth to effectively reduce the cogging torque and torque ripple are presented. Two design examples are provided.

8-1 Conclusions

The conclusions of this work are as follows:

1. Through the theoretical study of motors and gear trains, new design concepts were stimulated that provided a theoretical foundation for the integrated device.
2. Via the analysis of existing designs, the design requirements and constraints of the integrated device were derived, thus making the integrated device achieve the desired functions.
3. The design concepts of the integrated device were obtained subject to the design requirements and constraints. In this study, the integrated design not only meets the demand of power transmission but also improves motor characteristics.

4. A design procedure is proposed to systematically generate integrated devices.
5. The use of graphs on the mechanism synthesis can simplify the complex structures of mechanisms and clearly present the topological structures and kinematic characteristics.
6. Yan's creative mechanism design methodology was applied. The three-link gear mechanism resulted in one feasible new design concept, and the four-link gear mechanism resulted in six feasible new design concepts.
7. The 1-D and 2-D equivalent magnetic circuit methods for analyzing the magnetostatic field of a DC commutator motor were applied and verified using an FEA.
8. The Carter's coefficient was obtained to model the permeance in the presence of slotting and gear-teeth.
9. By comparing the analytical results with the FEA results, the differences in the air-gap flux density were 3.21% and 3.06% for the 1-D and 2-D methods, respectively.
10. The major difference between these two methods is that the 1-D method only shows the average air-gap flux density, and the 2-D method presents the distribution of the air-gap flux density.
11. The flux linkages, the first derivative of the flux linkage, cogging torques, electromagnetic torques, and torque ripples of two sets of gear-teeth integrated on the rotor were analyzed to verify the effects of the gear profiles.
12. The number of teeth were derived, and the corresponding design constraints were determined.

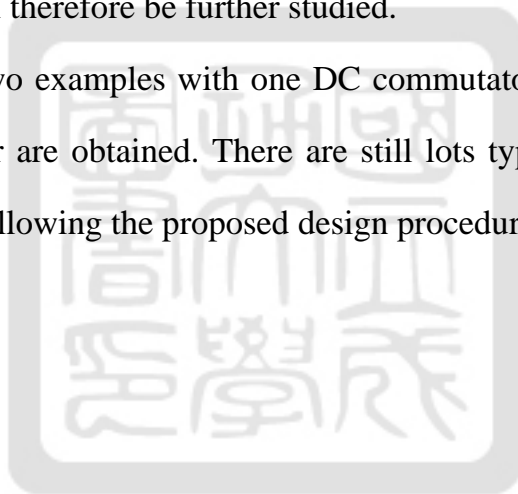
13. The planetary gear teeth and ring gear teeth are related to the sun gear teeth. The number of teeth of the transmission was derived, where $T_1' = T_1''$ was 82 teeth; T_2 was 56 teeth, and T_4 was 20 teeth, and where this was the integer solution of the second stage sun gear. The velocity ratio was 0.0796. The planet gear of the second stage PGT T_5 was derived as 31 teeth.
14. The dynamic loading was derived as 686.2 N.
15. The maximum stress of the gear profile implemented on the DC integrated device was 7.94 MPa, and the material yielding stress was 312 MPa. The gear strength was adequate for torque transmission.
16. The flux linkages and the first derivative of the flux linkage ψ were analyzed to compare the existing design with the integrated devices. The affection of the integrated gear-teeth on the flux linkage and the first derivative of the flux linkage ψ could be ignored, and the magnetic characteristics remained the same.
17. Two gear profiles with feasible numbers of teeth integrated on the rotor were provided to effectively reduce the cogging torque. The cogging torques were greatly reduced by 92.02% in the 3rd case and by 20.10% in the 2nd case, respectively. The results showed that the gear-teeth integrated on the rotor of the motor act as dummy slots, which reduce the cogging torque efficiently.
18. By analyzing the standard deviation and torque ripple, it was found that the electromagnetic torque could remain the same.
19. A feasible design concept of the integrated design of permanent-magnet rotating electric motors with gear mechanisms was synthesized, and the design requirements and constraints were determined.

20. The feasible numbers of gear teeth to effectively reduce the cogging torque and torque ripple were presented. The results showed that the proposed integrated device performed better than the existing design by reducing the cogging torque by 92.02% and the torque ripple by 50.14%.
21. The proposed design also enhanced the torque density by 16.66% for the same rate of output torque.
22. An AC induction motor and gear trains were applied as an example.
23. The 3D model of the designed gear train was developed, for which the required reduction ratio was 6.8.
24. The strength of the gear profile implement on the DC integrated device was analyzed for which the maximum stress was found to be 98.32 MPa, and the yielding stress was found to be 312 MPa. This shows that the gear train as capable of transmission.
25. The integrated gear profiles had no effects on the flux linkage, the induced voltages, or the current.
26. The torque of the integrated design was reduced by 8.96% when the torque ripple was reduced by 14.23%. The torque density was increased by 1.75%. This shows that the integrated device provides a more stable and efficient output torque than the existing design.

8-2 Suggestions

The study provides a design procedure for the integrated design of electric motors with gear mechanisms, which includes not only a configuration design but also an electromagnetic analysis. However, there are several relevant areas that are worthy of future study:

1. According to the results of the design examples presented in Chapter 7, a prototype of the AC induction motor can be constructed. The output performances of the prototype can be measured so as to verify the FEA results.
2. Since the material properties of the existing motor are changeable, which may change motor characteristics, the selection of materials should go through a more complete assessment.
3. There are several assumptions within the equivalent magnetic circuit methods, and the difference between the analytical results and practical applications can therefore be further studied.
4. In this work, two examples with one DC commutator motor and one AC induction motor are obtained. There are still lots types of motors can be integrated by following the proposed design procedure.



References

- [1] 許正和，2002，*機構構造設計學*，高立圖書有限公司，台北，台灣。
- [2] 賴介村，梁嘉生，1994，電動輪圈馬達傳動裝置，中華民國專利第 244,042 號。
- [3] 蕭雲隆，1996，輪圈馬達改良構造，中華民國專利第 300,682 號。
- [4] 許俊甫，2001，內齒輪外旋轉之輪鼓式馬達，中華民國專利第 501,330 號。
- [5] 亞伯特·帕米羅，2002，具有內齒輪系的低度輪廓馬達，中華民國專利第 556,394 號。
- [6] 武智哲雄，2005，電動車椅的驅動裝置所使用的齒輪馬達，中華民國專利第 I238,226 號。
- [7] 河野功，倡原功，2009，小齒輪一體型馬達及門開閉用戟齒輪馬達，中華民國專利第 I305,972 號。
- [8] Fukui, K., 1986, Geared Motor, U. S. Patent No. 4,626,722.
- [9] Kondoh, M. and Minegishi, K., 1996, Low Speed Geared Motor, U. S. Patent No. 5,497,041.
- [10] Kinoshita, S. and Sakagami, K., 2000, Geared Motor, U. S. Patent No. 6,031,308.
- [11] Minegishi, K. and Tamenaga, J., 2002, Geared Motor and Geared Motor Series, U. S. Patent No. 6,485,394.
- [12] Torii, K., Adachi, T., Sakai, H., and Omori, S., 2003, Geared Motor Having Worm Wheel Drivingly Connected to Output Shaft, U. S. Patent No. 6,591,707.
- [13] Nagai, A. and Agematsu, I., 2004, Geared Motor, U. S. Patent No. 6,745,639.
- [14] Saito, T. and Katoh, M., 2004, Starter Motor Having Planetary Gear Device for Reducing Rotational Speed of Electric Motor, U. S. Patent No. 6,782,770.

- [15] Michael, C., Heinrich, Z., and Ju, K., 2007, Planetary Gear, Gear Motor and Series of Gear Motors, U. S. Patent No. 7,182,709.
- [16] Kovach, J. A., Furches, L. K., Kimpel, R. D., Zhang, H., Collett, R. E., and Martinelli, L. A., 2008, Multiple Gear Motor Drive, U. S. Patent No. US2008/0113838.
- [17] Chang, D. S., 2009, Modular Gear Train Mechanism with an Internal Motor, U. S. Patent No. US2009/0227412.
- [18] Saya, T., 2009, Motor with Reduction Gear, European Patent No. EP 2,103,842.
- [19] Oriental Motor General Catalogue, 2008, Oriental Motor Co., Tokyo, Japan.
- [20] 旋轉馬達技術手冊，2008，大銀微系統股份有限公司，台中，台灣。
- [21] DC 直流無刷馬達綜合型錄，2009，泰映科技股份有限公司，台北，台灣。
- [22] Davis, R. I. and Lorenz, R. D., 2003, "Engine Torque Ripple Cancellation with an Integrated Starter Alternator in a Hybrid Electric Vehicle: Implementation and Control," *IEEE Transactions on Industry Applications*, Vol. 39, No. 6, pp. 1765-1774.
- [23] Fahimi, B., Emadi, A., and Sepe, R. B., 2004, "A Switched Reluctance Machine-Based Starter/Alternator for More Electric Cars," *IEEE Transactions on Energy Conversion*, Vol. 19, No. 1, pp. 116-124.
- [24] NAFTC eNews, 2005, "Integrated Starter-Generator," <http://www.naftc.wvu.edu/naftc%20enews/October%2005/hydrogen.html>.
- [25] Electric Coolant Pump Catalogue, 2009, Pierburg Pump Co., Neuss, Germany.
- [26] Suzuki, K., Inaguma, Y., Haga, K., and Nakayama, T., 1995, "Integrated Electro-Hydraulic Power Steering System with Low Electric Energy Consumption," *Society of Automotive Engineers*, Paper No. 950580, pp. 948-954.
- [27] Cho, C. P., Fussell, B. K., and Hung, J. Y., 1996, "A Novel Integrated

- Electric Motor/Pump for Underwater Applications,” *Journal of Applied Physics*, Vol. 79, No. 8, pp. 5548-5550.
- [28] Miller, T. J. E. and Hendershot, Jr., J. R., 1994, *Design of Brushless Permanent Magnet Motors*, Clarendon Press, Oxford.
- [29] Hanselman, D. C., 2003, *Brushless Permanent-Magnet Motor Design, 2nd edition*, The Writers’ Collective, Cranston, Rhode Island.
- [30] 秋山勇治、萩野弘司，1990.12，無刷直流馬達的設計及應用，中國生產力中心小型馬達設計開發講座，台北，台灣。
- [31] 唐任遠，1997，*現代永磁電機理論與設計*，機械工業出版社，北京，中國。
- [32] Qu, R. and Lipo, T. A., 2004, “Analysis and Modeling of Air-Gap and Zigzag Leakage Fluxes in a Surface-Mounted Permanent-Magnet Machine,” *IEEE Transactions on Industry Applications*, Vol. 40, No. 1, pp. 121-127.
- [33] Yang, Y. P., Luh, Y. P., and Cheung, C. H., 2004, "Design and Control of Axial-Flux Brushless DC Wheel Motors for Electric Vehicles—Part I : Multi-Objective Optimal Design and Analysis," *IEEE Transactions on Magnetics*, Vol. 40, No. 4, pp. 1873-1882.
- [34] Hwang, C. C. and Cho, Y. H., 2001, “Effects of Leakage Flux on Magnetic Fields of Interior Permanent Magnet Synchronous Motors,” *IEEE Transactions on Magnetics*, Vol. 37, No. 4, pp. 3021-3024.
- [35] Hwang, C. C., Chang, S. M., Pan, C. T., and Chang, T. Y., 2002, “Estimation of Parameters of Interior Permanent Magnet Synchronous Motors,” *Journal of Magnetism and Magnetic Materials*, Vol. 239, pp. 600-603.
- [36] Tsai, W. B. and Chang, T. Y., 1996, “Magnetic Modeling of Brushless Permanent Magnet Motors with Embedded Magnets,” *Proceedings of the 17th Symposium on Electrical Power Engineering*, Hsinchu, Taiwan, pp. 752-756.
- [37] 鄒繼斌、劉寶廷、崔淑梅、鄭萍，1998年，*磁路與磁場*，哈爾濱工

業大學出版社，哈爾濱，中國。

- [38] Huang, C. C. and Tsai, M. C., 2001, "A Novel Two-phases Spindles Motor for DVD Applications", *IEEE Transactions On Magnetics*, vol. 37, pp. 3825~3820.
- [39] Momen, M. F. and Datta, S., 2009 , "Analysis of Flux Leakage in a Segmented Core Brushless Permanent Magnet Motor," *IEEE Transactions on Energy Conversion*, Vol. 24 , No. 1 , pp. 77-81.
- [40] Hsu, L. Y., Tsai, M. C., and Huang, C. C., 2003, "Efficiency Optimization of Brushless Permanent Magnet Motors Using Penalty Genetic Algorithms," *IEEE International Electric Machines and Drives Conference (IEMDC)*, Madison WI, USA.
- [41] Hsu, L. Y. and Tsai, M. C., 2004, "Tooth Shape Optimization of Brushless Permanent Magnet Motors for Reducing Torque Ripples," *Journal of Magnetism and Magnetic Materials*, Vol. 282, pp. 193-197.
- [42] Hauge, B., 1962, *The Principles of Electromagnetism Applied to Electrical Machines*, Dover, New York, U.S.A.
- [43] Boules, N., 1985, "Prediction of No-Load Flux Density Distribution in Permanent Magnet Machines," *IEEE Transactions on Industry Applications*, Vol. 21, No. 4, pp. 633-642.
- [44] Rasmussen, K. F., Davies, J. H., Miller, T. J. E., McGilp, M. I., and Olaru, M., 2000, "Analytical and Numerical Computation of Air-Gap Magnetic Fields in Brushless Motors with Surface Permanent Magnets," *IEEE Transactions on Industry Applications*, Vol. 36, No. 6, pp. 1547-1554.
- [45] Kumar, P. and Bauer, P., 2008, "Improved Analytical Model of a Permanent-Magnet Brushless DC Motor," *IEEE Transactions on Magnetics*, Vol. 44, No. 10, pp. 2299-2309.
- [46] Jian, L., Chau, K. T., Gong, Y., Yu, C., and Li, W., 2009 , "Analytical Calculation of Magnetic Field in Surface-Inset Permanent Magnet Motors," *IEEE Transactions on Magnetics*, Vol.45, No. 10, pp.

- 4688-4691.
- [47] Liu, Z. J. and Li, J. T., 2008, “Accurate Prediction of Magnetic Field and Magnetic Forces in Permanent Magnet Motors Using an Analytical Solution,” *IEEE Transactions on Energy Conversion*, Vol. 23, No. 3, pp. 717-726.
- [48] Markovic, M. and Perriard, Y., 2009, “Optimization Design of a Segmented Halbach Permanent-Magnet Motor Using an Analytical Model,” *IEEE Transactions on Magnetics*, Vol. 45, No. 7, pp. 2955-2960.
- [49] Zhu, Z. Q., Howe, D., Bolte, E., and Ackermann, B., 1993, “Instantaneous Magnetic Field Distribution in Brushless Permanent Magnet DC Motors, Part I: Open-Circuit Field,” *IEEE Transactions on Magnetics*, Vol. 29, No. 1, pp. 124-135.
- [50] Zhu, Z. Q. and Howe, D., 1993, “Instantaneous Magnetic Field Distribution in Brushless Permanent Magnet DC Motors, Part II: Armature-Reaction Field,” *IEEE Transactions on Magnetics*, Vol. 29, No. 1, pp. 136-142.
- [51] Zhu, Z. Q. and Howe, D., 1993, “Instantaneous Magnetic Field Distribution in Brushless Permanent Magnet DC Motors, Part III: Effect of Stator Slotting,” *IEEE Transactions on Magnetics*, Vol. 29, No. 1, pp. 143-151.
- [52] Zhu, Z. Q., Howe, D., and Xia, Z. P., 1994, “Prediction of Open-Circuit Airgap Field Distribution in Brushless Machines Having an Inset Permanent Magnet Rotor Topology,” *IEEE Transactions on Magnetics*, Vol. 30, No. 1, pp. 98-107.
- [53] Zhu, Z. Q., Howe, D., and Chan, C. C., 2002, “Improved Analytical Model for Predicting the Magnetic Field Distribution in Brushless Permanent-Magnet Machines,” *IEEE Transactions on Magnetics*, Vol. 38, No. 1, pp. 229-238.
- [54] Atallah, K., Calverley, S. D., and Howe, D., 2004, “Design, Analysis, and

- Realization of a High-Performance Magnetic Gear,” *IEE Proceedings B Electric Power Applications*, Vol. 151, No. 2, pp. 135-143.
- [55] Lee, K. S., Debortoil, M. J., Lee, M. J., and Salon, S. J., 1991, “Coupling Finite Elements and Analytical Solution in the Airgap of Electric Machines,” *IEEE Transactions on Magnetics*, Vol. 27, No. 5, pp. 3955-3957.
- [56] Mizutani, R. and Matsui, N., 2000, “Design and Analysis of Low-Speed, High-Torque Permanent Magnet Motors,” *Electrical Engineering in Japan*, Vol. 132, No. 3, pp. 48-56.
- [57] Kim, T. H., Choi, J. H., Ko, K. C., and Lee, J., 2003, “Finite-Element Analysis of Brushless DC Motor Considering Freewheeling Diodes and DC Link Voltage Ripple,” *IEEE Transactions on Magnetics*, Vol. 39, No. 5, pp. 3274-3276.
- [58] Ohnishi, T. and Takahashi, N., 2000, “Optimal Design of Efficient IPM Motor Using Finite Element Method,” *IEEE Transactions on Magnetics*, Vol. 36, No. 5, pp. 3537-3539.
- [59] Tsai, M. C., Weng, M. H., and Hsieh, M. F., 2002, “Computer-Aided Design and Analysis of New Fan Motors,” *IEEE Transactions on Magnetics*, Vol. 38, No. 5, pp. 3467-3474.
- [60] Lacombe, G., Foggia, A., Marechal, Y., Brunotte, X., and Wendling P., 2007, “From General Finite-Element Simulation Software to Engineering-Focused Software: Example for Brushless Permanent Magnet Motors Design,” *IEEE Transactions on Magnetics*, Vol. 43, No. 4, pp. 1657-1660.
- [61] Hsu, Y. S., Tsai, M. C., and Hsieh, M. F., 2008, “Novel Stator Design of Fan Motors Using Soft Magnetic Composites,” *Journal of Applied Physics*, Vol. 103, No. 7, Paper No. 07F109.
- [62] Wrobel, R. and Mellor, P. H., 2008, “Design Considerations of a Direct Drive Brushless Machine With Concentrated Windings,” *IEEE Transactions on Energy Conversion*, Vol. 23, No. 1, pp. 1-8.

- [63] Yan, G. J., Hsu, L. Y., Wang, J. H., Tsai, M. C., and Wu, X. Y., 2009, "Axial-Flux Permanent Magnet Brushless Motor for Slim Vortex Pumps," *IEEE Transactions on Magnetics*, Vol. 45, No. 10, pp. 4732-4735.
- [64] Upadhyay, P. R., Rajagopal, K. R., and Singh, B. P., 2004, "Design of a Compact Winding for an Axial-Flux Permanent-Magnet Brushless DC Motor Used in an Electric Two-Wheel Vehicle," *IEEE Transactions on Magnetics*, Vol.40, No.4, pp.2026-2028.
- [65] Sim, D. J., Cho, D. H., Chun, J. S., Jung, H. K., and Chung, T. K., 1997, "Efficiency Optimization of Interior Permanent Magnet Synchronous Motor Using Genetic Algorithms," *IEEE Transactions on Magnetics*, Vol. 33, No. 2, pp. 1880-1883.
- [66] Cho, D. H., Jung, H. K., and Sim, D. J., 1999, "Multiobjective Optimal Design of Interior Permanent Magnet Synchronous Motors Considering Improved Core Loss Formula," *IEEE Transactions on Energy Conversion*, Vol. 14, No. 4, pp. 1347-1352.
- [67] Hosokawa, Y., Noguchi, S., Yamashita, H., and Tanimoto, S., 2002, "An Optimal Design Method for Efficiency of Permanent Magnet Motors," *Electrical Engineering in Japan*, Vol. 138, No. 3, pp. 72-79.
- [68] Hwang, C. C., Lyu, L. Y., Liu, C. T., and Li, P. L., 2008, "Optimal Design of an SPM Motor Using Genetic Algorithms and Taguchi Method," *IEEE Transactions on Magnetics*, Vol. 44, No. 11, pp. 4325-4328.
- [69] Isfahani, A. H., Vaez-Zadeh, S., and Rahman, M. A., 2008, "Using Modular Poles for Shape Optimization of Flux Density Distribution in Permanent-Magnet Machines," *IEEE Transactions on Magnetics*, Vol. 44, No. 8, pp. 2009-2015.
- [70] Luomi, J., Zwysig, C., Looser, A., and Kolar, J. W., 2009, "Efficiency Optimization of a 100-W 500000-r/min Permanent-Magnet Machine Including Air-Friction Losses," *IEEE Transactions on Industrial Applications*, Vol. 45, No. 4, pp. 1368-1377.

- [71] Yang, Y. P., Wang, J. P., Wu, S. W., and Luh, Y. P., 2004, "Design and Control of Axial-Flux Brushless DC Wheel Motors for Electric Vehicles- Part II: Optimal Current Waveforms and Performance Test," *IEEE Transactions on Magnetics*, Vol. 40, No. 4, pp. 1883-1891.
- [72] Jahns, T. M. and Soong, W. L., 1996, "Pulsating Torque Minimization Techniques for Permanent Magnet AC Motor Drives- A Review," *IEEE Transactions on Industrial Electronics*, Vol. 43, No. 2, pp. 321-330.
- [73] Keyhani, A. and Studer, C. B., 1999, "Study of Cogging Torque in Permanent Magnet Machines," *Electric Machines and Power Systems*, Vol. 27, pp. 665-678.
- [74] Islam, R., Husain, I., Fardoun, A., and McLaughlin, K., 2009, "Permanent-Magnet Synchronous Motor Magnet Designs With Skewing for Torque Ripple and Cogging Torque Reduction," *IEEE Transactions on Industry Applications*, Vol. 45, No. 1, pp. 152-160.
- [75] Sakabe, S., Shinoda, Y., and Yokoyama, H., 1990, "Effect of Interpole on Cogging Torque of Two-Phase Permanent Magnet Motor," *Electrical Engineering in Japan*, Vol. 110, No. 4, pp. 131-138.
- [76] Rizzo, M., Savini, A., and Turowski, J., 1991, "Influence of Number of Poles on the Torque of DC Brushless Motors with Auxiliary Salient Poles," *IEEE Transactions on Magnetics*, Vol. 27, No. 6, pp. 5420-5422.
- [77] Goto, M. and Kobayashi, K., 1983, "An Analysis of the Cogging Torque of a DC Motor and a New Technique of Reducing the Cogging Torque," *Electrical Engineering in Japan*, Vol. 103, No. 5, pp. 711-718.
- [78] Zeroug, H., Boukais, B., and Saharoui, H., 2002, "Analysis of Torque Ripple in a BDCM," *IEEE Transactions on Magnetics*, Vol. 38, No. 2, pp. 1293-1296.
- [79] Li, T. and Slemon, G., 1988, "Reduction of Cogging Torque in Permanent Magnet Motors," *IEEE Transactions on Magnetics*, Vol. 24, No. 6, pp. 2901-2903.
- [80] Eom, J. B., Hwang, S. M., Kim, T. J., Jeong, W. B., and Kang, B. S.,

- 2001, "Minimization of Cogging Torque in Permanent Magnet Motors by Teeth Pairing and Magnet Arc Design Using Genetic Algorithm," *Journal of Magnetism and Magnetic Materials*, Vol. 226, No. 2, pp. 1229-1231.
- [81] Chung, T. K., Kim, S. K., and Hahn, S. Y, 1997, "Optimal Pole Shape Design for the Reduction of Cogging Torque of Brushless DC Motor Using Evolution Strategy," *IEEE Transactions on Magnetics*, Vol. 33, No. 2, pp. 1908-1911.
- [82] Yao, Y. D., Huang, D. R., Wang, J. C., Liou, S. H., and Wang, S. J., 1997, "Simulation Study of the reduction of Cogging Torque in Permanent Magnet Motors," *IEEE Transactions on Magnetics*, Vol. 33, No. 5, pp. 4095-4097.
- [83] Yao, Y. D., Huang, D. R., Wang, J. C., and Wang, S. J., 1998, "Study of a High Efficiency and Low Cogging Torque Spindle Motor," *IEEE Transactions on Magnetics*, Vol. 34, No. 2, pp. 465-467.
- [84] Lin, Y. K., Hu, Y. N., Lin, T. K., Lin, H. N., Chang, Y. H., Chen, C. Y., Wang, S. J., Ying, T. F., 2000, "A Method to Reduce the Cogging Torque of Spindle Motors," *Journal of Magnetism and Magnetic Materials*, Vol. 209, No. 2-3, pp. 180-182.
- [85] Hsu, L. Y. and Tsai, M. C., 2004, "Tooth Shape Optimization of Brushless Permanent Magnet Motors for Reducing Torque Ripples," *Journal of Magnetism and Magnetic Materials*, Vol. 282, pp. 193-197.
- [86] Zhu, Z. Q., Chen, J. T., Wu, L. J., and Howe, D., 2008, "Influence of Stator Asymmetry on Cogging Torque of Permanent Magnet Brushless Machines," *IEEE Transactions on Magnetics*, Vol. 44, No. 11, pp. 3851-3854.
- [87] Ackermann, B., Janssen, J. H. H., Sottek, R., and Steen, R. I., 1992, "New Technique for Reduction Cogging Torque in a Class of Brushless DC Motors," *IEE Proceedings-B*, Vol. 339, No. 4, pp. 315-320.
- [88] Ishikawa, T., and Slemon, G. R., 1993, "A Method of Reducing Ripple

- Torque in Permanent Magnet Motors without Skewing,” *IEEE Transactions on Magnetics*, Vol. 29, No. 2, pp. 2028-2031.
- [89] Jiang, X., Xing, J., Li, Y., and Lu, Y., 2009, “Theoretical and Simulation Analysis of Influences of Stator Tooth Width on Cogging Torque of BLDC Motors,” *IEEE Transactions on Magnetics*, Vol. 45, No. 10, pp. 4601-4604.
- [90] Choi, J. H., Kim, J. H., Kim, D. H., and Baek, Y. S., 2009, “Design and Parametric Analysis of Axial Flux PM Motors With Minimized Cogging Torque,” *IEEE Transactions on Magnetics*, Vol. 45, No. 6, pp. 2855-2858.
- [91] Freudenstein, F., 1971, “An Application of Boolean Algebra to the Motion of Epicyclic Drives,” *ASME Journal of Engineering for Industry*, Vol. 93B, pp. 176-182.
- [92] Buchsbaum, F. and Freudenstein, F., 1970, “Synthesis of Kinematic Structure of Geared Kinematic Chains and Other Mechanisms,” *Journal of Mechanisms*, Vol. 5, pp. 357-392.
- [93] Tsai, L. W., 1987, “An Application of the Linkage Characteristic Polynomial to the Topological Synthesis of Epicyclic Gear Trains,” *ASME Journal of Mechanisms, Transmissions, and Automation in Design*, Vol. 109, No. 3, pp. 329-337
- [94] Chatterjee, G. and Tsai, L. W., 1994, “Enumeration of Epicyclic-Type Automatic Transmission Gear Trains,” *Journal of Passenger Cars: Mechanical Systems*, Vol. 103, pp. 1415-1426.
- [95] Tsai, L. W., 1995, “An Application of Graph Theory to the Detection of Fundamental Circuits in Epicyclic Gear Trains,” Technical Report TR 1995-97, Digital Repository at the University of Maryland, Maryland, U.S.A.
- [96] Olson, D. G., Erdman, A. G., and Riley, D. R., 1991, “Topological Analysis of Single-Degree-of-Freedom Planetary Gear Trains,” *ASME Journal of Mechanical Design*, Vol. 113, No. 1, pp. 10-16.

- [97] Hsu, C. H. and Lam, K. T., 1992, "A New Graph Representation for the Automatic Kinematic Analysis of Planetary Spur-Gear Trains," *ASME Journal of Mechanical Design*, Vol. 114, No. 1, pp. 196-200.
- [98] Hsu, C. H., 1993, "Synthesis of Kinematic Structure of Epicyclic Gear Trains by Admissible Graph Method," *Journal of Franklin Institute*, Vol. 330, No. 5, pp. 913-927.
- [99] Hsu, C. H. and Hsu, J. J., 1997, "An Efficient Methodology for the Structural Synthesis of Geared kinematic Chains," *Mechanism and Machine Theory*, Vol. 32, pp. 957-973.
- [100] Hsu, C. H. and Hsu, J. J., 2000, "Epicyclic Gear Trains for Automotive Automatic Transmissions," *Institution of Mechanical Engineers, Part D, Journal of Automobile Engineering*, Vol. 214, pp. 523-532.
- [101] Freudenstein, F. and Yang, A. T., 1972, "Kinematics and Statics of a Coupled Epicyclic Spur-Gear Train," *Mechanism and Machine Theory*, Vol. 7, pp. 263-275.
- [102] Yan, H. S. and Hsieh, L. C., 1991, "Kinematic Analysis of General Planetary Gear Trains," *Proceedings of the 8th World Congress on the Theory of Machines and Mechanisms*, Prague, Czechoslovakia, Vol. 6, pp. 153-157.
- [103] Hsieh, L. C. and Yan, H. S., 1992, "Generalized Kinematic Analysis of Planetary Gear Trains," *International Journal of Vehicle Design*, Vol. 13, Nos. 5/6, pp. 494-504.
- [104] Mogalapalli, S. N., Magrba, E. B., and Tasi, L. W., 1993, "A CAD System for the Optimization of Gear Ratios for Automotives Automatic Transmission," *SAE Paper No. 930,675*.
- [105] Simionescu, P. A., Beale, D., and Dozier, G. V., 2006, "Teeth-Number Synthesis of a Multispeed Planetary Transmission Using an Estimation of Distribution Algorithm," *ASME Journal of Mechanical Design*, Vol. 128, pp. 108-115.
- [106] Hsu, C. H., 2002, "An Analytic Methodology for the Kinematic

- Synthesis of Epicyclic Gear Mechanisms,” *ASME Journal of Mechanical Design*, Vol. 124, pp. 574-576.
- [107] 顏鴻森，蔡明祺，王心德，洪銀農，洪銀樹，2001，馬達與齒輪整合之裝置，中華民國專利第 434,977 號。
- [108] 顏鴻森，吳益彰，2006，整合行星齒輪系之直流無刷馬達，中華民國專利第 I253800 號。
- [109] Yan, H. S. and Wu, Y. C., 2006, “A Novel Design of a Brushless DC Motor Integrated with an Embedded Planetary Gear Train,” *IEEE/ASME Transactions on Mechatronics*, Vol. 11, No. 5, pp. 551-557.
- [110] Yan, H. S. and Wu, Y. C., 2006, “A Novel Configuration for a Brushless DC Motor with an Integrated Planetary Gear Train,” *Journal of Magnetism and Magnetic Materials*, Vol. 301, No. 2, pp. 532-540.
- [111] Yan, H. S. and Wu, Y. C., 2007, “Geared Motor with Planetary Gear Assembly,” U. S. Patent No. 7,211,016.
- [112] 吳益彰，顏鴻森，2007，“一種新型齒輪馬達之構想設計”，第十屆全國機構與機器設計學術研討會，台中，台灣，論文編號 A12。
- [113] 吳益彰，顏鴻森，2008，“整合式行星齒輪系與永磁無刷馬達之構想設計”，中國機械工程學會第二十五屆全國學術研討會，彰化，台灣，論文編號 csme25-493。
- [114] Yan, H. S., Wang, H. T., and Liu, J. Y., 2006, “Structural Synthesis of Novel Integrated DC Gear Motors,” *Mechanism and Machine Theory*, Vol. 41, No. 11, pp. 1289-1305.
- [115] 林均瑜，2007，“整合風力發電機與齒輪箱之構形設計”，國立成功大學機械工程學系碩士論文，台南，台灣。
- [116] Wu, Y. C., Chen, G. C., and Yan, H. S., “Optimization Design of a DC Commutator Motor with an Integrated Planetary Gear Train. ”, *IEEE Transactions on Magnetics*, 2011. Vol. 47, No. 10: pp. 4461-4464.
- [117] 王思為，2015，“一種新型充電式電鑽之設計”，國立成功大學機械工程學系碩士論文，台南，台灣。

- [118] 李若瑜，2016，” 整合行星齒輪式減速機切換式磁阻馬達之設計與分析”，國立成功大學機械工程學系碩士論文，台南，台灣。
- [119] 王紹宇，2017，” 整合行星齒輪式減速機與混合型步進馬達之設計與分析”，國立成功大學機械工程學系碩士論文，台南，台灣。
- [120] 吳益彰，林伯煒，2008，”整合式驅動馬達與內變速器之概念設計”，*Motor Express*，第 303 期，國立成功大學馬達科技研究中心，台南，台灣。
- [121] 蔡明祺，林博正，陳添智，王明賢，2005，同心式馬達設計與控制應用，*國科會專題計畫結案報告*，NSC91-2213-E-006-123。
- [122] 蔡明祺，林博正，杜黎蓉，2003，雙同心軸馬達，*中華民國發明專利*第 181543 號。
- [123] 蔡明祺，林博正，杜黎蓉，2003，無段變速馬達，*中華民國發明專利*第 183349 號。
- [124] Wang, L. L., Shen, J. X., Wang, Y., and Wang, K., 2008, “A Novel Magnetic-Geared Outer-Rotor Permanent-Magnet Brushless Motor,” *4th IET International Conference on Power Electronics, Machines, and Drives*, York, UK, pp. 33-36.
- [125] Wang, L. L., Shen, J. X., Luk, P. C. K., Fei, W. Z., Wang, C. F., and Hao, H., 2009, “Development of a Magnetic-Geared Permanent-Magnet Brushless Motor,” *IEEE Transactions on Magnetics*, Vol. 45, No. 10, pp. 4578-4581.
- [126] Chau, K. T., Zhang, D., Jiang, J. Z., Liu, C., Zhang, Y., 2007, “Design of a Magnetic-Geared Outer-Rotor Permanent-Magnet Brushless Motor for Electric Vehicles,” *IEEE Transactions on Magnetics*, Vol. 43, No. 6, pp. 2504-2506.
- [127] Jian, L., Chau, K. T., and Jiang, J. Z., 2009, “A Magnetic-Geared Outer-Rotor Permanent-Magnet Brushless Machine for Wind Power Generation,” *IEEE Transactions on Industrial Applications*, Vol. 45, No. 3, pp. 954-962.

- [128] Yan, H. S. and Wu, L. I., 2014, *Mechanism (in Chinese)*, 4th Edition, Tunghua Books Co. Ltd., Taipei, Taiwan.
- [129] Hsu, C. H., 2006, *Creative Mechanism Design (in Chinese)*, Gau Lih Books Co. Ltd., Taipei, Taiwan.
- [130] French, M.J., 1999, *Conceptual Design for Engineers*, Design council/Springer-Verlag, London, U.K..
- [131] Slemon, G. R., 1990, "An equivalent circuit approach to analysis of synchronous machines with saliency and saturation," *IEEE Transactions on Energy Conversion*, Vol. 5, No. 3, pp. 538-544.
- [132] Wu, Y. C. and Jian B. S., 2015, "Magnetic field analysis of a coaxial magnetic gear mechanism by two-dimensional equivalent magnetic circuit network method and finite-element method," *Applied Mathematical Modelling*, Vol. 39, No.19, pp. 5746 – 5758.
- [133] China Steel Corporation, 1971, *Electromagnetic Characteristics of Electromagnetic Coil (in Chinese)*, Kaohsiung, Taiwan.

Copyright

本論文非經顏鴻森教授同意不得影印。

The material contained in this thesis cannot be copied without the permission from Professor Hong-Sen Yen.

Signature(簽章)： 